NEW METHODOLOGIES OF SOLID STATE NMR AND BIOPHYSICAL STUDIES OF ANTIMICROBIAL AND DESIGNED PEPTIDES IN MODEL AND NATURAL MEMBRANES

by

BARBARA PERRONE

NEW METHODOLOGIES OF SOLID STATE NMR AND BIOPHYSICAL STUDIES OF ANTIMICROBIAL AND DESIGNED PEPTIDES IN MODEL AND NATURAL MEMBRANES

by

BARBARA PERRONE

A dissertation submitted for the degree of

DOCTOR OF PHILOSOPHY

at the

Université de Strasbourg

Strasbourg

France

September, 2011

BARBARA PERRONE:
New Methodologies of Solid-State NMR and Biophysical Studies of Antimicrobial and Designed Peptides in Model and Natural Membranes, © September 2011

SUPERVISOR:
Prof. Dr. B.Bechinger

LOCATION:
Membrane Biophysics and NMR Laboratory
Chemistry Institute
University of Strasbourg
Strasbourg, France

NEW METHODOLOGIES OF SOLID STATE NMR AND BIOPHYSICAL STUDIES OF ANTIMICROBIAL AND DESIGNED PEPTIDES IN MODEL AND NATURAL MEMBRANES

by

BARBARA PERRONE

A dissertation submitted for the degree of

DOCTOR OF PHILOSOPHY

Université de Strasbourg

Strasbourg, France

2011

C. MARQUES, H.d.R., CNRS	Présidente
R. WILLUMEIT, Prof., GKSS Research Center	Rapporteur
N. C. NIELSEN, Prof., University of Aarhus	Rapporteur
B. A. WALLACE, Prof. University of London	Examinateur
B. BECHINGER, Prof., Université de Strasbourg	Directeur de thèse

ABSTRACT

Solid-state NMR (SS-NMR) spectroscopy is a powerful tool to investigate structural details of membrane-associated peptides. In particular, the tilt angle of α-helical peptides reconstituted in non-oriented membranes can be derived by line-shape analysis of ^{15}N powder patterns. This approach allow a better control on several parameters such as pH, salt concentration, etc. with respect to mechanically oriented samples used in oriented SS-NMR spectroscopy.

Anyway, the spectra of peptides undergoing to fast uniaxial rotation diffusion around the membrane normal are characterized by distortions close to the isotropic chemical shift (Magic Angle Hole, MAH) that prevent to reach a satisfying fit quality. In this thesis work we developed a method that recovers the theoretical powder pattern line-shape based on ROtor-Directed Exchange of Orientations Cross-Polarization (RODEO). The method was successfully applied to designed peptides in unoriented membranes resulting in tilt angles values in agreement with published data. Finally we proved that RODEO can be applied in complex membrane systems, such as lipid mixture extracted from natural membranes, and, for the first time, we obtained an estimation of the alignment of an antimicrobial peptide in vivo, in Escherichia coli bacteria.

In the second part of this work, we report some unexpected results of biophysical investigations conducted to elucidate the insertion mechanism of the antimicrobial peptide LAH4 in zwitterionic membranes. It was previously shown that the LAH4-helix adopts an in-plane orientation in acidic conditions, while, at neutral pH, the peptide adopts a trans-membrane orientation. In contrast, we found that when citrate buffer is added to regulate the pH at 5, the peptide inserts in a transmembrane manner. Some possible explanations are suggested.

RÉSUMÉ

La spectroscopie de Résonance Magnétique Nucléaire des solides est un outil puissant pour l'étude structurale des peptides et protéines membranaires. En particulier l'angle d'inclinaison par rapport à la membrane de peptides structurés en hélice alpha et marqués en ^{15}N peut être obtenu par l'analyse des spectres de poudre provenant de systèmes peptides/membranes non-orientés par rapport au champ magnétique statique. Cette approche permet un meilleur contrôle sur plusieurs paramètres tels que la concentration en sel, le pH, etc.. par rapport aux échantillons que nécessite l'analyse par spectroscopie RMN de systèmes orientés sur plaques de verre. Cependant, les spectres de poudre de ces systèmes peptide/membrane présentent d'importantes distorsions à proximité du déplacement chimique isotrope (Magic Angle Hole, MAH) qui empêchent d'atteindre une qualité satisfaisante des paramètres RMN mesurés. Dans ce travail de thèse nous avons développé une nouvelle méthode qui récupère la forme théorique des spectres de poudre : l'expérience RODEO (ROtor-Directed Exchange of Orientations). La méthode a été appliquée avec succès à des peptides insérés dans des membranes non orientées et elle aboutit des valeurs d'angles d'inclinaison en accord avec les données publiées. Enfin nous avons prouvé que l'expérience RODEO pouvait être appliquée à des systèmes membranaires complexes, comme par exemple un mélange de lipides extraits de membranes naturelles, et, pour la première fois, nous avons obtenu une estimation de l'alignement d'un peptide antimicrobien in vivo, dans des bactéries Escherichia coli. Dans la deuxième partie de ce travail, nous rapportons quelques résultats inattendus des enquêtes biophysiques menées pour élucider le mécanisme d'insertion du peptide antimicrobien LAH4 dans les membranes zwitterioniques. Il a été précédemment montré que l'hélice LAH4 est orientée parallèlement à la surface de la membrane dans des conditions acides, tandis que, à pH neutre, le peptide adopte une orientation trans-membranaire. En revanche, nous avons constaté que lorsque le tampon citrate est ajouté pour réguler le pH à 5, le peptide s'insère de manière transmembranaire. Quelques explications possibles sont proposées.

PUBLICATIONS

Some ideas and figures have appeared previously in the following publications:

Pubblications in journals and books

- Raya, J., Perrone, B., Bechinger, B., and Hirschinger, J. "Undistorted chemical shift powder spectra obtained by using rotor-driven exchange of orientations cross-polarization (RODEO-CP)". Accepted by *Chemical Physics Letters*
- Bechinger, B., Bertani, P., Werten, S., Mendonça de Moraes, C., Aisenbrey, C., Mason, A.J., Perrone, B., Prudhon, M., Sudheendra, U.S., and Vidovic, V. "The structural and topological analysis of membrane polypeptides by oriented solid-state NMR spectroscopy: Sample preparation and theory". Chapter 8 in "*Membrane-active peptides: Methods and results on structure and function*" International University Line, La Jolla, California, USA; editor Miguel Castanho (2009)
- Mason, A.J., P. Bertani, G. Moulay, A. Marquette, B. Perrone, A.F. Drake, A. Kichler, and B. Bechinger. (2007). "Membrane interaction of chrysophsin-1, a histidine-rich antimicrobial peptide from red sea bream". *Biochemistry*. 46: 15175-15187.

Posters and oral communications

- Perrone, B., Bertani, P., Mason, J., and Bechinger, B., "Solid State NMR of peptides on oriented lipids" poster presented at the *"Atelier RMN & Matière Molle"*, Arcachon, France, 3^{rd} to 5^{th} June 2007
- Perrone, B., Bertani, P., Raya, J. and Bechinger, B., "Orientation and Rotational Diffusion Studies of Alpha Helical Peptides into Non Oriented Phospholipids", poster presented at the *XIII Congrès GEIMM,* Mittelwihr 2008, France, 4^{th} -7^{th} Mai 2008
- Perrone, B., Miles, A.J., Bechinger, B., Hoffman, S.V., and Wallace, B.A., "Oriented Synchrotron Radiation Circular Dichroism and Linear Dichroism Spectroscopy of Peptides in Model Membranes" poster presented at the 53^{rd} *Biophysical Society Annual Meeting*, Boston, USA, 28^{th} February to 4^{th} March 2009.
- "New Methodologies of investigation of model peptides-lipids systems by Solid-State NMR and application to the study of the antimicrobial peptide LAH4", talk presented at the joint conferences *14th Meeting of the Swedish Neutron Scattering Society* and *Final Biocontrol Meeting*, Lund, Sweden, 24^{th} -27^{th} August 2010.
- "Biophysical studies of the transfetion peptide LAH4 in zwitterionic and charged model membranes", talk presented at the lab

meeting of *MEMPHYS, Center for Biomembrane Physics*, Odense, Denmark, 20^{th} January 2010

- "Orientation of alpha helical peptides in membrane: Solid State NMR and Circular Dichroism in comparison" talk presented at the workshop *Structure and Function of Membrane Proteins*, Freiburg, Germany, 24^{th}-25^{th} September 2009.
- "Structural investigations of syntetic peptides by NMR and CD-SRCD Spectroscopy", talk presented at the *3rd Biocontrol Annual Meeting*, Bonn, Germany, 1^{st}-2^{nd} July 2009.
- "Investigation of the structural basis of the mechanism of transfection for therapeutic approaches" talk presented at the "*UK Circular Dichroism Winter Workshop*", Warwick University, Warwick, UK, 3^{rd} December 2007.
- "NMR and SRCD Spectroscopy of membrane peptides. A Marie Curie's Project" , talk presented at the student meeting of the University of Padova, *Physicists One Year After: Review of Experiences in the Research and Work World*, Padova, Italy 23^{rd} December 2007.

« *All you need to be a shinobi is the guts to never give up!* »

— Jiraiya —

in *"Naruto"* by Masashi Kishimoto

CONTENTS

LIST OF FIGURES

ACRONYMS

AMP Anti-Microbial Peptide

AMPs Anti-Microbial Peptides

APHH-CP Adiabatic Passage though the Hartman-Hahn Cross Polarization

APHH-RODEO-CP Adiabatic Passage though the Hartman-Hahn RODEO Cross Polarization

CD Cicular Dichroism

CP Cross Polarization

CP-MAS Cross Polarization with Magic Angle Spinning

CS Chemical Shift

CSA Chemical Shift Anisotropy

CWCP Continuous Wave Cross Polarization

CW-RODEO-CP Continuous Wave ROtor-Directed Exchange of Orientations Cross-Polarization

DLS Dynamic Light Scattering

DMPC DiMyristoyl Phosphatidyl Choline

DNP Dynamic Nuclear Polarization

FID Free Free Induction Decay

HH Hartmann-Hahn

HPLC High-Performance Liquid Chromatography

LPS Lipopolysaccharides

MA Magic Angle

MALDI-TOF Matrix-Assisted Laser Desorption/Ionization by Time of Fly

MAH Magic Angle Hole

MAS Magic Angle Spinning

MLV Multi-Lamellar Vesicles

MOIST Mismatch-Optimized IS Transfer

NEO Native Exchange of Orientations

NMR Nuclear Magnetic Resonance

OCD Oriented Cicular Dichroism

PAF Principal Axis Frame

POPC 1-palmitoyl-2-oleoyl-sn-glycero-3-phosphocholine

POPG 1-palmitoyl-2-oleoylglycero-3-phosphoglycerol

RF Radio Frequency

RODEO ROtor-Directed Exchange of Orientations

RODEO-CP ROtor-Directed Exchange of Orientations Cross-Polarization

SAXS Small Angle X-ray Scattering

SDS Sodium dodecyl sulfate

SS-NMR Solid State NMR

TLE Total Lipid Extract

TOH Transient Oscilation Holes

TFE Tri-fluoro ethanol

ULV Uni-Lamellar Vesicles

VACP Variable-Amplitude Cross Polarization

Part I

INTRODUCTION AND MOTIVATIONS

1 GENERAL INTRODUCTION AND MOTIVATIONS

CONTENT OF THE CHAPTER:

In this chapter we are going to give the reader some general information on the topics approached in this thesis. The reasons for conducting this research work are described in the frame of their respective context.

1.1 ANTIMICROBIAL PEPTIDES

Motivations

Anti-Microbial Peptides (AMPs) possess a broad spectrum of activity toward several types of organisms and a certain degree of selectivity for bacteria cells. Despite their ancient lineage, their efficiency as defensive weapons is conserved, suggesting that bacteria did not developed a resistance mechanism which increases their biomedical interest as therapeutic agents.

Structural features

Structural characteristics of AMPs can be quite heterogeneous: there is no standard amino-acid composition, they can assume alpha-helix or beta structure or even both, they may be linear or cyclic.

Based on their structural features, AMPs can be divided in four major groups:

1. linear peptides, without cysteines, unstructured in solution but helical in presence of membranes
2. linear peptides, without cysteines but rich in prolines and arginines
3. peptides with one disulfide bond
4. peptides carrying more then one disulfide bonds, forming mainly β-sheets structures with antiparallel chains

Even within the first group of AMPs, the most studied, there is a considerable variation of structural proprieties, as their chain length, hydrophobicity and distribution of charges. Nevertheless, they present some common characteristics: their positive charge, their amphiphaticity and the fact that they arrange their hydrophobic residues to face the interior of the bacterial membrane, while the hydrophilic side stay is pointed toward the membrane-water interface.

Selectivity towards bacterial membranes

Even when two AMPs have similar physico-chemical characteristics, their antimicrobial activity may be very different. The reasons beyond the different susceptibility of different cells towards a certain AMPs are a key step to understand in order to efficiently develop low-toxicity drugs selective against pathogens.

Whereas the Gram positive single barrier and the Gram negative inner membranes are both composed of negatively charged phospholipids, the mammalian membranes are constituted mainly of zwitterionic lipids and cholesterol. It is thought to be the net positive charge of the AMPs that allow them to interact preferentially with negatively charged bacterial membranes.

Killing mechanism

A common characteristic observed in membrane-active peptides is their capability to disturb bilayer integrity, either by creation of defects, disruption or pore formation. The permeation of microbial membranes seems to be an early and necessary step in killing microbes, if not the lethal step that kills the bacteria. Once the membrane is damaged, several path may lead to the cell death, as modifications of the microbial metabolism due to the collapse of the transmembrane electrochemical gradients, the inhibition of cellular respiration, the cell swelling and the osmolysis caused by the increased flow of water and ions.

Mechanisms of membrane permeation

The permeation of the cytoplasmic membrane of the cell has been proposed to proceed via several mechanisms. In this section a brief overview of some the most cited mechanisms in the literature will be presented.

TRANSMEMBRANE PORE FORMATION Some antimicrobial peptides form transmembrane pores once a certain peptide/lipid ratio is reached. Indeed, pore formation occurs spontaneously in pure lipid vesicles under tension, and the same mechanism is proposed by Huang [6] to explain the membrane permeation. The peptide binding to the membrane surface causes a local membrane area expansion and therefore an equivalent local tension. According to the author, "even at extremely low concentrations, antimicrobial peptides can induce, by fluctuations, transient pores [...]" and "stable pores appear only when the peptide concentration exceeds a threshold".

The pore may be formed by the peptide alone, aggregated in α helical bundle with the hydrophilic peptide facing the interior region of the pore ("barrel-stave" model, cf. Figure 1 A) or may involve lipid molecules, tilted from the lamellar normal to form a toroidal hole ("toroidal-pore", cf. Figure 1 C). The first mechanism well describes the experimental findings of alamethicin [7], while the second mechanism was invoked to explain the formation of structures which resembles 'worm-holes' [8, 9] at high magainin concentrations.

"CARPET-LIKE" MECHANISM In the carpet-like mechanism, amphiphatic peptides initially bind to the surface of the membrane and partially cover it in a carpet-like fashion. The membrane is permeated only after a peptide threshold concentration has been reached(cf. Figure 1 B).

In contrast to the "barrel-stave" mechanism, the peptide does not insert in the core of the membrane, but rather binds to lipids headgroups. Peptide-lipid binding is driven by electrostatic and hydrophobic interactions and the peptide disrupts the bilayer in a detergent-like

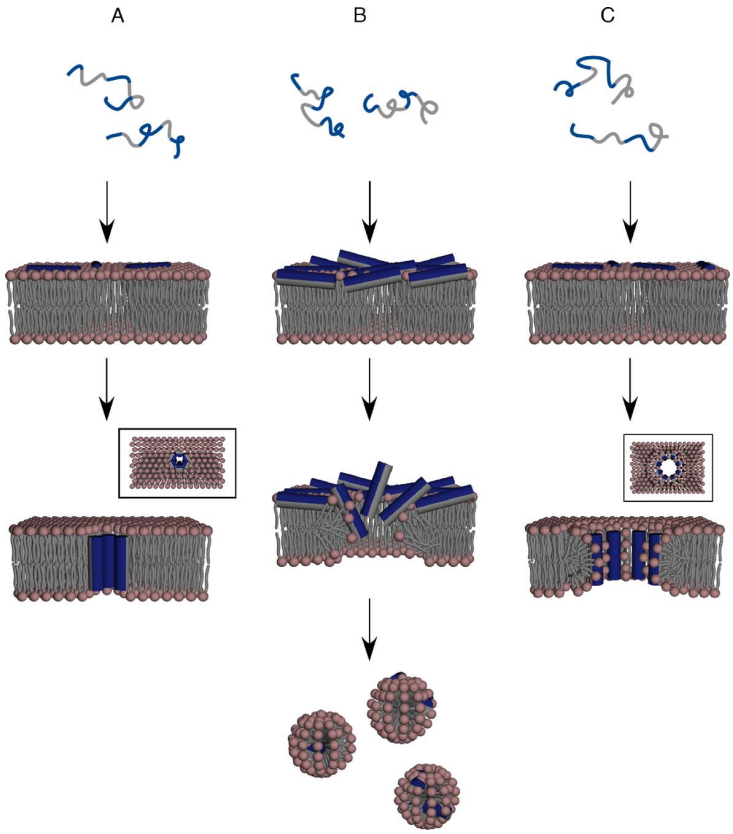

Figure 1: Schematic illustration of the bilayer permeabilization mechanisms induced by α-helical antimicrobial peptides: (A) "barrel-stave", (B) "carpet-like" (detergent-like), and (C) "toroidal-pore" (wormhole). The hydrophilic and hydrophobic faces of the peptides are colored in blue and gray, respectively. The top-views for the "barrel-stave" and the "toroidal-pore" models are shown in boxes. Image adapted from [1].

manner, maintaining a surface-orientation (in-plane). Upon a critical threshold concentration is reached, the peptides are thought to form transient holes, disrupt the bilayer curvature, and finally disintegrate the membrane, leading eventually to micelle formation.

This mechanism implies that a high concentration of the peptide has to be reached before the membrane permeation occurs. The concentrations at the membrane level is still a discussed matter[10] and even if high peptide densities have been observed at the surface of bacterial cells, membrane-activities have been demonstrated at much reduced peptide-to-lipid ratios.

Low peptide-to-lipid ratios are considered sufficient to dissipate the ionic gradient across cell membranes or to develop antibiotic activity [11, 12, 13] through small openings, while bigger pores and higher peptide-to-lipid ratios are required for the cell lysis [14, 15, 16].

"DETERGENT-LIKE" MODEL The "detergent-like" model [2] is a more general model, based on the detergent-like properties of AMPs. Notably, the "detergent-like" model is not in contradiction with the above mentioned "toroidal-pore" or "carpet-like" models, instead they are included as 'special cases'.

This model is based on the observation that antimicrobial peptides and detergents have several general features in common, such as the leakage of fluorescent dyes at similar concentrations [17, 18], the stepwise changes in conductivity and the detergent-to-lipid ratio dependency on the membrane disruption action (cf. Figure 1). In particular, at very low detergent-to-lipid ratios, they can have neutral or event stabilizing effects on the bilayer [19**?**]. At intermediate concentrations, openings might form temporarily while, at higher detergent-to-lipid ratios, membrane disintegration becomes apparent. Additional support for the detergent-like model arises from the observation that antibiotic or model peptides too short to span the membrane exhibit channel-like activities as well, and that in-plane oriented amphipathic peptides posses antimicrobial activity (see references cited in [2]).

Neither amphipathic helix nor detergent molecules, when intercalated into a lipid bilayer, fill the volume at the level of the fatty acyl chains and in the lipid head group region equally well, creating a void in the hydrophobic region of the membrane bilayer (cf. Figure 4 E, [2, 3] and references therein). The wide spectrum of membrane morphologies is then the response to the molecular shape of lipid together and the broad ensemble of variables that can modify the packing of the membrane. Thus, the action of amphipathic peptides can be understood within the frame of a phase diagram (see Figure 1), in which a wide variety of parameters and conditions, as the peptide-to-lipid ratio, the detailed membrane composition, temperature, hydration and buffer composition, have also be taken in account.

Other mechanisms

The breakdown of the permeability barrier in bacteria is not always closely correlated with cytotoxic activity [20] and more recent investigations give evidence that the antibiotic activity may also develop due to interactions of these peptides with intracellular targets (for a review see [21]).

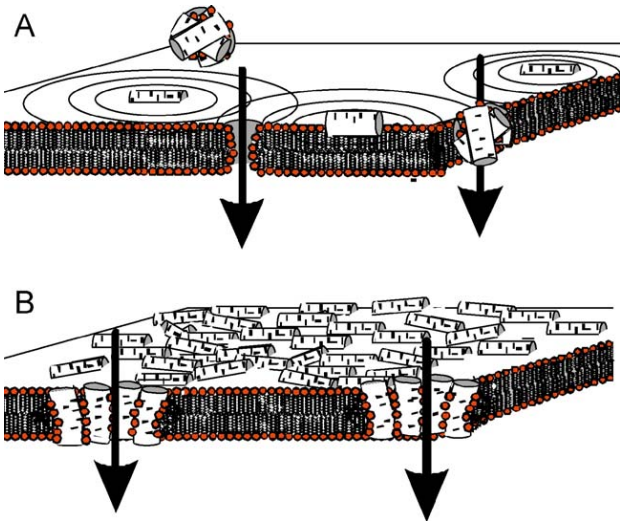

Figure 2: Models describing the interactions of linear cationic amphipathic peptides with membranes. (A) At low concentrations three effects of detergent-like molecules are shown. A peptide micelle 'hits' the membrane, thereby adsorbing a few lipid molecules concomitant with pore formation (top). The micelle can also 'insert' in the membrane resulting in a 'micellar aggregate channel' (right side). Furthermore, as in the presence of detergents in-plane oriented amphipathic peptides destabilize the membrane within a diameter of several nanometers (circles). Lateral diffusion of the peptides along the membrane surface results in transient changes in local peptide density and the temporary collapse of the membrane ohmic resistance when peptides approach each other. (B) At higher concentrations the membrane disintegrates as described by the carpet-, torroidal pore- or wormhole models. Figure and caption from [2].

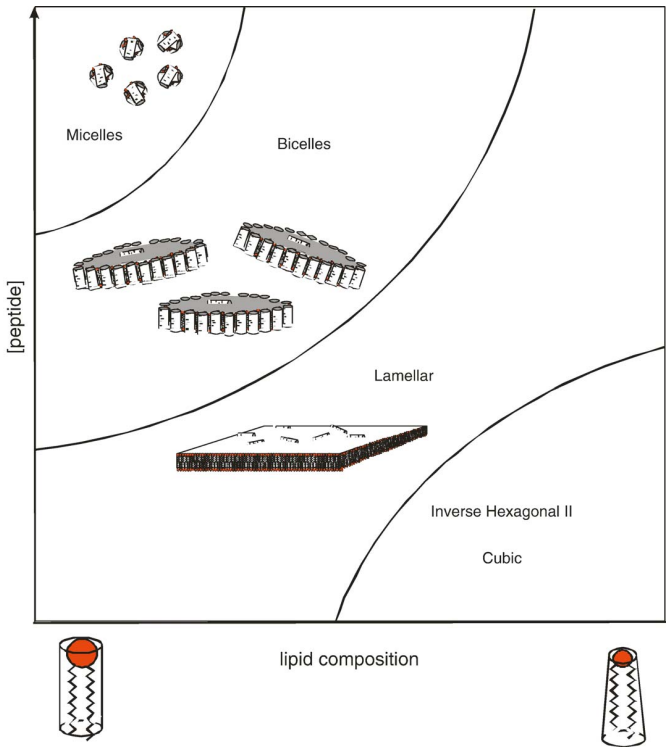

Figure 3: Schematic phase diagram of antibiotic peptide/phospholipid mixtures. A variety of macroscopic phases are obtained as a function of peptide/ lipid ratios and lipid composition. Here two lipids with different molecular shapes are mixed and their effect on the macroscopic phase transition in the presence of antibiotic peptides is shown. For a complete description of antibiotic activities other parameters such as temperature, pH, or cholesterol concentration would have to be considered. Figure and caption from [2].

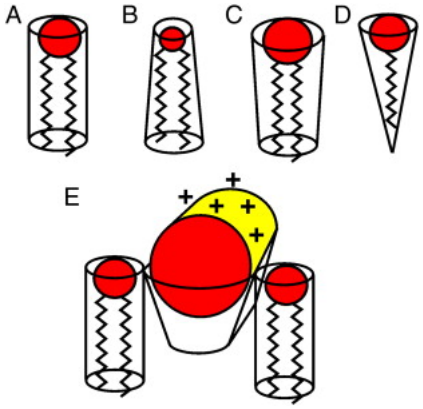

Figure 4: The molecular shape of lipids and in-plane oriented amphiphatic peptides is illustrated. Whereas lipids such as diacylphosphatidylcholines are represented by a cylindrical molecular shape (A), the decreased size of the phsophatidylethanolamine head group results in an inverted truncated cone structure (B). In contrast a truncated cone is obtained for double chained lipids with larger head groups (C) or a cone in the presence of only one alkyl chain such as lyso-lipids or detergents (D). An in-plane oriented cationic peptide that inserts into the membrane interface resembles a wedge similar to a cone or truncated cone structure (E). For comparison two PC lipids are shown next to the peptide indicating that the latter does not fill the depth of the PC unperturbed monolayer. Figure and caption from [3].

Other membrane-dependent processes may be involved in the action of some peptides, such as translocation of the peptide across the membrane to the cytoplasm or facilitation of the trans-bilayer lipid diffusion leading to loss of lipids asymmetry in the membrane. Once inserted in the cytoplasm, the peptide might alter the normal cell activities by binding to DNA, inhibition of nucleic acids and protein synthesis, inhibition of enzymatic activity, activation of autolytic enzymes, alteration of the cytoplasmic membrane or inhibition of the cell-wall synthesis [21].

Nevertheless, the membrane has to be crossed to allow penetration into the cell interior and to reach the final target.

... *and* in vivo?

Many studies have been performed in model bilayers mimicking the bacteria and mammalian membranes with the goal of correlate their proprieties and biological activity. However it is evident that there is a major difference between living cells and model membranes.

In vivo, Anti-Microbial Peptide (AMP)s have to pass through the cell wall before they come in contact with the cytoplasmic membrane and this process is depending on many factors, such as structure and oligomeric state of the peptide, and characteristics of the microbial surface. In particular, the structure and composition of the Lipopolysaccharides (LPS) in the bacterial cell wall may play a capital role in the overall efficiency of the peptide antimicrobial action and in the resistance mechanism developed by the bacteria.

In this regard, effective definitions of "antimicrobial activity" and "specificity" should take into consideration the physiological conditions *in vivo*. These include the concentration of antimicrobial peptide at

the site of the infection, the role of synergistic substances (such as other antimicrobial peptides or the absence of divalent cations), the role of inhibiting substances that might be present (like physiological concentrations of salt and proteins) and the unusual characteristics of bacteria replicating in vivo, particularly those in biofilms. It is therefore important to study the mechanism of action of these peptides in their appropriate environments to reach the final goal of a successful development of more efficient, broad-spectrum antimicrobial agents.

1.2 SOLID-STATE NMR

Solid-state NMR as a tool to investigate biological membranes

When dealing with membrane-associated peptides and proteins, classical structural techniques such as X-ray diffraction and liquid-state Nuclear Magnetic Resonance (NMR) encounter experimental difficulties. For example, even if new emerging strategies to crystallize membrane proteins exist [22, 23], to obtain well-ordered 3-dimensional crystals of a good size is still a challenge. On the other hand, the insolubility in aqueous media is the major problem of the application of liquid-state NMR to membrane protein studies. Organic solvents or detergents are used to mimic the hydrophobic lipid environment, however the resolution is strongly related with the tumbling rates of the molecules, causing overlap of the signals in large proteins, complexes or protein-detergent micelles spectra.

SS-NMR spectroscopy is a powerful tool to investigate structural details of peptides and proteins directly in the membrane medium. This highly versatile technique gives access to atomic-level information about the conformation, dynamics, orientation, depth of insertion of membrane proteins, and lipid–protein interactions. The outstanding propriety of SS-NMR is the fact that is able to provide several structural information of proteins and peptides near to physiological conditions. Furthermore, with the same technique also the structural modification of the phospholipids caused by the presence of the peptide can be investigated, allowing one to obtain a wide view of the protein-membrane interactions. This is a major advantage with respect to other techniques because membrane proteins require the presence of the lipid environment to maintain their native conformation and their functions [24].

By the use of selectively labelled amino acids is possible to study specific elements of the structure, as angles or distances, of the polypeptide or of the peptide-lipid complex. In order reduce the complexity of the spectra and to obtain the necessary resolution uni-axially aligned samples are used. The alignment can be obtained by several ways, the more commons ones are to use magnetic oriented bicelles or mechanically oriented samples. Diamagnetic proprieties of lipids are at the basis of the magnetic orientation of bicelles (discotic phospholipids particles) in the presence of a strong magnetic field but the stability and degree of orientation achievable by this approach depend critically on sample composition and experimental conditions. The second approach takes advantage of the self-assembly propriety of lipids, that organize themselves in ordered multilayers on solid supports like glass or quartz or even plastic. The use of multilayers permit also to check the quality of the alignment of the membrane by ^{31}P naturally present in phospholipids. The ^{31}P spectrum allows one to evaluate how the

phase and the aliment of the membrane are modified by the peptide or by other environmental conditions, such as hydration, temperature, pH, etc. Moreover, by using deuterated lipids is also possible to check the perturbation that the host molecule provokes on the alkyl chains in terms of order parameter variations.

The Magic Angle Hole

One major problem of SS-NMR techniques is the low sensitivity. To gain in signal-to-noise ratio, the spectra of low abundance nuclei, as ^{15}N and ^{13}C, are recorded by CP techniques. The process of magnetization transfer is driven by the dipolar coupling between protons near to the labelled ^{15}N or ^{13}C, and, for ^{15}N backbone-labeled peptides, mainly by the directly bounded ^{1}H. The angular dependence of the dipolar coupling is such that it vanishes at the magic angle. This causes, under certain conditions, the appearance of a problematic "hole" in correspondence to the isotropic chemical shift σ_{iso} [25], [26, 27] that deform the powder pattern line-shapes and prevent to reach a satisfying fit quality.

For common rigid solids this effect is usually not visible, since spin diffusion acts in a way to homogenize the magnetization across the whole powder pattern. However, there is a special case in which the peculiarity of the magic angle become obvious and it is when the spins of interest are subject to uniaxial motion. Under these conditions, the spin diffusion process is drastically slowed down and the system behave as an isolated spin pair with null magnetization at the magic angle.

> *Aim of the first part of this thesis work is to develop a method that recovers the theoretical powder pattern line-shape of samples subject to fast uniaxial motion.*
>
> A propaedeutic study on cross-polarization schemes will be developed in Chapter 3 and the full method will be introduced and described in Chapter 4.

To set up our method we used ferrocene, an organometallic compound constituted of two cyclopentadienyl rings bound on opposite sides of a central Fe atom. It was observed by nuclear magnetic resonance [28] that the two rings rapidly rotate about their five-fold symmetry axes (see 5). As a result, inter-ring and intermolecular dipolar interactions are strongly reduced and the directly bound $^{1}H-^{13}C$ pairs are well isolated, at least, as long as the dipolar vector is not oriented in proximity of the magic angle. The dynamic of the process of cross polarization between a directly bound proton and a ^{13}C carbon shows the same aspects of the dynamic of a ^{15}N labelled backbone amide of a peptide in liquid crystals. In addition, it has the advantage of a $T_{1\rho}$ long enough to record an undistorted line-shape spectrum to use as comparison and requires a relatively short measurement time (about 1 hour) for each spectrum.

This type of systems is biologically relevant, since amide backbone sites in α–helical peptides show this kind of dynamics when reconstituted in membranes. Biological samples are not suitable to set up a methodology because of their low sensitivity, due to the low concentration of ^{15}N labels aggravated by the dilution in the membrane. Additional problems arise from sample dehydration and degradation, preventing to reach a long-term stability necessary for methodological studies.

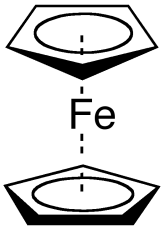

Figure 5: Ferrocene. The rotation occurs around the axis connecting the center of the two rings and the Fe^{2+} ion.

Unoriented membranes and powder pattern analysis

The mechanical alignment is a conceptually simple method to obtain the orientation, however it is not so simple to achieve from the experimental point of view. It can result challenging to obtain well-aligned membranes in case of unfavourable interactions of lipids with the solid support, especially for negatively charged lipids, or disruption of the alignment caused by the peptide or the protein themselves. The problem can be avoided when recurring to non-oriented samples in which the fast uniaxial rotation diffusion around the membrane normal of the protein still permit to determine the orientation respect to the axis of rotational averaging [29, 30, 31, 32]. This method, as additional advantage, allows a more controlled sample preparation, in terms of pH and salt concentration, opening the way for measurements even in living cells.

The presence of deviations from the averaged powder pattern lineshape complicates dramatically the interpretation of the spectra, aggravated by the poor resolution obtained from non-oriented samples. In the presence of distorted spectra discerning populations of spins with different orientation can result in a difficult task. In case of multiple labels present in the sample the task became even more difficult. To expand the application of this approach to the study of more complex systems and topologies, a methodology to record a undistorted spectra has to be developed

> *The second aim of this research work is to develop and apply a method for the analysis of powder spectra which consent to extract an estimation of the tilt and pitch angles of helical peptides in unoriented membranes.*
>
> The achievement of this goal is described in Chapter 5.

Application to natural membranes and in vivo

Membrane-active peptides and proteins, so far, are studied only in model systems, as micelles or bi-layers. Rarely in lipid extracts or isolated bacterial membranes [33]. Bacteriorhodopsin in the purple membrane of *Halobacterium salinarium* is one of the few examples available [34, 35, 36]. Concerning antimicrobial peptides, PGLa and other peptides were studied in native membranes [37] and in living bacteria [38] by ^{31}P NMR spectroscopy. Ieronimo et *al*. also studied the orientation of PGLa by ^{19}F NMR [37] including fluoridated amino acid analogs in the peptide sequence. However, the effects of such substitution may alter the protein structure, stability or biological activity [39].

The fact that our method can be efficiently applied, as seen in Chapter 5, to obtain topological information of peptides in non-oriented samples, enable us to extend its application to more complex systems, as natural membranes. This kind of studies may open a new approach to prove the mechanism of action of antimicrobial peptides in the context of sophisticated much more complex membrane systems or *in vivo*. From these studies a more detailed description of the AMPs action may result, accounting for many additional variables that are not easily included in model membrane experiments , such as the complexity of the membrane composition or the presence of glycolipids. Additionally, the use of unoriented samples permits to obtain a good control over environmental parameters such as pH or salts concentration, that may affect the oligomeric state of the peptide or the strength of the electrostatic interactions with the lipid surface.

> *The third goal of this thesis is to demonstrate the applicability of the RODEO method to complex membrane systems, such as lipid mixture extracted from natural membrane, and in vivo, in Escherichia coli bacteria.*
>
> With this objective, in Chapter 6 we will apply the RODEO method for the structural study of the antimicrobial peptide PLAH4 directly in natural membranes and in vivo.

1.3 BIOPHYSICAL STUDIES OF THE ANTIMICROBIAL PEPTIDE LAH4 IN PRESENCE OF CITRATE BUFFER

LAH4 is an amphiphatic histidine-rich peptide that possess both antibiotic [40, 41] and DNA delivery [42, 43] capabilities. Because of the protonation of the imidazole rings, LAH4 increases its overall net charge from +5 to +9 in response to the acidification of the environment from the neutral condition to pH ca. 5. It was shown [40, 44] that when the histidines are protonated, the LAH4-helix adopts an in-plane orientation at the membrane surface. In contrast, when the histidine are uncharged, the peptide adopts a trans-membrane orientation with the lysine residues acting as anchors at the membrane surfaces.

The mechanism of action of this peptide in zwitterionic and charged membrane at neutral pH was already studied [41, 45, 46], while less is known on the mechanism of membrane disruption under acidic conditions [40].

To clarify the different aspects of the mechanism of action of the peptide we started some biophysical characterization of the peptide-lipid interaction in acidic conditions. However, when citrate buffer was added to regulate the pH, some unexpected results were obtained.

> *The forth aim of this thesis is to describe the effect of the addition of citrate buffer to the insertion mechanism of the antimicrobial peptide LAH4 in zwitterionic membranes.*
>
> The results obtained by different biophysical techniques are reported in Chapter 7.

SYNTHÈSE DU TRAVAIL DE THÈSE

CONTENU DU CHAPITRE:

Dans ce chapitre, nous allons donner au lecteur quelques informations générales sur les thèmes abordés dans cette thèse. Les raisons pour effectuer ce travail de recherche sont décrits dans le cadre de leur respectif contexte.

1.4 LES PEPTIDES ANTIMICROBIENS

Motivations

Les peptides antimicrobiens (AMPs) possède un large spectre d'activité vers plusieurs types d'organismes et un certain degré de sélectivité pour les cellules de bactéries. Malgré leur ancienne lignée, leur efficacité comme armes défensives est conservée, ce qui suggère que les bactéries n'ont pas développé un mécanisme de résistance qui augmente leur intérêt biomédical en tant qu'agents thérapeutiques.

Les caractéristiques structurelles

Les caractéristiques structurelles de peuvent être très hétérogènes: il n'existe aucune norme composition en acides aminés, ils peuvent assumer hélice alpha ou de structure bêta ou même les deux, ils peuvent être linéaires ou cycliques.

Basé sur leurs caractéristiques structurelles, AMPs peuvent être divisé en quatre grands groupes:

1. peptides linéaires, sans cystéines, non structurées dans la solution, mais hélicoïdale en présence de membranes
2. peptides linéaires, sans cystéines, mais riche en prolines et arginines
3. peptides avec un pont disulfure
4. peptides portant plus d'un des ponts disulfure, formant essentiellement structures de bêta-feuilles avec des chaînes antiparallèles

Même au sein du premier groupe de AMPs le plus étudié, il ya une variation considérable de propriétés structurelles, comme leur longueur de chaîne, l'hydrophobicité et la répartition des charges. Néanmoins, elles présentent certaines caractéristiques communes: leur charge positive, leur amphiphaticity et le fait qu'ils organisent leurs résidus hydrophobes pour faire face à l'intérieur de la membrane bactérienne, tandis que le séjour côté hydrophile est pointé vers l'interface membrane-eau.

Sélectivité envers les membranes bactériennes

Même lorsque deux AMPs ont similaires caractéristiques physico-chimiques, leur activité antimicrobienne peut être très différente. Compraindre

les raisons de la susceptibilité différente des différentes cellules vers une certaine peptide antimicrobien est une étape clé pour développer efficacement les médicaments à faible toxicité sélective contre les pathogènes.

Alors que la membrane des bacteries est composée de phospholipides chargés négativement, les membranes de mammifères sont constituées essentiellement de lipides zwitterioniques et le cholestérol. Il est la charge nette positive de les AMPs qui leur permettent d'interagir préférentiellement avec les membranes bactériennes chargées négativement.

Mécanisme

Une caractéristique commune observée dans les peptides qui agissent sur la membrane est leur capacité à perturber l'intégrité de la bicouche, soit par création de défauts, la perturbation ou la formation de pores. La perméation des membranes microbiennes semble être une étape précoce et nécessaire dans tuant les microbes, si ce n'est l'étape mortelle qui tue les bactéries. Une fois que la membrane est endommagée, plusieurs parcours peuvent conduire à la mort cellulaire, comme des modifications du métabolisme microbien dû à l'effondrement des gradients transmembranaires électrochimique, l'inhibition de la respiration cellulaire, le gonflement des cellules et l'osmolysis causée par l'augmentation du débit d'eau et des ions.

Mécanismes de la perméabilité membranaire

La perméation de la membrane cytoplasmique de la cellule a été proposé de procéder par le biais de plusieurs mécanismes. Dans cette section un bref aperçu de certains des mécanismes les plus cités dans la littérature sera présentée.

FORMATION DE PORES TRANSMEMBRANAIRES Certains peptides antimicrobiens pores transmembranaires forment une fois certains rapports peptide/lipide est atteint. En effet, la formation des pores se produit spontanément dans des vésicules lipidiques pures sous tension, et le même mécanisme est proposé par Huang [6] pour expliquer la perméabilité membranaire. La liaison du peptide à la surface de la membrane provoque une expansion à membrane locale zone et donc une tension équivalente locales. Selon l'auteur, "même à des concentrations extrêmement faibles, les peptides antimicrobiens peuvent induire, par les fluctuations, des pores transitoires [...]" et "pores stables apparaissent seulement lorsque la concentration de peptide dépasse un seuil".

Le pore peut être formé par le peptide seul, agrégées avec le peptide hydrophile posent à la région intérieure de la porosité ("barrel-stave model", voir Figure 1 A) ou peut impliquer des lipides molécules, inclinée de la normale lamellaire pour former un trou toroïdal ("toroidal pore", voir Figure 1 C). Le premier mécanisme ainsi décrit les résultats expérimentaux de alaméthicine [7], tandis que le second mécanisme a été invoqué pour expliquer la formation de structures qui ressemble à «trous de ver» [6, 8] à des concentrations élevées de magainine.

MÉCANISME "À TAPIS" Dans le mécanisme à tapis, les peptides amphiphatiques d'abord se lieront partiellement à la surface de la membrane et le couvriront d'une manière semblable à un tapis. La membrane est perforé seulement après un seuil de concentration de peptide a été obtenu (voir Figure 1 B).

Contrairement à le mécanisme precedente, le peptide ne s' insére pas dans le noyau de la membrane, mais plutôt lie les groupes de tête de lipides. La liaison du peptide aux lipides est entraîné par des interactions électrostatiques et hydrophobes et le peptide perturbe la bicouche de façon "détergent-like", le maintien d'une surface d'orientation (en avion). À l'atteintment d'une concentration critique les peptides sont pensés former des trous, perturber la courbure de la bicouche, et finalement désintégrer la membrane, aboutissant finalement à la formation de micelles.

Ce mécanisme implique que une forte concentration du peptide doit être atteint avant la perméation membranaire survient. La concentration au niveau de la membrane est encore un sujet discuté [10] et même si des densités élevées de peptides ont été observés à la surface des cellules bactériennes, activités antibiotiques sur la membrane ont été démontrés à rapports peptide/lipids beaucoup plus réduites. Faibles concentrations sont considérées comme suffisantes pour dissiper le gradient ionique à travers les membranes cellulaires ou pour développer une activité antibiotique [11, 12, 13] à travers de petites ouvertures, tandis que concentrations supérieures sont nécessaires pour générer des pores et pour la lyse de la cellule [14, 15, 16].

MODÈLE "DETERGENT-LIKE" Le modèle "détergent-like" [2] est un modèle plus général, sur la base des propriétés détergentes des peptides antimicrobiens. Notamment, ce modèle n'est pas en contradiction avec les models mentionnés ci-dessus: ils sont inclus comme des «cas spéciaux».

Ce modèle est basé sur l'observation que des peptides antimicrobiens et les détergents ont plusieurs caractéristiques générales en commun, tels que les fuites de colorants fluorescents à des concentrations similaires [17, 18], les changements par étapes de la conductivité et dépendance du rapport peptide/lipide de la rupture de la membrane (voir Figure 1). En particulier, à très faible raports détergent-lipide, ils peuvent avoir des effets neutres ou de stabilisantion sur la bicouche [19**?**]. À des concentrations intermédiaires, des ouvertures pourraient se former temporairement, et à concentrations supérieures, la désintégration membrane devient apparente. Un appui supplémentaire pour le modèle à détergent, vient de l'observation que des peptides avec une séquence trop courte pour traverser la membrane présentent aussi des activités antibiotiques, et que des peptides amphipathiques d'activité orientée dans le plan de la membrane possèdent aussi proprietés antibiotiques (voir les références citées dans [2]).

Ni les hélices amphipathiques, ni les molécules détergentes, quand intercalés dans une bicouche lipidique, remplissez le volume au niveau des chaînes alkyliques et dans la région de la tête du groupe de lipides, en créant un vide dans la région hydrophobe de la bicouche membranaire (voir Figure 4). Le large spectre des morphologies membrane est alors la réponse à la forme moléculaire de lipides et à l'ensemble de variables qui peuvent modifier l'emballage de la membrane. Ainsi, l'action des peptides amphiphiles peuvent être compris dans le cadre

d'un diagramme de phase (voir Figure 1), dans lequel une grande variété de paramètres et les conditions, comme le rapport peptide-lipide, la composition détaillée de la membrane, la température, l'hydratation et la composition du tampon, ont également pris en compte.

D'AUTRES MÉCANISMES La rupture de la barrière de perméabilité dans les bactéries ne sont pas toujours en corrélation étroite avec l'activité cytotoxique [20] et les enquêtes les plus récentes donnent la preuve que l'activité antibiotique peut également se développer en raison des interactions de ces peptides avec des cibles intracellulaires (pour une revue voir [21]) .

D'autres processus peuvent être impliqués dans l'action de certains peptides, comme la translocation du peptide à travers la membrane vers le cytoplasme ou la facilitation de la diffusion des lipides trans-bicouche conduisant à la perte d'asymétrie des lipides dans la membrane. Une fois inséré dans le cytoplasme, le peptide pourrait modifier les activités cellulaires normales en se liant à l'ADN, ou par l'inhibition des acides nucléiques et de la synthèse des protéines, par l'inhibition de l'activité enzymatique, par l'activation des enzymes autolytiques, par l'altération de la membrane cytoplasmique ou encore pae l'inhibition de la synthèse de la paroi cellulaire [21].

Néanmoins, la membrane doit être franchi pour permettre la pénétration dans l'intérieur de la cellule et d'atteindre l'objectif final.

... et in vivo?

De nombreuses études ont été réalisées dans des bicouches modèle mimant les bactéries et les membranes des mammifères dans le but de corréler leurs propriétés et l'activité biologique. Cependant il est évident qu'il ya une différence majeure entre les cellules vivantes et des membranes modèles.

In vivo, les peptides antimicrobiens doivent passer à travers la paroi des cellules avant qu'elles entrent en contact avec la membrane cytoplasmique et ce processus est fonction de nombreux facteurs, tels que la structure et l'état oligomérique du peptide et les caractéristiques de la surface microbienne. En particulier, la structure et la composition de la paroi cellulaire bactérienne peut jouer un rôle capital dans l'efficacité globale de l'action peptide antimicrobien et dans le mécanisme de résistance développée par les bactéries.

À cet égard, les définitions en vigueur d '«activité antimicrobienne» et «spécificité» doit prendre en considération les conditions physiologiques *in vivo*. Il s'agit notamment de la concentration de peptide antimicrobien sur le site de l'infection, le rôle des substances synergiques (comme d'autres peptides antimicrobiens ou l'absence de cations divalents), le rôle des substances inhibitrices qui pourraient être présents (comme des concentrations physiologiques de sel et de protéines) et les caractéristiques inhabituelles de bactéries, en particulier ceux dans les biofilms. Il est donc important d'étudier le mécanisme d'action de ces peptides dans leurs environnements appropriés pour atteindre l'objectif final d'un développement réussi de d'agents antimicrobiens plus efficaces et à large spectre .

1.5 RMN DU SOLIDE

RMN des solides comme un outil pour étudier les membranes biologiques

Les techniques classiques de structure telles que diffraction des rayons X et de l'état liquide RMN rencontrons des difficultés expérimentales lorsque les peptides et les protéines étudiés sont associée à la membrane. Par exemple, même si de nouvelles stratégies émergent à cristalliser les protéines membranaires existent [22, 23], d'obtenir des cristaux de bonne taille et bien ordonnée en 3 dimensions est toujours un défi. D'autre part, l'insolubilité en milieu aqueux des protéines membranaires est le problème majeur pour la spectroscopie par RMN du liquide. Les solvants organiques ou détergents sont utilisés pour mimer l'environnement lipidique hydrophobe, cependant la résolution est fortement liée aux taux de tumbling des molécules, provoquant le chevauchement des signaux en spectre des protéines de grande taille ou des complexes protéine-détergent.

La spectroscopie RMN du solide est un outil puissant pour étudier les détails structuraux des peptides et des protéines directement dans le milieu membranaire. Cette technique très polyvalente permet d'accéder à l'échelle atomique des informations sur la conformation, la dynamique, l'orientation, la profondeur d'insertion des protéines membranaires et lipides-protéines. L'opportunité exceptionnelle de la spectroscopie RMN du solide est le fait qui elle est capable de fournir plusieurs informations structurales des protéines et des peptides proches des conditions physiologiques. En outre, avec la même technique aussi la modification structurelle des phospholipides causée par la présence du peptide peut être étudié, permettant d'obtenir une large vue sur les interactions protéine-membrane. Ceci est un avantage majeur par rapport aux autres techniques, car les protéines membranaires nécessitent la présence de l'environnement lipidique de maintenir leur conformation native et leurs fonctions [24].

Par le marquage sélective des acides aminés il est possible d'étudier des éléments spécifiques de la structure, comme les angles ou les distances, du polypeptide ou du complexe peptide-lipide. Afin de réduire la complexité des spectres et d'obtenir la résolution nécessaire, des échantillons alignées sont utilisés. L'alignement peut être obtenue de plusieurs manières, les plus communes sont utilisation des bicelles magnétiquement orientée ou des échantillons mécaniquement orientés. Les propriétés diamagnétiques des lipides sont à la base de l'orientation magnétique de bicelles en présence d'un fort champ magnétique, mais la stabilité et le degré d'orientation réalisable par cette approche dépend essentiellement de la composition de l'échantillon et des conditions expérimentales. La seconde approche tire parti de la propriété d'auto-assemblage des lipides, qui s'organisent en multicouches ordonnée sur des supports solides comme le verre ou le quartz ou même sur la plastique. L'utilisation de multicouches permettent aussi de vérifier la qualité de l'alignement de la membrane par spectroscopie RMN du ^{31}P naturellement présents dans les phospholipides. Le spectre ^{31}P permet d'évaluer comment la phase et l'aliment de la membrane sont modifiées par le peptide ou par d'autres conditions environnementales, telles que l'hydratation, la température, pH, etc De plus, en utilisant les lipides deutérés est également possible vérifier la perturbation que la molécule

hôte provoque sur les chaînes alkyliques en termes de variations des paramètres de ordre.

Le "magic angle hole"

Un problème majeur des techniques de RMN du solide est la faible sensibilité. Pour gagner en rapport signal-bruit, les spectres des noyaux de faible abondance, commele ^{15}N et le ^{13}C, sont enregistrés par les techniques de polarization croisé (CP). Le processus de transfert de magnétisation est entraîné par le couplage dipolaire entre les protons à proximité du noyaux ^{15}N ou ^{13}C, et principalement par le proton directement attaché. La dépendance angulaire du couplage dipolaire est tel qu'il disparaît à l'angle magique. Cela provoque, sous certaines conditions, l'apparition d'une problématique «trou» en correspondance du déplacement chimique isotrope σ_{iso} [25, 26, 27] qui déforment la forme du spectre de poudre et de empêche d'atteindre une qualité de "fit" satisfaisant.

Pour communs solides rigides cet effet n'est généralement pas visibles, car la diffusion de spin agit de manière à homogénéiser l'aimantation. Cependant, il y a un cas particulier dans lequel la particularité de l'angle magique devien évident et c'est quand les spins des intérêts sont soumis à un mouvement uniaxiale. Dans ces conditions, le processus de diffusion de spin est considérablement ralentie et le système se comporte comme une paire de spins isolée avec une aimantation nulle à l'angle magique.

But de la première partie de ce travail de thèse est de développer une méthode qui récupère la forme théorique des spectre de poudre pour d'échantillons soumis à diffusion uniaxiale rapide.

Une étude sur la polarisation croisée serait développés dans Chapter 3 et la méthode complète sera présentée et décrite dans Chapter 4.

Pour mettre en place notre méthode, nous avons utilisé le ferrocène, un composé organométallique constitué de deux anneaux cyclopentadiényle liés sur les côtés opposés d'un atome central Fe. La dynamique du processus de polarisation croisée entre le ^{13}C et son proton directement lié montre les mêmes aspects de la dynamique d'un ^{15}N dans une amide d'un peptide dans les cristaux liquides. En outre, le ferrocene a l'avantage d'une $T_{1\rho}$ assez long pour enregistrer une forme du spectre de poudre non faussée à utiliser comme comparaison. En plus, le ferrocene nécessite un temps de mesure relativement courte (environ 1 heure) pour chaque spectre.

Ce type de systèmes est biologiquement pertinent, car les sites amidiques marquées en ^{15}N dans les peptides hélicoïdaux montrent ce genre de dynamique lorsqu'ils sont reconstituées dans des membranes. Les échantillons biologiques ne sont pas appropriées pour mettre en place une méthodologie en raison de leur faible sensibilité. D'autres problèmes découlent de la déshydratation et la dégradation de l'échantillon, ce qui empêche d'atteindre une stabilité à long terme nécessaires pour les études méthodologiques.

Membranes non orientés et analyse des spectres de poudre

L'alignement mécanique des membranes sur plaques de verre est une méthode conceptuellement simple d'obtenir l'orientation des peptides par rapport à la normale à la membrane, mais il n'est pas si simple à

réaliser du point de vue expérimental. Il peut résulter difficile d'obtenir des bicouches bien alignées en cas d'interactions défavorables de lipides avec le support solide, surtout pour les lipides chargés négativement, ou en cas d'une perturbation de l'alignement provoquée par le peptide ou par la protéine eux-mêmes. Le problème peut être évité récurrents à des échantillons non-orientés dans lesquels il y a une rapide diffusion autour de la normale à la membrane. Cette méthode, comme avantage supplémentaire, permet une préparation des échantillons plus contrôlé, en termes de pH et de la concentration de sel, ouvrant la voie à des mesures même dans des cellules vivantes.

La présence de déviations par rapport à la forme théorique des spectres de poudre complique considérablement l'interprétation des spectres, aggravée par la faible résolution obtenues à partir d'échantillons non-orientés. En présence plurieuses populations de spins avec orientations différentes l'interprétation peut divenir une tâche difficile. En cas de plusieurs marquages présentes dans l'échantillon, la tâche peut devenir encore plus difficile. Pour étendre l'application de cette approche à l'étude des systèmes et des topologies plus complexes, une méthodologie pour enregistrer des spectre de poudre non faussée par distortions doit être développée.

Le deuxième objectif de ce travail de recherche est de développer et appliquer une méthode pour l'analyse des spectres de poudre qui permit une estimation de l'angle d'inclinaison des peptides hélicoïdaux dans les membranes non orientés.

La réalisation de cet objectif est décrit dans Chapter 5.

Application à membranes naturelles et in vivo

Les peptides et les protéines membranaires, jusqu'ici, sont étudiées que dans des systèmes modèles, comme les micelles ou les bi-couches. Rarement dans les extraits lipidiques ou membranes bactériennes isolées [33]. Bactériorhodopsine étudiée dans la membrane pourpre de Halobacterium Salinarium est l'un des rares exemples disponibles [34, 35, 36]. Concernant les peptides antimicrobiens, PGLA et autres peptides ont été étudiés dans les membranes natives [37] et en bactéries vivantes par spectroscopie RMN du phosphore. Ieronimo et al. ont également étudié l'orientation de PGLA par ^{19}F RMN. Toutefois, les effets d'une telle substitution peut modifier la structure, la stabilité ou l'activité biologique [39] des protéines.

Le fait que notre méthode peut être appliquée efficacement pour obtenir des informations topologiques des peptides dans des échantillons non-orientés,, comme on démontré dans Chapter 4, nous permette d'étendre son application à des systèmes plus complexes, comme les membranes naturelles. Ce genre d'études peut ouvrir une nouvelle approche pour prouver le mécanisme d'action des peptides antimicrobiens dans le contexte des systèmes membranaires sophistiqués ou *in vivo*. De ces études, une description plus détaillée de l'action des peptides antimicrobiens peut se développer, avec l'inclusion de nombreuses autres variables qui ne sont pas facilement prises en compte dans les expériences conduites dans des membranes modèles, tels que la complexité de la composition de la membrane ou la présence de glycolipides. De plus, l'utilisation d'échantillons non orientés permet d'obtenir un bon contrôle sur les paramètres environnementaux, tels que la concentration

de pH ou de sels, qui peuvent affecter l'état oligomérique du peptide ou la force de l'interaction électrostatique avec la surface des lipides.

Le troisième objectif de cette thèse est de démontrer l'applicabilité de la méthode RODEO pour les systèmes membranaires complexes, comme une mélange de lipides extraits de une membrane naturelle, et *in vivo*, chez les bactéries *Escherichia coli*.

Avec cet objectif, dans Chapter 6 nous allons appliquer la méthode RODEO pour l'étude structurale du peptide antimicrobien PLAH4 directement dans les membranes naturelles et *in vivo*.

1.6 DES ÉTUDES BIOPHYSIQUES DU LAH4 PEPTIDE ANTIMICROBIEN, EN PRÉSENCE DE TAMPON CITRATE

LAH4 est un peptide amphiphatiques riche en histidines qui possèdent à la fois capacités antibiotiques [40, 41] et de tranfection de l'ADN [42, 43]. En réponse à l'acidification de l'environnement, LAH4 augmente sa charge globale nette de +5 à +9. Il a été montré [40, 44] que lorsque les histidines sont protonés, l'hélice adopte une orientation parallele à la surface de la membrane. En revanche, lorsque l'histidine sont déchargées, le peptide adopte une orientation trans-membranaire avec les résidus lysines agissant comme des ancres à la surface de membrane.

Le mécanisme d'action de ce peptide dans la membrane zwitterioniques et chargé à pH neutre a déjà été étudiée [45, 41, 46], tandis que moins est connu sur le mécanisme de rupture de la membrane dans des conditions acides [40].

Afin de clarifier les différents aspects du mécanisme d'action du peptide, nous avons commencé une caractérisation biophysique de l'interaction peptide-lipide dans des conditions acides. Toutefois, lorsque le tampon de citrate a été ajouté à réguler le pH, des résultats inattendus ont été obtenus.

Le dernier objectif de cette thèse est de décrire l'effet de l'addition du tampon citrate sur le mécanisme d'insertion du peptide LAH4 dans les membranes zwitterioniques.

Les résultats obtenus par différentes techniques biophysiques sont rapportés dans Chapter 7.

Part II

NEW METHODOLOGIES OF SOLID-STATE NMR SPECTROSCOPY

2 INTRODUCTION ON SOLID-STATE NMR SPECTROSCOPY

CONTENT OF THE CHAPTER:

In this chapter we are going to introduce some basic concepts of SS-NMR Spectroscopy. First we briefly review some application of SS-NMR to the study of biological problems. In the following paragraphs we are going to describe some basics ideas of the physics phenomena involved in the acquisition of a NMR measurement and finally we will describe the structural information deducible from a NMR a not-oriented spectra.

2.1 PHYSICAL PRINCIPLES OF NUCLEAR MAGNETIC RESONANCE SPECTROSCOPY

NMR spectroscopies are all based on the interactions between nuclear spin with magnetic and electric fields. Applying an electromagnetic pulse to nuclei in a external strong magnetic filed, B_0, cause the absorption of energy and its consequent release. The frequency of the radiation (in the range of some tenths of MHz) emitted back from the nucleus depends mainly from the interaction between nuclear spin and the magnetic field (Zeeman effect). Also the surrounding of the nucleus play an important role in the fine structure of the spectra, since the nuclei in neighbour atoms posses magnetic and electronic dipole, they can modify the local magnetic and electronic fields. These modifications are described by mean of a so called internal Hamiltonian, H_{int} to distinguish them from the external interactions with the static magnetic field represented by the Zeeman Hamiltonian, H_Z) and the radio frequency pulse represented by the radio frequency Hamiltonian, H_{RF}, characteristic of the specific sequence of pulses used during the experiment. The internal interactions are weaker compared to the external ones, and can usually be treated as an perturbation of the Zeeman Hamiltonian (the shift resulting in the spectra goes from few Hz to several kHz). The sought information on the microscopic structure of spin probe environment are can be extrapolated from the interaction between the spin probe and the surrounding electronic cloud, expressed by the Chemical Shift Hamiltonian, H_{CS}, and by the coupling with the other neighbouring spins, expressed by the Dipolar Hamiltonian, Homonuclear, H_{Dhomo}, or Heteronuclear, $H_{Dhetero}$, depending both the spins are of the same kind or of a different nuclear species. Quadrupolar nuclei, like Deuterium, have an additional way to interact with the surrounding described by the Quadrupolar Hamiltonian, H_Q. To summarize, the main interactions acting on solid-state NMR are described by the Hamiltonian below:

$$H = H_Z + H_{RF} + H_{CS} + H_D + H_Q$$

A more specific description of these terms can be found in several NMR books, i.e. [47].

2.1.1 *The Zeeman interaction*

The principal and strongest interaction of a nucleus in a static magnetic field B_0 is the Zeeman interaction, described by the Zeeman Hamiltonian, H_Z:

$$H_Z = -\overrightarrow{\mu} \cdot \overrightarrow{B_0} \tag{2.1}$$

where $\overrightarrow{\mu}$ is the nuclear magnetic moment operator. Considering its expression in therms of the nuclear spin operator I and choosing a coordinate system in which the static magnetic field is parallel to the z axis, we can rewrite equation (2.1) as:

$$H_Z = -B_{0z} I_z = -\hbar \gamma B_{oz} m$$

where m is the magnetic quantum number. For spin ½, the transition between the two eigenstates occurs at the so called Larmor frequency given by

$$\nu = \frac{\gamma \hbar B_{0z}}{2\pi}$$

All the other spin interactions can be treated as perturbation of the Zeeman Hamiltonian and the transitions between these perturbed states give the observed NMR spectra.

2.1.2 *The chemical shielding Hamiltonian*

The chemical shielding Hamiltonian can be included as a screen effect in the Zeeman Hamiltonian:

$$H = H_Z + H_{CS} = \gamma \hbar (1 - \boldsymbol{\sigma}) \overrightarrow{I} \cdot \overrightarrow{B_0} \tag{2.2}$$

where the shielding tensor, $\boldsymbol{\sigma}$, is a second-rank tensor of the type:

$$\boldsymbol{\sigma} = \begin{pmatrix} \sigma_{xx} & \sigma_{xy} & \sigma_{xz} \\ \sigma_{yx} & \sigma_{yy} & \sigma_{yz} \\ \sigma_{zx} & \sigma_{zy} & \sigma_{zz} \end{pmatrix}$$

The contribution to the frequency of the observed NMR signal from the chemical shielding is given by:

$$\omega_{CS} = \gamma \sigma_{zz} B_0 = -\omega_0 \sigma_{zz}. \tag{2.3}$$

In general the spatial distribution of electrons around the nucleus is not symmetric but, choosing the correct frame, the Principal Axis Frame (PAF) , it is always possible to diagonalize the tensor:

$$\boldsymbol{\sigma}_{\mathbf{PAF}} = \begin{pmatrix} \sigma_{11} & 0 & 0 \\ 0 & \sigma_{22} & 0 \\ 0 & 0 & \sigma_{33} \end{pmatrix}$$

The shielding tensor can be conveniently represented by an ellipsoid fixed within the molecule and centered on the nucleus under examination: the principal axes of the ellipsoid coincide then with the principal axis frame, as sketched in Figure 6.The length of three main axis, *a*,*b*,*c*, are related with the main tensor elements by:

$$a = \frac{1}{\sqrt{\sigma_{11}}}, \quad b = \frac{1}{\sqrt{\sigma_{22}}}, \quad c = \frac{1}{\sqrt{\sigma_{33}}}$$

The shielding effect of the electronic cloud is maximum when the narrowest part of the tensor, the shorter axis of the ellipsoid, *c*, is oriented along the $\overrightarrow{B_0}$ vector , whereas the shield is less effective when the widest part of the electronic cloud, the longest axis, *a*, is co-aligned with the external magnetic field.

Three quantities defined from the principal values are frequently used to describe characterize the shielding tensor. They are the isotropic value, σ_{iso}, the anisotropy, Δ, and the asymmetry, η:

$$\sigma_{iso} = \frac{1}{3}(\sigma_{xx} + \sigma_{yy} + \sigma_{zz}) = \frac{1}{3}(\sigma_{11} + \sigma_{22} + \sigma_{33})$$

[1]

$$\Delta = \sigma_{33} - \sigma_{iso}$$

$$\eta = \frac{\sigma_{11} - \sigma_{22}}{\Delta}$$

The intersection of the ellipsoid with the magnetic field direction $\overrightarrow{B_0}$ cut a vector which length, $\frac{1}{\sqrt{\sigma_{zz}}}$, depends on the molecular orientation. Expressing the molecular orientation in terms of the Euler's angles (Θ,Φ, see Figure 6) we can write the relationship:

$$\sigma_{zz} = \sigma_{11}\sin^2\Theta\cos^2\Phi + \sigma_{22}\sin^2\Theta\sin^2\Phi + \sigma_{33}\cos^2\Theta \tag{2.4}$$

and by the equation (2.3) we obtain the link between the measured frequency ω_{CS} and the principal elements of the tensor.

In case of axial symmetry, as for a prolate tensor with $\sigma_{11} = \sigma_{22} = \sigma_\perp$ and $\sigma_{33} = \sigma_\parallel$, the equation (2.4) can be rewritten as:

$$\sigma_{zz} = \sigma_\perp + (\sigma_\parallel - \sigma_\perp)\cos^2\Theta \tag{2.5}$$

1 Equivalence satisfied thanks to the propriety of invariance of every tensor trace respect to changes of reference system.

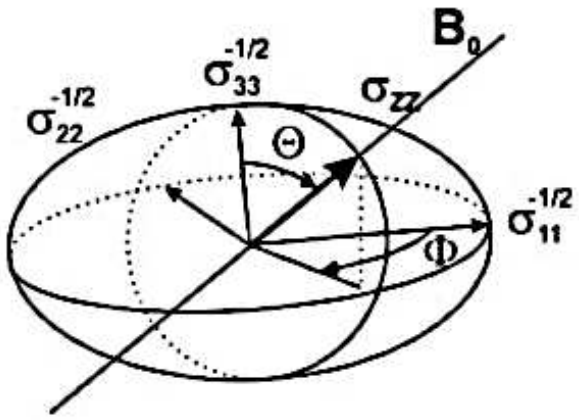

Figure 6: Ellipsoid representing the ^{15}N chemical shift tensor in the molecular frame.

When performing NMR experiments, absolute frequencies are not measured. Instead, a reference compound is used and frequencies are quoted as chemical shifts with respect to that substance:

$$\delta = \frac{\nu - \nu_{ref}}{\nu_{ref}} = \frac{\sigma_{zz}^{lab}(ref) - \sigma_{zz}^{lab}}{1 - \sigma_{zz}^{lab}(ref)} \approx \sigma_{zz}^{lab}(ref) - \sigma_{zz}^{lab}$$

[2]

The isotropic chemical shift, chemical shift anisotropy and asymmetry are defined in an analogous manner to the shielding anisotropy and asymmetry:

$$\delta_{iso} = \frac{1}{3}(\delta_{11} + \delta_{22} + \delta_{33})$$

$$\Delta_{cs} = \delta_{11} - \delta_{iso}$$

$$\eta_{cs} = \frac{\delta_{33} - \delta_{11}}{\Delta_{cs}}$$

where δ_{11}, δ_{22} and δ_{33} are the chemical shift principal values labelled by convention as $\delta_{11} \geqslant \delta_{22} \geqslant \delta_{33}$.

Observed chemical shifts are related to the chemical shift tensor through:

$$\delta = \delta_{iso} + \frac{1}{2}\Delta_{cs}\left(3\cos^2\Theta - 1 + \eta_{cs}\sin^2\Theta\cos 2\Phi\right)$$

2.1.3 *The dipolar coupling*

The dipolar coupling arises from the interaction between two nuclear magnetic moments. If the spins are of two different species (usually

2 Approximation valid if $1 >> \sigma_{zz}^{lab}$.

identified by I for the abundant spin and S for the rare spin) the interaction is said Heteronuclear. We refer to Homonuclear interaction when the two spin involved are of the same specie, as I-I or S-S. The Hamiltonian describing the dipolar coupling, for a pair of spins ½, I and S, has the form:

$$H_{D_{IS}} = -b(3\cos^2\theta - 1)I_z S_z \tag{2.6}$$

$$b = \left(\frac{\mu_0 \hbar}{4\pi}\right) \frac{\gamma_I \gamma_S}{r_{IS}^3} \tag{2.7}$$

where b is the dipolar coupling and describe the magnitude of the interaction between the two spins in terms of the gyromagnetic ratios of the two spins (γ_I,γ_S) and the internuclear distance, r_{IS}. As visible from equation (2.6), the strength of the dipolar interaction dependent on the orientation of the internuclear vector $\overrightarrow{r}_{IS}$ respect to the external magnetic field, individuated by the angle θ.

Within an amide bond the dipolar coupling between ^{15}N and ^{1}H spins can span several tens of kHz resulting in broad lines. In the solid state, the limited motions are not sufficient to average the dipolar coupling and chemical shift interactions. To have a recourse to the combination of decoupling techniques and sample alignment is mandatory to obtain narrow lines similar to those achievable by liquid- NMR. However, the dipolar coupling does not represent only a hindrance: it contains precious orientational information and it can be used to increase the sensitivity of rare, low gyromagnetic radius nuclei by coupling with neighbour protons.

2.2 CROSS POLARIZATION

CP is one of the most important technique in SS-NMR. It consent a drastic improvement in sensitivity by magnetization transfer from abundant spins such as ^{1}H to dilute spins such as ^{13}C or ^{15}N. The transfer occurs via heteronuclear coupling and the overall effect is a gain in signal-to-noise by a factor γ_I/γ_S and with the additional advantage of using shorter recycle times thanks to the faster relaxation of the protons.

The process of CP occurs in a similar way to the heat flow from a hotter to a colder objects in thermal contact. In our case, it is the magnetization that flow from highly polarized nuclei to nuclei with lower polarization though processes of spin flips. For heteronuclear couples, as $^{1}H - ^{15}N$ or $^{1}H - ^{13}C$, these spin-flips are not energy-conserving and the transitions have to be externally driven by the application of a radio-frequency Radio Frequency (RF) field. The dipolar contact is usually established by the HH method [48] that consists in the application of two continuous RF fields B_{1I} and B_{1S} on both spins at their respective resonance frequencies. When irradiated, both the spins rotate independently along an axis with speeds given by the frequency and amplitude of each RF fields. When the nutation frequencies are equal[3] an energy conserving dipolar contact is established between the

3 The nutation frequencies ω_I and ω_S are equal when: $\gamma_I B_{1I} = \omega_I = \omega_S = \gamma_S B_{1S}$. This relationship is known as the HH condition.

two spins and the polarization can be transferred from the I spins to the S spins.

The CP dynamics can be in first approximation be described by the use of a classical thermodynamic model. The I-S half -integer spin system is described by a lattice of huge heat capability and two subsystems, the I and S reservoirs. TheCP experiments take place in three steps (see scheme in Figure 7):

1. creation of a net magnetization of the I spin
2. transfer of polarization between the I and the S spins
3. observation of the Free Free Induction Decay (FID) on the S channel.

The first step is achieved by a $\frac{\pi}{2}$ pulse on the I spin system that allows to lower the temperature of the abundant spin reservoir. The pulse create a net I magnetization along the -y axis in the I rotating frame. In this same rotating frame, the S spin magnetization is zero, i.e. the spin temperature is infinite.

The the thermal contact between the I and S spins is realized by spin-locking the two spin systems for a certain time τ_{CP}. As the system approach the thermal equilibrium, the two spin temperature tend to equalize: the hot, dilute spin system S is cooled via thermal contact with the cold reservoir I. The two spin system are also in contact with the lattice and they lose magnetization by spin-lattice relaxation processes.

In the presence of fast tumbling or in spinning samples, problems in establishing and maintaining the HH matching condition can be encountered. In the past decades, several authors [49, 50, 51, 52, 53] studied the best way to realize this crucial step of CP process both in static and MAS - NMR using amplitude and/or frequency modulated radiofrequecy fields on one or both channels [4].

Finally, the last step of the CP sequence is the acquisition of the FID decay on the rare spin channel while a strong decoupling field is irradiating the proton channel.

2.3 UNIAXIALLY ORIENTED SAMPLES IN MODEL MEMBRANES

The sketch of the principal component for backbone ^{15}N nucleus in a peptide bond is reported in Figure 9. The less shielded direction, σ_{33}[5], lies in the peptide plane approximately 18 degrees away from the N-H bond [29]. The most shielded direction, σ_{11}, runs almost parallel to the C-N bond, while σ_{22} is pointing out of the peptide plane. The nature of the amide ^{15}N chemical shift in peptide backbone is complex: it is sensitive to the conformational changes [54] but also to several other factors (reviewed in [55] and [56]) that can modify the electronic shield, including torsional angles of both the residue of interest and neighbors residues, hydrogen bonding, solvent, etc.

When the ^{15}N labeled residue is part of a well-defined secondary structure, it is possible to extract information about the spatial arrangement of the specific domain from the chemical shift anisotropy. The geometry of a regular helix is such to have σ_{33} just few degrees away

4 More details on this aspect are going to be discussed in the next chapter.

5 In this chapter and in the following, we are going to use the same notation as in [29] indicating with σ_{ii} the components of the chemical shift tensor with the additional convention: $\sigma_{33} \geqslant \sigma_{22} \geqslant \sigma_{11}$.

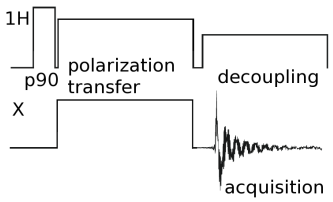

Figure 7: CWCP sequence. The proton channel is sketched on the top and the X-channel (may be ^{13}C or ^{15}N) is represented at the bottom. First a *p90* is applied to rotate the proton magnetization on the plane. The polarization is then transferred to the rare nuclei and finally the signal is acquired on the X-channel while decoupling the protons.

from the axis of the helix [29]. This fact has important consequence for the study of membrane active peptides in oriented membranes.

It is well known that membranes are dynamic objects, and several kind of motions are present involving not only the lipids but also the protein components embedded in the membrane. In particular, small polypeptides are subject to rotational diffusion around the normal of the liquid crystalline membrane, as sketched in Figure 10. When this kind of motion is fast enough (on the order of $\mu s - ms$) it causes the average of the chemical shift anisotropy and the otherwise anisotropic ^{15}N tensor can be approximated with a prolate tensor as in Figure 11 and we can use the equation (2.5). The following relations permit to connect the new averaged tensor components ($\sigma_{\parallel}$, $\sigma_{\perp}$) with the principal components of the static tensor ($\sigma_{11}, \sigma_{22}, \sigma_{33}$) by the Euler's rotation angles (α, β) (see Figure 8) as derived by Bechinger and Sizun in [29]:

$$\sigma_{\parallel} = \sigma_{11}\cos^2\alpha\sin^2\beta + \sigma_{22}\sin^2\alpha\sin^2\beta + \sigma_{33}\cos^2\beta \tag{2.8}$$

$$\sigma_{\perp} = \frac{\sigma_{11}(1-\cos^2\alpha\sin^2\beta) + \sigma_{22}(1-\sin^2\alpha\sin^2\beta) + \sigma_{33}\sin^2\beta)}{2} \tag{2.9}$$

$$\Delta\sigma = \frac{3\cos^2\beta - 1}{2}\left[\sigma_{33} - \frac{\sigma_{11}+\sigma_{22}}{2}\right] + (\sigma_{11}-\sigma_{22})\frac{3\cos 2\alpha\sin^2\beta}{4}$$

Let's discuss the two extremes possible configurations of an α-helical peptide inserted in a membrane, as sketched in Figure 65.

When the helix is inserted perfectly parallel to the membrane normal, like in Figure 12a, we have $\beta = 0$. The axis of motional averaging, the membrane normal $\hat{n}$, is then coincident with the main principal axis of the chemical shift static tensor σ_{33} (within the approximation that σ_{33} is parallel to the helix axis). Finally, the averaged chemical shift tensor

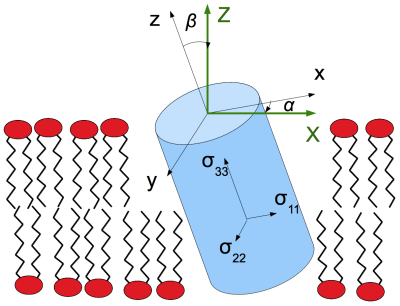

Figure 8: Relations between the molecular frame x,y,z in which the CS tensor has components σ_{11}, σ_{22}, σ_{33}, and the X,Y,Z frame, where the Z axis correspond to the membrane normal. The diffusion occurs around this axis and the resulting component of the motional-averaged CSA tensor depend on the Euler's angle α and β. In particular β correspond to the angle between the σ_{33} component (and in fist approximation, the helix axis) and the membrane normal, while α is the phase between the tensor component σ_{11} in the perpendicular plane and the X axis.

parallel to the motional averaging axis, $\sigma_{\parallel}$, is then coincident with σ_{33} and we have:

$$\beta = 0 \Longrightarrow \begin{cases} \sigma_{\parallel} = \sigma_{33} \\ \sigma_{\perp} = \frac{\sigma_{11}+\sigma_{22}}{2} \\ \Delta\sigma = \sigma_{33} - \frac{\sigma_{11}+\sigma_{22}}{2} \end{cases} \tag{2.10}$$

If the helix is instead sitting on the top of the bilayer, i.e. $\beta = \pi/2$ as in Figure 12b, then the motional averaging occurs around an axis that is perpendicular to σ_{33}, we have:

$$\beta = \pi/2 \Longrightarrow \begin{cases} \sigma_{\parallel} = \sigma_{11}\cos^2\alpha + \sigma_{22}\sin^2\alpha \\ \sigma_{\perp} = \frac{\sigma_{11}(1-\cos^2\alpha)+\sigma_{22}(1-\sin^2\alpha)+\sigma_{33}}{2} \\ \Delta\sigma = \sigma_{11}(\frac{1+3\cos 2\alpha}{4}) + \sigma_{22}(\frac{1-3\cos 2\alpha}{4}) - \frac{\sigma_{33}}{2} \end{cases} \tag{2.11}$$

In general, the measured chemical shift, σ_{zz}, depends then on the angle Θ between the membrane normal and the B_0 direction (cf. equation (2.4)). If glass supported multilayers are used, it is possible to achieve a uniform orientation of the phospholipids respect to the external magnetic field. Considering the most used configuration, with the membrane normal parallel to the static magnetic field direction, $\sigma_{\parallel}$ and the measurable σ_{zz} are coincident. We can re-write equation (5.1) as:

$$\begin{aligned} \sigma_{zz} = \sigma_{\parallel} \quad &= (\sigma_{33} - \left[\cos^2\alpha(\sigma_{11} - \sigma_{22}) + \sigma_{22}\right])\cos^2\beta + \\ &+ \left[\cos^2\alpha(\sigma_{11} - \sigma_{22}) + \sigma_{22}\right] \end{aligned}$$

In this last formula, the contain of the square brackets is a function of the pitch angle α and can assume only values in the narrow range between σ_{11} and σ_{22}. Considering $\sigma_{\perp} = \cos^2\alpha(\sigma_{11} - \sigma_{22})$ the averaged value between σ_{11} and σ_{22}, approximation justified because of the small difference between the two values and even more valid in

presence of rotational diffusion of the peptide around its axis, then the measured ^{15}N chemical shift is a direct indication of the tilt angle β:

$$\sigma_{zz} = (\sigma_{33} - \frac{\sigma_{11} + \sigma_{22}}{2})\cos^2\beta + \frac{\sigma_{11} + \sigma_{22}}{2}$$

The position of the single sharp line appearing in spectra of oriented samples is by consequence a direct indication of the tilt angle of the helix respect to the lipid bilayer: around 200 ppm for a transmembrane peptide with its main axis parallel to the membrane normal and in the range 65-85 ppm for peptides oriented parallel to the surface of the bilayer.

2.4 POWDER PATTERN LINE-SHAPES

The anisotropy of the SS-NMR spectroscopy became clearly visible in a spectrum of a static powder sample in which all the possible orientations are present. In this case, each single molecule, with its specific orientation, will give a contribution to the chemical shift Hamiltonian (cf. equation (2.2)) of the type described in equation (2.4). The NMR spectra of these kind of samples result from the overlap of all the individual lines from each single orientation. The resultant intensity at any given frequency is proportional to the number of molecular orientations which have that particular chemical shift. The line-shape of such a randomly distributed sample is know as "powder pattern" and it is illustrated in Figure 13 *A* for a general asymmetric tensor of a ^{15}N amide labeled peptide. The discontinuities in the line-shape give the three principal components of the chemical shift tensor: σ_{11} and σ_{22} gave main tensor elements have values in the range of 65 and 85 ppm respectively, while the third component, σ_{33}, is characterized by a much different value that appear beyond 200 ppm.

The powder patter line-shape is sensible to molecular exchange process as motional averaging [31]. For an unoriented sample, the motional axis is generally not parallel to B_0, instead all the possible orientation of the membrane has to be taken in account. The weighing over all the possible angles (α, β) with equal probability results in an averaged powder pattern line-shape whose edge and shoulder are directly related to the $\sigma_{\parallel}$ and $\sigma_{\perp}$ of the motinally averaged chemical shift tensor.

When the motional averaging occurs along the membrane normal, the powder pattern line-shape can be use to derive an estimation of the tilt angle of the peptide helix. In this case, a symmetric tensor can be used, with $\sigma_{\parallel}$ parallel to the axis of motion, i.e. parallel to the normal of the membrane, and the two identical components $\sigma_{\perp}$ on the orthogonal plane, as explained in Section 2.3. The spectra of a simulated proton-decoupled ^{15}N chemical shift powder pattern in presence of motional averaging around σ_{33} and around σ_{11} is reported in Figure 13 *B* and *C* respectively.

In conclusion, provided a reasonable estimation of the three chemical principal components of the static tensor is available, it is possible to derive an estimation of the tilt (β) and pitch angle (α) from the positions of the discontinuity and shoulder of the motionally averaged powder pattern spectra.

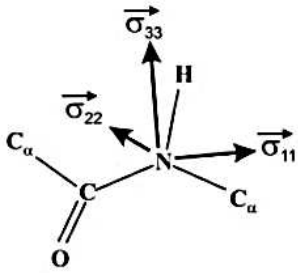

Figure 9: ^{15}N chemical shift tensor in a peptide bond.

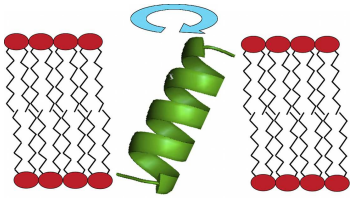

Figure 10: Alpha-helix peptide inserted in a phospholipidic bilayer subject to rotational diffusion around the membrane normal.

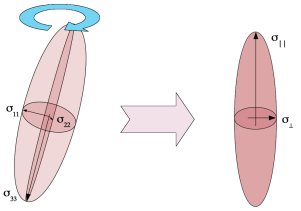

Figure 11: Effect of rotational diffusion on the chemical shielding tensor. After the averaging around the membrane normal the tensor became axially symmetric, with only two principal components: $\sigma_{\parallel}$ and $\sigma_{\perp}$.

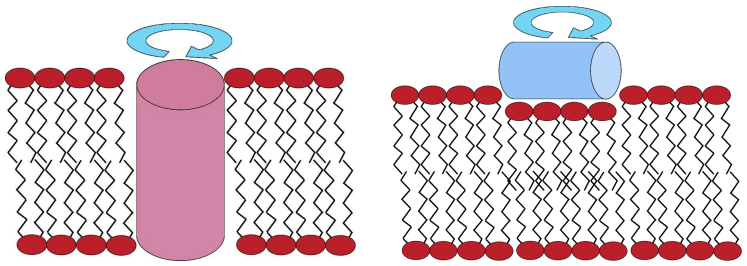

(a) Transmembrane alpha-helical peptide. (b) In-plane alpha-helical peptide.

Figure 12: Example of possible configurations for membrane-associated peptides.

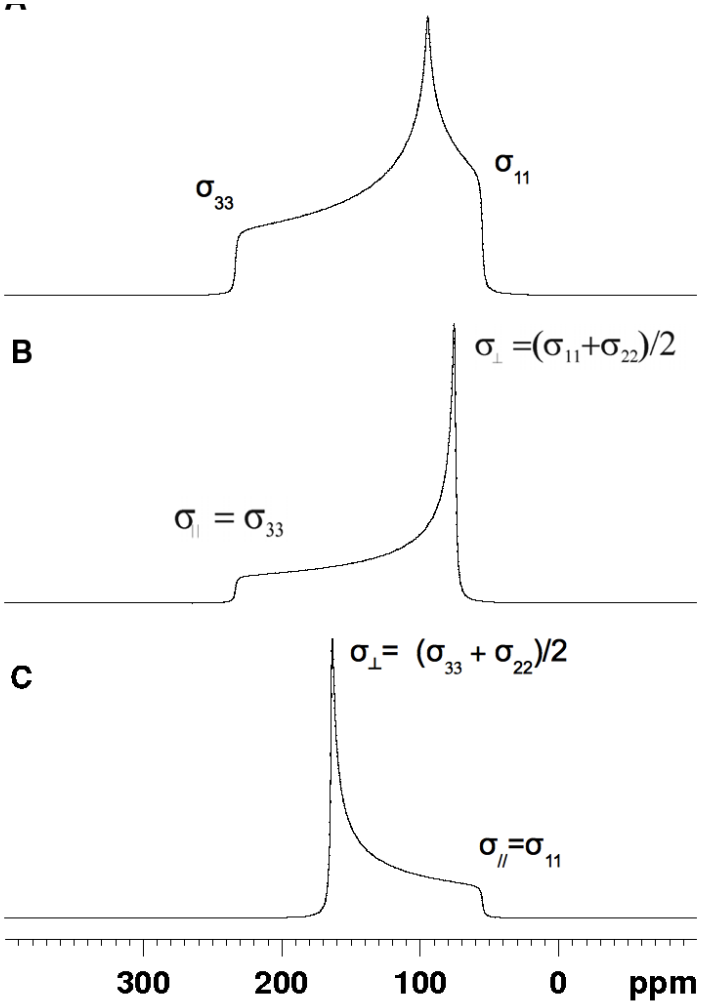

Figure 13: Simulated proton-decoupled ^{15}N chemical shift powder patter in absence of motional averaging (A), in case of motional averaging around the σ_{33} (B) and σ_{11} (C) main tensor element.

3

CROSS POLARIZATION STUDIES OF A MODEL COMPOUND WITH UNIAXIAL MOTION

CONTENTS OF THE CHAPTER:

In this chapter we are going to illustrate some peculiar features of cross-polarization of molecules with fast uniaxial motion. In particular we will present some results of SS-NMR static experiments conducted on ferrocene applying different contact pulse conditions, such as contact time and shape of the pulse.

3.1 INTRODUCTION

SS-NMR is a powerful tool to investigate structural details of peptides and proteins directly in the membrane. In particular, from powder pattern line-shape analysis it is possible to obtain the orientation of a ^{15}N-labeled molecule subject to fast uniaxial motion [29, 30, 25, 32]. However the powder spectra of these systems presents a deformation at the isotropic chemical shift, the so-called Magic Angle Hole MAH , [32] that causes significant deviations between experimental and simulated spectra line-shapes. A similar behavior was observed by Müller et al. for ferrocene [57].

In the same article, Müller, Kumar, Baumann, and Ernst derived a model (MKBE)[1] to describe CP dynamics by the introduction of two phenomenological spin diffusion time constants. In a continuous-wave cross-polarization CWCP experiment, described within this model, a quasi-equilibrium state must be reached to obtain undistorted powder spectra, otherwise the effects of dipolar oscillations superimpose, leading to a modulation of the line-shape [58, 59, 60]. Since the uniformity of the signal enhancement is based on spin diffusion, there is a chance to obtain undistorted line-shape if the contact time is long enough, i.e. much longer longer then the spin diffusion time constants. For solids like ferrocene, CP intervals in the order of some milliseconds allow the spin diffusion to transfer magnetization to the spins that are not polarized by the directly bounded protons, often leading to undistorted powder pattern line-shapes.

On the other end, the efficiency of CWCP degrades with mismatch of the HH condition, RF -field inhomogeneity and resonance offset. The set-up of the HH condition directly on a biological sample is usually not feasible because of sensitivity problems. Another reference compound is generally used to optimize the cross-polarization and this procedure may lead to severe HH condition mismatch. To overcome these problems, several techniques have been developed, such as Mismatch-Optimized IS Transfer (MOIST) [61], Variable-Amplitude Cross Polarization (VACP) [49], ramped-amplitude CP [62], APHH-CP and frequency modulated CP [63], whose efficiency is less dependent from the mismatch of the HH condition.

In the APHH-CP experiment the amplitude of one or both the RF fields is varied continuously from far below to far above the HH condition. If

1 We refer the reader to the next chapter for a more detailed description of this model.

the field variation is made slowly enough, the density operator can follow (and commute) with the Hamiltonian and a complete polarization transfer occurs. In cases where the nucleus from which the polarization originates is not part of a strongly coupled network, contact pulses which have RF amplitudes varying tangentially with time, perform much better than rectangular or ramped pulses [47].

In our study we investigated two strategies of removing MAH and additional transient oscillation distortions from CP spectra of ferrocene powder. In particular, we are going to explore the line-shape behaviour of CP experiments performed applying different shaped contact pulses and over several scales of contact times.

3.2 MATERIALS AND METHOD

All the experiments were conducted on ferrocene powder, purchased from Fluka Chemie and used without any further purification.

Solid-state nuclear magnetic resonance experiments were performed at room temperature on an AVANCE 500 MHz wide bore spectrometer (Bruker, Wissembourg, France) operating at frequencies of 500.13 MHz for ^{1}H and of 125.73 MHz for ^{13}C. The spectrometer was equipped with a triple resonance MAS probe (operating in double mode) designed for 3.2 mm zirconia rotors. All the experiments were performed in static conditions.

In the CWCP experiments, the proton and carbon radiofrequency fields were calibrated directly on the ferrocene sample using a two-dimensional nutation experiment [64] and adjusted to fulfill the Hartmann-Hahn condition: $\frac{\omega_{1I}}{2\pi} = \frac{\omega_{1S}}{2\pi}$ =47.2 kHz.

For the shaped-pulse experiments, the proton RF field was set constant to 47.2 kHz while the carbon field was ramped during the contact time accordingly to the curves sketched out in Table 1, Table 2, Table 3, Table 4, Table 5, Table 6, and Table 7 (Figure 14a and Figure 14b). All the curves, except ramp (Table 9), triangular and rectangular profiles (Table 8), are built by the tangent amplitude modulation designed by Baldus *et al*. [65] changing the phase α from 45 to 89.9 degrees and are named accordingly to this parameter. [2]

The profiles are banded together in two sets, set*A*, with the carbon RF field increasing from 0 to 94.4 kHz and set*B*, whose ^{13}C fields span amplitudes limited within 31.7 to 56.6 kHz. For the set*A*, the modulation has the same magnitude as the mean amplitude, i.e. the ^{13}C field at the HH condition, while for the set*B* the amplitude varies only 20% around the HH condition.

Except for the triangular curve, all the others are symmetric in time and amplitude with respect to the mid point, which means that HH condition is always crossed at half of the contact time and with an amplitude equal to the mean amplitude.

CP experiments were performed not only with different contact pulse shapes but also length and several contact times were investigated, from 50 µs up to 10 ms.

Proton decoupling during acquisition was performed using the pulse sequence SPINAL-64 [66]. Recycle time applied was 40 s and 192 scans

2 Acting on the phase α implies a modification of the initial and final slope of the profile and but also on the angle at which the HH condition is crossed. The closer the phase get to 90 degrees, the more adiabatic the passage though the HH condition.

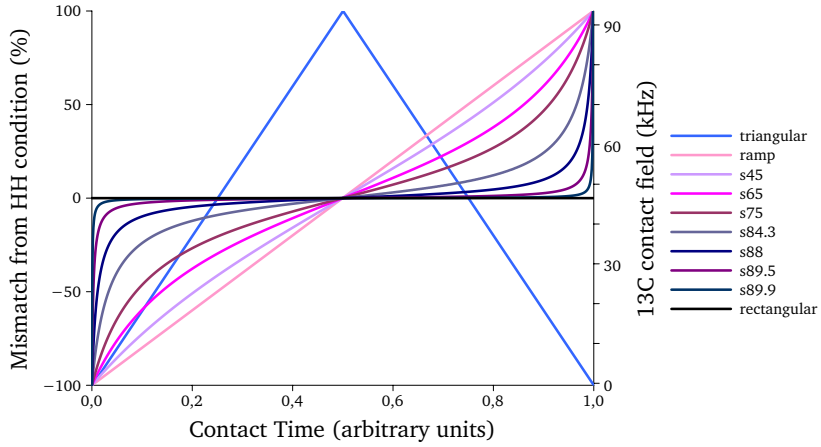

(a) Set A of shaped-pulses applied on ^{13}C channel. The modulation of the field intensity grows from zero up to twice the value of the ^{13}C field at the HH condition.

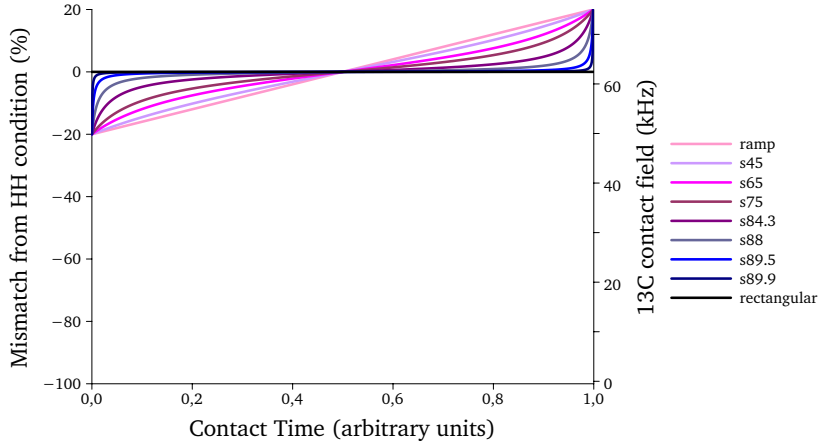

(b) Set B of shaped-pulses applied on ^{13}C channel. The modulation of the field intensity is restricted within $\pm 20\%$ the value of the ^{13}C field at the HH condition.

Figure 14: Comparison of the ^{13}C shaped-pulses used in the experiments.

were recorded. A left shift of 24 points and a Lorentzian broadening of 100 Hz were applied prior to Fourier transform.

The spectra were analysed and fitted by using the commercial software Topspin 2.01 (Bruker Biospin, Rheinstetten, Germany).

3.3 RESULTS

3.3.1 *CWCP experiments*

In order to investigate the efficiency of the processes of spin diffusion alone in recovering the loss of magnetization at the magic angle (MAH in Figure 15), we performed several CWCP experiments with a *rectangular* pulse (Table 8), varying the contact time. The results are reported in Figure 15 for contact times of 50 µs, 150 µs, 350 µs, 1 ms, 3 ms and 10 ms. As we can see from the t_{cp}-evolution of the line-shapes and the confront with the simulated spectra, a contact time of the order of 3 ms has to be used in order to refill the MAH in a CWCP experiment. For short contact times ($t_{cp} \leqslant 1$ ms) the presence of the MAH deviates the

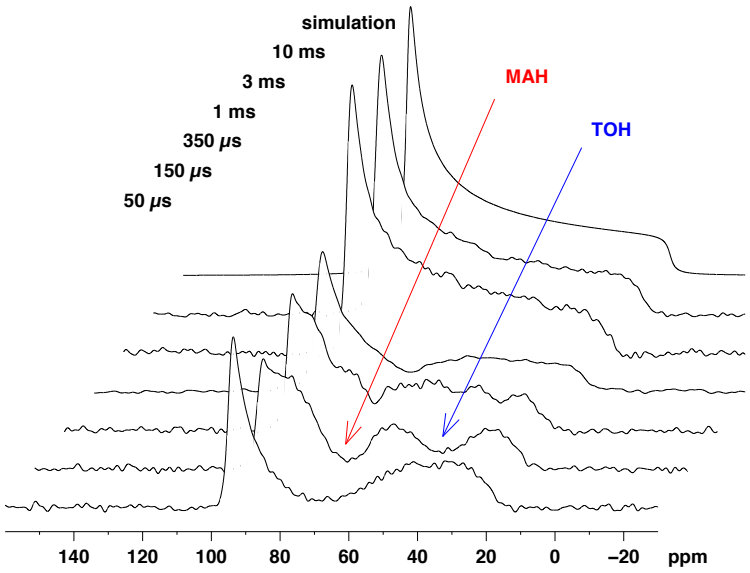

Figure 15: Static $^{1}H-^{13}C$ CWCP experiment on Ferrocene with various contact times and comparison with the simulated spectrum. MAH and TOH are clearly visible in the spectrum recorded with $t_{cp} = 150$ μs. Spectra recorded applying the *rectangular* pulse (Table 8).

spectra from a pure powder spectrum. Moreover, the presence of TOH is reveled at intermediate contact times (150 -350 μs).

3.3.2 *APHH-CP experiments*

Several different contact pulses were tested to evaluate the effect of pulse profile and HH mismatch on the process of magnetization transfer. The shaped pulses were applied on the carbon channel and are sketched in Table 1, Table 2, Table 3, Table 4, Table 5, Table 6, Table 7 Figure 14a, Figure 14b, Table 9, and Table 8. Each experiment was repeated at various contact times: 50 μs, 150 μs, 350 μs, 1 ms and 3 ms.

CONTACT TIMES = 50 μs The spectra reported in Figure 16 and Figure 17 refer to APHH-CP experiments performed with different shaped pulses (from setA and setB respectively) and with a contact time of 50 μs. For such a short contact time, none of the used shaped-pulses is able to refill the MAH, as can be observed from the comparison with the *rectangular* CWCP performed with a very long contact time (10 ms). Shaped-pulses with smaller mismatch (setB, Figure 17) have all a behaviour similar to the *rectangular* CWCP (Figure 17) both in terms of line-shape and overall intensity. Instead, the shaped-pulses of setA Figure 16 exhibit an increase of the signal intensity with the phase α: the more the shaped pulse resembles the rectangular pulse, the more is the overall intensity.

CONTACT TIMES = 150 μs In Figure 16 and Figure 17 are shown the spectra of APHH-CP experiments performed with a contact time of 150 μs and the same shaped pulses previously tested. The shaped pulses of setA (Figure 16) give again an overall intensity dependency

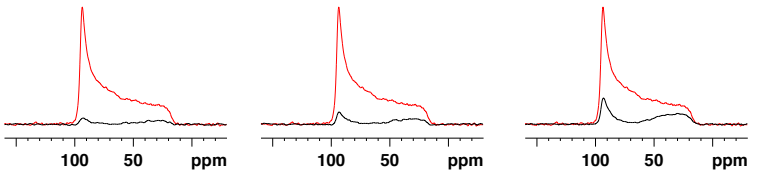

(a) *ramp* shaped-pulse, setA (cf. Table 9). (b) *s45* shaped-pulse, setA (cf. Table 1). (c) *s65* shaped-pulse, setA (cf. Table 2).

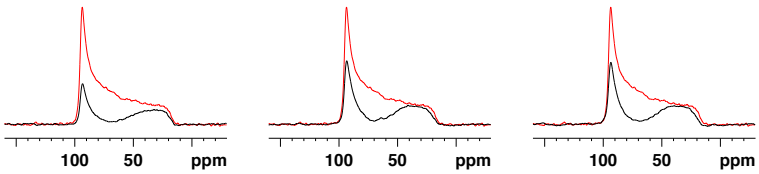

(d) *s75* shaped-pulse, setA (cf. Table 3). (e) *s84.3* shaped-pulse, setA (cf. Table 4). (f) *s88* shaped-pulse, setA (cf. Table 5).

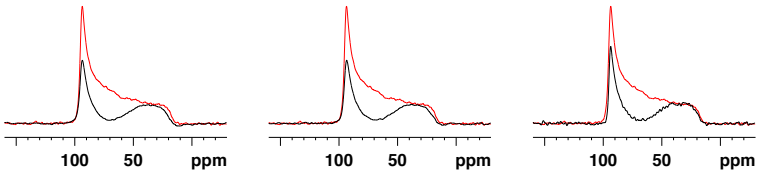

(g) *s89.5* shaped-pulse, setA (cf. Table 6). (h) *s89.9* shaped-pulse, setA (cf. Table 7). (i) *rectangular* (cf. Table 8).

Figure 16: APHH-CP, t_{cp} = 50 µs, SHAPE VARIATION ON SETA. In black, static $^{1}H-^{13}C$ cross-polarization experiments on ferrocene performed with t_{cp} =50 µs and each of the shaped-pulses of setA (Figure 14a). In red, confront with the CWCP experiment performed with t_{cp} =10 ms and the *rectangular* pulse shape (Table 8).

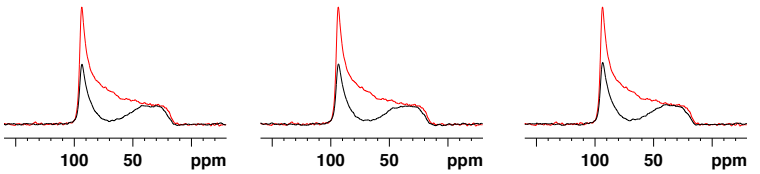

(a) *ramp* shaped-pulse, setB (cf. Table 9). (b) *s45* shaped-pulse, setB (cf. Table 1). (c) *s65* shaped-pulse, setB (cf. Table 2).

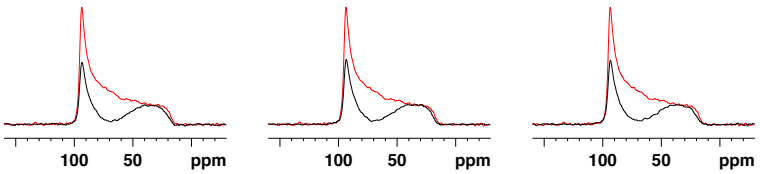

(d) *s75* shaped-pulse, setA (cf. Table 3). (e) *s84.3* shaped-pulse, setB (cf. Table 4). (f) *s88* shaped-pulse, setB (cf. Table 5).

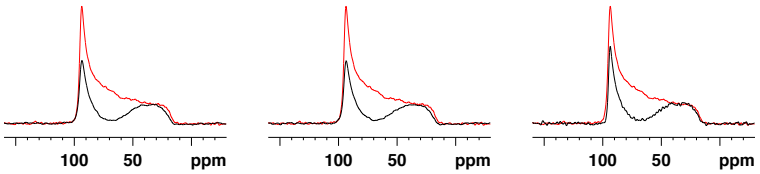

(g) *s89.5* shaped-pulse, setB (cf. Table 6). (h) *s89.9* shaped-pulse, setB (cf. Table 7). (i) *rectangular* (cf. Table 8).

Figure 17: APHH-CP, t_{cp} = 50 µs, SHAPE VARIATION ON SETB. In black, static $^{1}H-^{13}C$ cross-polarization experiments on ferrocene performed with t_{cp} =50 µs and each of the shaped-pulses of setB (Figure 14b). In red, confront with the CWCP experiment performed with t_{cp} =10 ms and the *rectangular* pulse shape (Table 8).

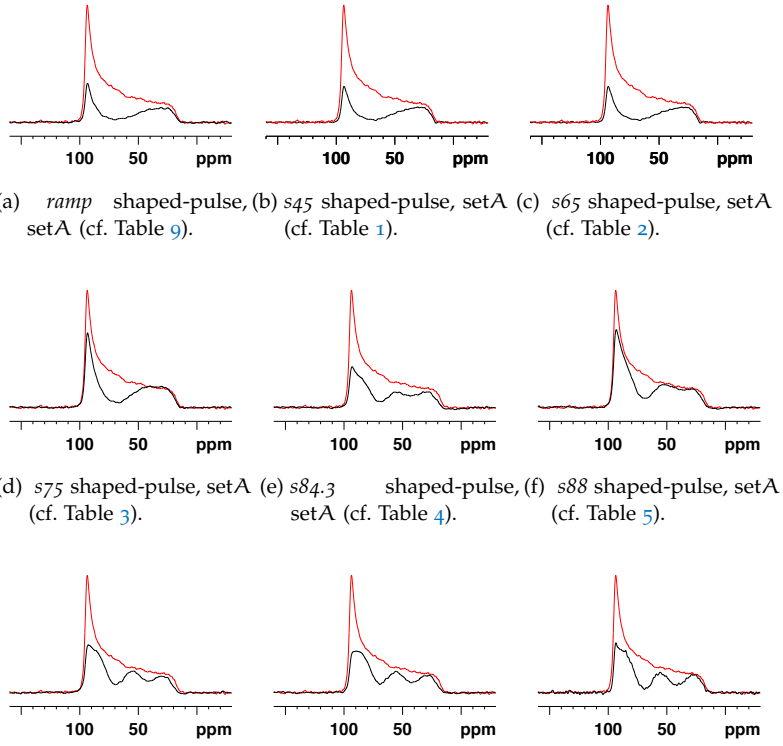

(a) *ramp* shaped-pulse, setA (cf. Table 9). (b) *s45* shaped-pulse, setA (cf. Table 1). (c) *s65* shaped-pulse, setA (cf. Table 2).

(d) *s75* shaped-pulse, setA (cf. Table 3). (e) *s84.3* shaped-pulse, setA (cf. Table 4). (f) *s88* shaped-pulse, setA (cf. Table 5).

(g) *s89.5* shaped-pulse, setA (cf. Table 6). (h) *s89.9* shaped-pulse, setA (cf. Table 7). (i) *rectangular* (cf. Table 8).

Figure 18: APHH-CP, $t_{cp} = 150$ µs, SHAPE VARIATION ON SETA. In black, static $^{1}H-^{13}C$ cross-polarization experiments on ferrocene performed with t_{cp} =150 µs and each of the shaped-pulses of setA (Figure 14a). In red, confront with the CWCP experiment performed with t_{cp} =10 ms and the *rectangular* pulse shape (Table 8).

on the parameter α. The spectra line shapes resembles the spectrum obtained with *ramp* pulse (Table 9) for the first three tested shaped pulses (Figure 18b, Figure 18c and Figure 18d) while starting with the pulse shape *s84.3* a transient hole is clearly appearing around 40 ppm. The behavior of the APHH-CP spectra obtained with the pulse shapes of setB is very similar with respect to the precedent set of shaped pulses. The only difference is an increase of the overall intensity of the first three spectra.

CONTACT TIMES = 350 µs The spectra reported in Figure 20 and Figure 21 refer to APHH-CP experiments performed with different shaped pulses (from setA and setB respectively) and with a contact time of 350 µs. In the spectra obtained with the pulse shapes of setA, there is a general increase in the overall intensity and, additionally, the right shoulder appears sharper. By consequence, the spectra obtained with *ramp*-like pulse shapes (Figure 20a, Figure 20b, Figure 20c, and Figure 20d) show an apparently deeper MAH, because the intensity improvement does not affect the isotropic chemical shift neighbourhood. The spectra obtained with *rectangular*-like pulse shapes (Figure 20e, Figure 20f, Figure 20g, Figure 20h, and Figure 20i), are still characterized by distorted line shapes at the isotropic chemical shift, with additional distortions due to the presence of the TOH.

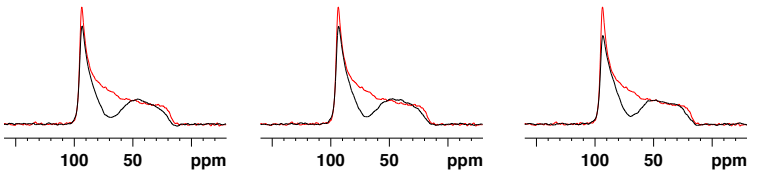

(a) *ramp* shaped-pulse, setB (cf. Table 9). (b) *s45* shaped-pulse, setB (cf. Table 1). (c) *s65* shaped-pulse, setB (cf. Table 2).

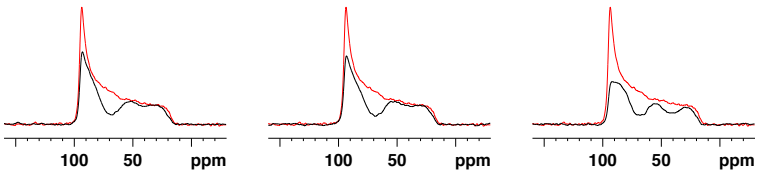

(d) *s75* shaped-pulse, setA (cf. Table 3). (e) *s84.3* shaped-pulse, setB (cf. Table 4). (f) *s88* shaped-pulse, setB (cf. Table 5).

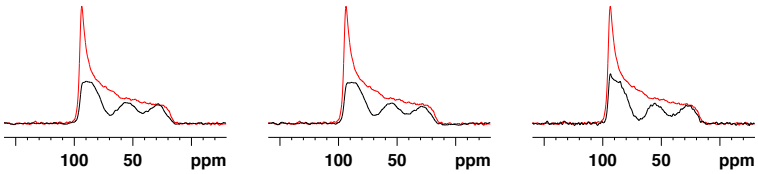

(g) *s89.5* shaped-pulse, setB (cf. Table 6). (h) *s89.9* shaped-pulse, setB (cf. Table 7). (i) *rectangular* (cf. Table 8).

Figure 19: APHH-CP, $t_{cp} = 150$ µs, SHAPE VARIATION ON SETB. In black, static $^{1}H-^{13}C$ cross-polarization experiments on ferrocene performed with t_{cp} =150 µs and each of the shaped-pulses of setA (Figure 14b). In red, confront with the CWCP experiment performed with t_{cp} =10 ms and the *rectangular* pulse shape (Table 8).

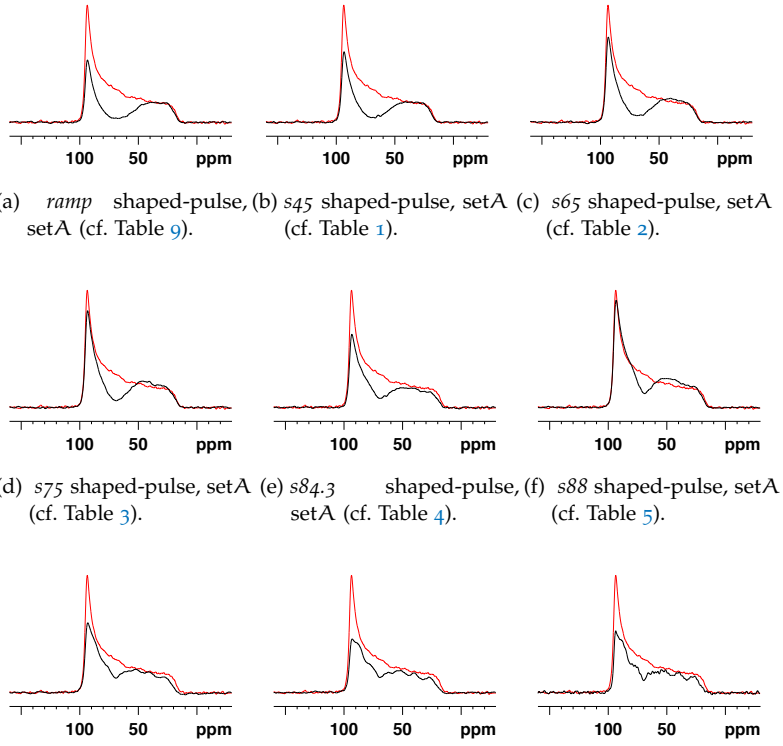

(a) *ramp* shaped-pulse, setA (cf. Table 9). (b) *s45* shaped-pulse, setA (cf. Table 1). (c) *s65* shaped-pulse, setA (cf. Table 2).

(d) *s75* shaped-pulse, setA (cf. Table 3). (e) *s84.3* shaped-pulse, setA (cf. Table 4). (f) *s88* shaped-pulse, setA (cf. Table 5).

(g) *s89.5* shaped-pulse, setA (cf. Table 6). (h) *s89.9* shaped-pulse, setA (cf. Table 7). (i) *rectangular* (cf. Table 8).

Figure 20: APHH-CP, t_{cp} = 350 µs, SHAPE VARIATION ON SETA. In black, static $^{1}H-^{13}C$ cross-polarization experiments on ferrocene performed with t_{cp} =350 µs and each of the shaped-pulses of setA (Figure 14a). In red, confront with the CWCP experiment performed with t_{cp} =10 ms and the *rectangular* pulse shape (Table 8).

The behaviour of the CP spectra obtained with the pulse shapes of setB is again very similar with respect to the pulse shapes of setA and only an increase of the overall intensity of the first three spectra can be noticed. The best compromise for limiting line-shape distortions and increasing the sensitivity, are the shape pulses *s84.3* of setB and *s88* of setA, that consent to to reach up to 30% more signal intensity eliminating the TOHs distortions.

CONTACT TIMES = 1 MS In Figure 22 and Figure 23 are shown the spectra of APHH-CP experiments performed with a contact time of 1 ms and the same shaped pulses previously tested.

At this contact time none of the excitation schemes tested was able to refill the MAH although some improvement can be observed with respect to shorter t_{cp}. Specifically, the overall intensity and the signal at the isotropic chemical shift increase if a *rectangular*-like pulse shape (Figure 23e, Figure 23f, and Figure 23g) is used. For these pulses, also the TOH is partially refilled. The APHH-CP spectra obtained with the pulse shapes of setB are all very similar, both in terms of intensity and line shape, until the pulse profile does not resemble the *rectangular* pulse shape to closely (i.e. for $\alpha \leqslant 84.3$). The pulse shapes *s89.9* and the *s84.3* are those that give the maximum signal for the setA and setB, respectively, and the gain with respect to the *rectangular* CWCP is about

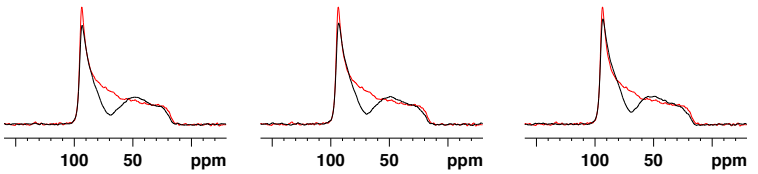

(a) *ramp* shaped-pulse, setB (cf. Table 9). (b) *s45* shaped-pulse, setB (cf. Table 1). (c) *s65* shaped-pulse, setB (cf. Table 2).

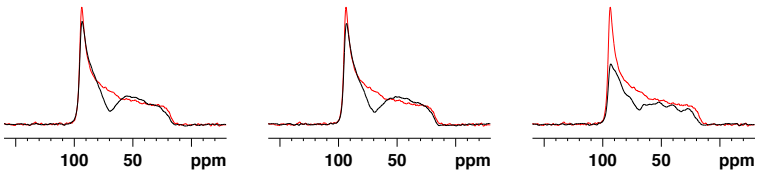

(d) *s75* shaped-pulse, setA (cf. Table 3). (e) *s84.3* shaped-pulse, setB (cf. Table 4). (f) *s88* shaped-pulse, setB (cf. Table 5).

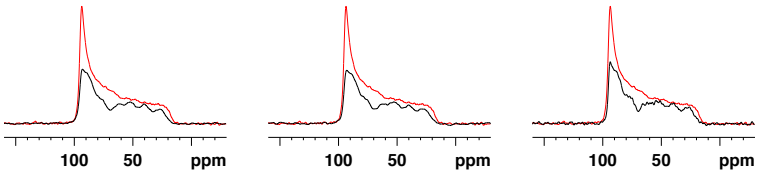

(g) *s89.5* shaped-pulse, setB (cf. Table 6). (h) *s89.9* shaped-pulse, setB (cf. Table 7). (i) *rectangular* (cf. Table 8).

Figure 21: APHH-CP, $t_{cp} = 350$ µs, SHAPE VARIATION ON SETB. In black, static $^{1}H-^{13}C$ cross-polarization experiments on ferrocene performed with t_{cp} =350 µs and each of the shaped-pulses of setB (Figure 14b). In red, confront with the CWCP experiment performed with t_{cp} =10 ms and the *rectangular* pulse shape (Table 8).

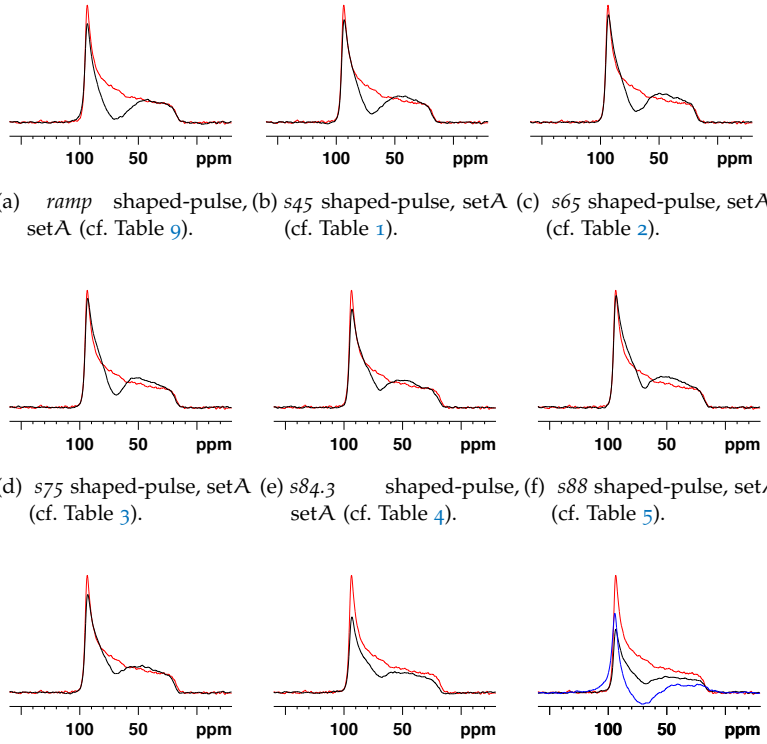

(a) *ramp* shaped-pulse, setA (cf. Table 9). (b) *s45* shaped-pulse, setA (cf. Table 1). (c) *s65* shaped-pulse, setA (cf. Table 2).

(d) *s75* shaped-pulse, setA (cf. Table 3). (e) *s84.3* shaped-pulse, setA (cf. Table 4). (f) *s88* shaped-pulse, setA (cf. Table 5).

(g) *s89.5* shaped-pulse, setA (cf. Table 6). (h) *s89.9* shaped-pulse, setA (cf. Table 7). (i) *rectangular* and *triangular* (cf. Table 8).

Figure 22: APHH-CP, t_{cp} = 1 ms, SHAPE VARIATION ON SETA. In black, static $^{1}H-^{13}C$ cross-polarization experiments on ferrocene performed with t_{cp} =1 ms and each of the shaped-pulses of setA (Figure 14a). In red, confront with the CWCP experiment performed with t_{cp} =10 ms and the *rectangular* pulse shape (Table 8).

60% in both cases. Finally, the use of the triangular excitation profile dramatically distorts the spectrum, as shown in blue in Figure 23i.

CONTACT TIMES = 3 MS The spectra reported in Figure 24 and Figure 25 refer to APHH-CP experiments performed with different shaped pulses (from setA and setB respectively) and with a contact time of 3 ms.

For the *rectangular* CWCP experiment (Figure 25i), a contact time of 3 ms is long enough to homogenize the magnetization and to recover the theoretical shape (Figure 15). The comparison with the spectrum obtained with a longer contact time shows that there is a small decrease in signal intensity with respect to t_{cp} =10 ms. This effect is probably due to relaxation processes.

Applying shaped pulses similar to the *ramp* causes the reappearing of the MAH (Figure 24b, Figure 24c, and Figure 24d). Only when the shaped pulses are approaching the *rectangular* pulse shape, the spectral line-shape is restored, with a limited gain in signal intensity with respect to *rectangular* CWCP. The impact on the line-shape is minor if the amplitude modulation is limited within 80-120% of the HH matching power (setB).

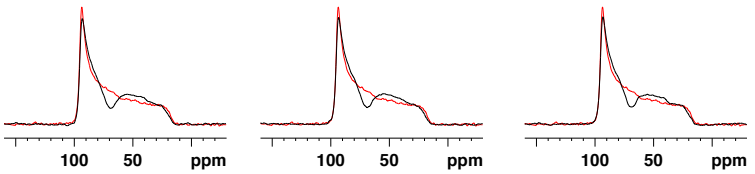

(a) *ramp* shaped-pulse, setB (cf. Table 9). (b) *s45* shaped-pulse, setB (cf. Table 1). (c) *s65* shaped-pulse, setB (cf. Table 2).

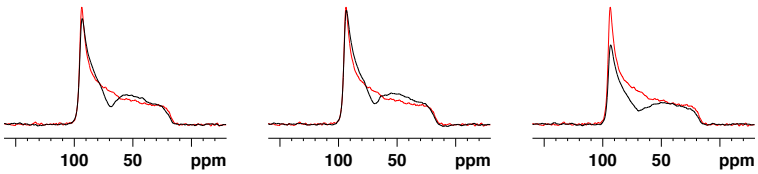

(d) *s75* shaped-pulse, setA (cf. Table 3). (e) *s84.3* shaped-pulse, setB (cf. Table 4). (f) *s88* shaped-pulse, setB (cf. Table 5).

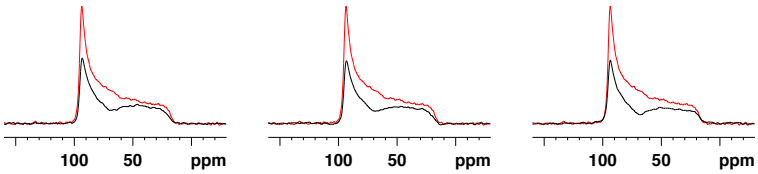

(g) *s89.5* shaped-pulse, setB (cf. Table 6). (h) *s89.9* shaped-pulse, setB (cf. Table 7). (i) *rectangular* (cf. Table 8).

Figure 23: APHH-CP, $t_{cp} = 1$ ms, SHAPE VARIATION ON SETB. In black, static $^{1}H-^{13}C$ cross-polarization experiments on ferrocene performed with t_{cp} =1 ms and each of the shaped-pulses of setB (Figure 14b). In red, confront with the CWCP experiment performed with t_{cp} =10 ms and the *rectangular* pulse shape (Table 8).

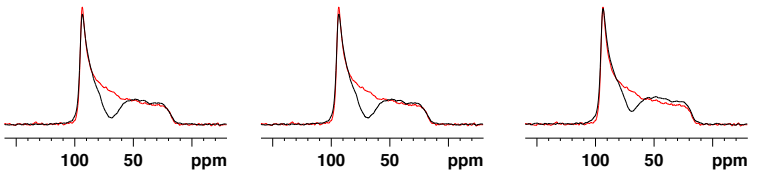

(a) *ramp* shaped-pulse, setA (cf. Table 9). (b) *s45* shaped-pulse, setA (cf. Table 1). (c) *s65* shaped-pulse, setA (cf. Table 2).

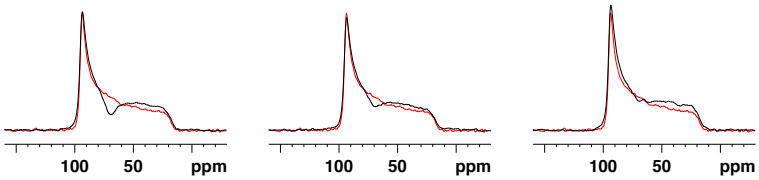

(d) *s75* shaped-pulse, setA (cf. Table 3). (e) *s84.3* shaped-pulse, setA (cf. Table 4). (f) *s88* shaped-pulse, setA (cf. Table 5).

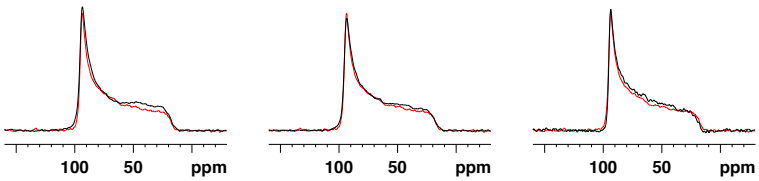

(g) *s89.5* shaped-pulse, setA (cf. Table 6). (h) *s89.9* shaped-pulse, setA (cf. Table 7). (i) *rectangular* (cf. Table 8).

Figure 24: APHH-CP, t_{cp} =3 ms, SHAPE VARIATION ON SETA. In black, static $^{1}H-^{13}C$ cross-polarization experiments on ferrocene performed with t_{cp} =3 ms and each of the shaped-pulses of setA (Figure 14a). In red, confront with the CWCP experiment performed with t_{cp} =10 ms and the *rectangular* pulse shape (Table 8).

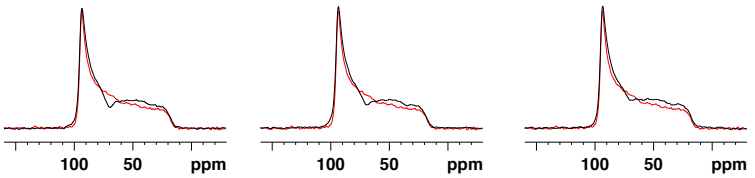

(a) *ramp* shaped-pulse, setB (cf. Table 9). (b) *s45* shaped-pulse, setA (cf. Table 1). (c) *s65* shaped-pulse, setB (cf. Table 2).

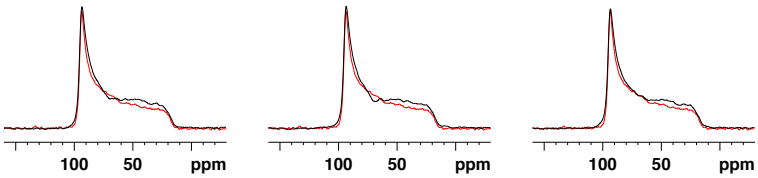

(d) *s75* shaped-pulse, setB (cf. Table 3). (e) *s84.3* shaped-pulse, setB (cf. Table 4). (f) *s88* shaped-pulse, setB (cf. Table 5).

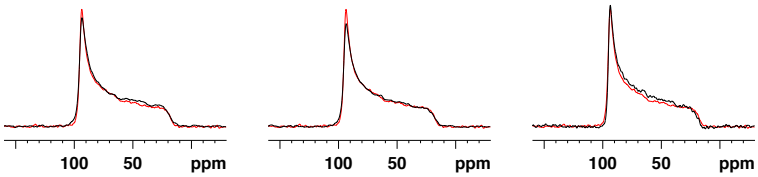

(g) *s89.5* shaped-pulse, setB (cf. Table 6). (h) *s89.9* shaped-pulse, setB (cf. Table 7). (i) *rectangular* (cf. Table 8).

Figure 25: APHH-CP, t_{cp} = 3 ms , SHAPE VARIATION ON SETB. In black, static $^{1}H-^{13}C$ cross-polarization experiments on ferrocene performed with t_{cp} =3 ms and each of the shaped-pulses of setB (Figure 14b). In red, confront with the CWCP experiment performed with t_{cp} =10 ms and the *rectangular* pulse shape (Table 8).

3.4 CONCLUSIONS AND DISCUSSION

In this chapter we examined how the contact time and shape of the excitation pulse affect the line-shape of ferrocene spectra obtained by $^{1}H - ^{13}C$ CWCP and APHH-CP.

In a standard CWCP experiment performed with a rectangular pulse profile (cf. Figure 15) the ^{13}C signal shows a net decrease of intensity in the proximity of the isotropic value. This effect, referred in literature as MAH, is known for ferrocene already since the early '70s [57] and in biological molecules subjected to fast uniaxial motion, such as lipids and peptides in membranes [27, 67, 31]. For intermediate contact times (150-350 μs), not only the MAH but also a TOH appears in the spectra. This additional distortion arises from the oscillatory terms of the density matrix, $\sigma(t)$, when $\sigma(0)$ does not commute with the Hamiltonian [68, 57]. For much longer contact times (3-10 ms), both the TOH and the MAH disappear (as shown in in Figure 15).

We can obtain an undistorted powder pattern line-shape from a standard CWCP experiment by choosing a contact time long enough to permit the spin diffusion to homogenize the magnetization. However, it has to be noted that this approach is not feasible for samples with fast spin relaxation, such as peptides in membranes, since the CP signals decay drastically after 1 ms because of the short $T_{1\rho}$. Another additional problem of long contact times is the consequent sample heating, that can accelerate the deterioration of sensitive biological samples.

Introducing shaped-pulses, instead of performing a CWCP experiment, in general do not act favourably in the process of recovering the MAH intensity. The hole at the isotropic frequency is still visible even for contact times as long as 3 ms (Figure 24), at which the CWCP is already efficiently recovering the lost magnetization. For such long intervals, even the gain in signal-to-noise of shaped-pulses is negligible when compared to rectangular pulses, since the system has the time to reach a quasi-equilibrium state. If the protons do not relax too fast, it is more advantageous to use long contact times with a standard rectangular pulse (CWCP) instead of tangent amplitude-modulated pulses (APHH-CP).

For very short contact times (cf. Figure 17 and Figure 16), the use of APHH-CP instead of CWCP does not affect the spectral line-shapes but only the intensity, resulting in a loss of signal intensity. Indeed, for contact times of a few tenths of microseconds, regular CWCP performed with a rectangular pulse shape is preferable over APHH-CP.

For intermediate contact times (Figure 19, Figure 18, Figure 20, and Figure 21), the transients caused by dipolar oscillations visibly degrade the shape of the spectra, as Hediger et al.[51] demonstrated already. In this regime, the adiabatic pulses (*s89.9* and *s84.3*) are preferable over the rectangular CWCP since they refill the transient holes. Reducing the magnitude of the pulse amplitude modulation increases also the total intensity of the spectrum and it is possible to gain up to 30% in signal intensity.

In conclusion, the use of APHH-CP is convenient only in this intermediate regime, i.e. when the contact time assumes values of the order of few hundreds of microseconds. Then, there is an effective gain in signal and the removal of the transients respect to the regular CWCP sequence.

However, we want to stress the point that the MAH problem is still not solved: the adiabatic pulses do not act on the isotropic frequency signal at all. On the contrary, the fact that the shaped-pulses increase the signal of the other frequencies, makes the MAH to look more pronounced when compared to a spectra obtained by regular CWCP.

s45 SHAPED PULSE

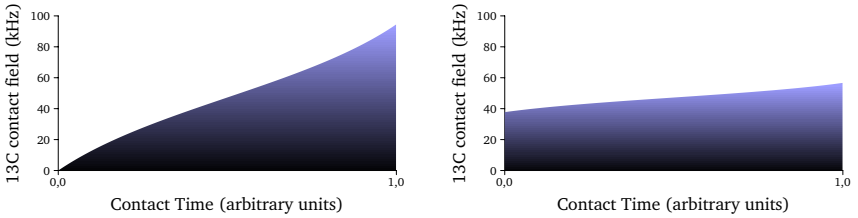

Table 1: Shaped pulse *s45*. In A the intensity of the contact field grows from 0 up to twice the HH condition. In B only a limited variation (±20%) of the intensity around the HH condition is performed.

s65 SHAPED PULSE

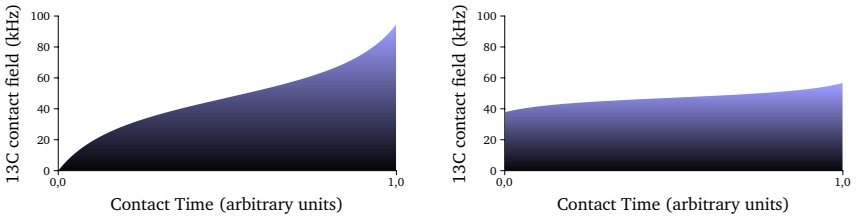

Table 2: Shaped pulse *s65*. In A the intensity of the contact field grows from 0 up to twice the HH condition. In B only a limited variation (±20%) of the intensity around the HH condition is performed.

s75 SHAPED PULSE

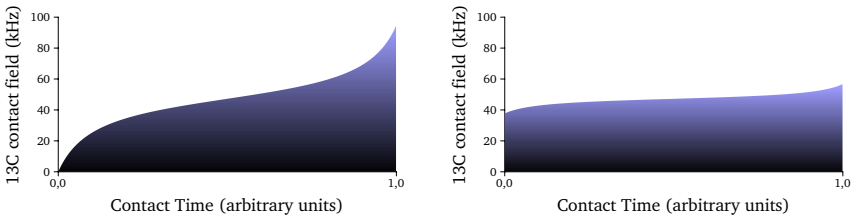

Table 3: Shaped pulse *s75*. In A the intensity of the contact field grows from 0 up to twice the HH condition. In B only a limited variation (±20%) of the intensity around the HH condition is performed.

s84.3 SHAPED PULSE

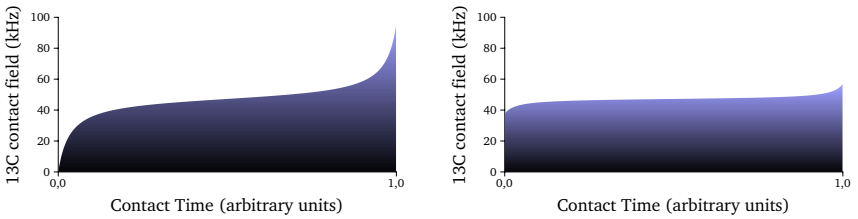

Table 4: Shaped pulse *s84.3*. In A the intensity of the contact field grows from 0 up to twice the HH condition. In B only a limited variation (±20%) of the intensity around the HH condition is performed.

s88 SHAPED PULSE

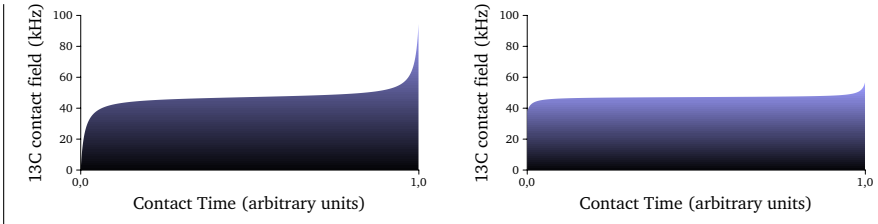

Table 5: Shaped pulse *s*88. In A the intensity of the contact field grows from 0 up to twice the HH condition. In B only a limited variation (±20%) of the intensity around the HH condition is performed.

s89.5 SHAPED PULSE

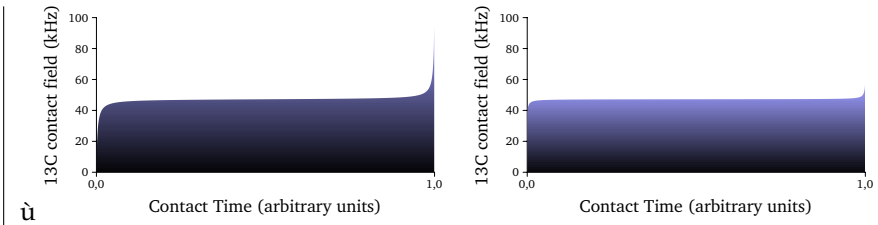

Table 6: Shaped pulse *s*89.5. In A the intensity of the contact field grows from 0 up to twice the HH condition. In B only a limited variation (±20%) of the intensity around the HH condition is performed.

s89.9 SHAPED PULSE

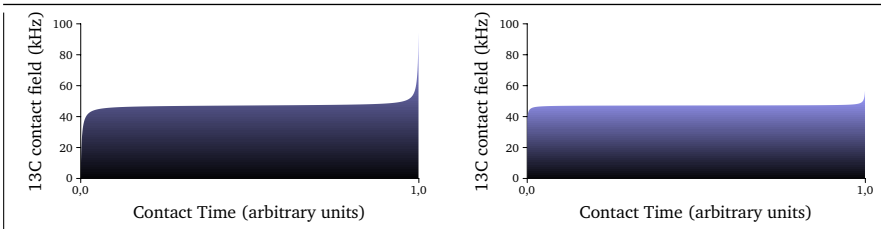

Table 7: Shaped pulse *s*89.9. In A the intensity of the contact field grows from 0 up to twice the HH condition. In B only a limited variation (±20%) of the intensity around the HH condition is performed.

TRIANGULAR AND RECTANGULAR PULSES

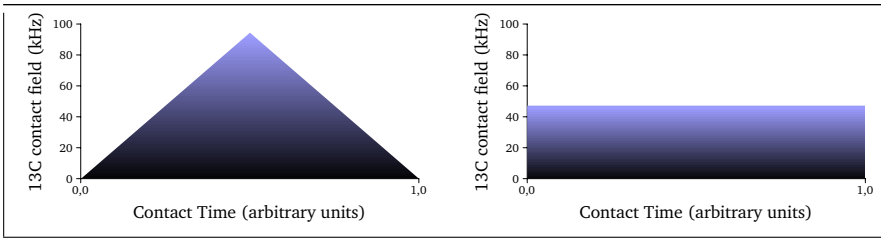

Table 8: Shaped pulse triangular (left) and rectangular (right). For the triangular shape, the intensity of the contact field varies between 0 and twice the HH condition. For the rectangular shape, the amplitude of the field stays constantly at the HH condition value.

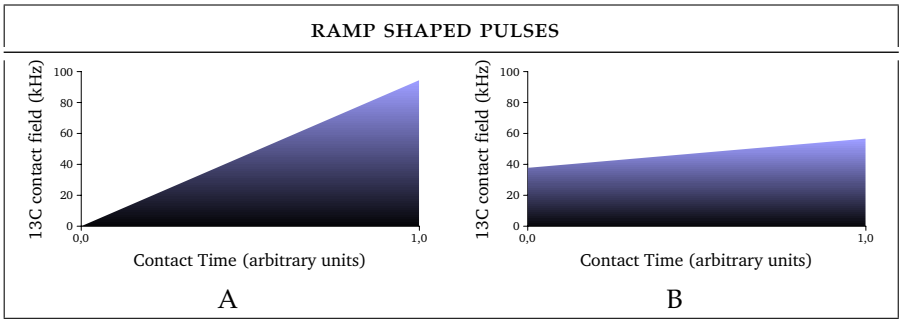

Table 9: Shaped pulse ramp. In A the intensity of the contact field grows from 0 up to twice the HH condition. In B only a limited variation ($\pm$20%) of the intensity around the HH condition is performed.

4

ROTOR-DIRECTED EXCHANGE OF ORIENTATIONS CROSS-POLARIZATION

CONTENTS OF THE CHAPTER:

In this chapter we are going to present a new cross-polarization scheme which consents to obtain undistorted chemical shift powder spectra with short contact times. The efficiency of the sequence in suppressing line-shape distortions as magic angle hole and transient oscillations is demonstrated on a powder sample of ferrocene.

4.1 INTRODUCTION

Pattern line-shape analysis of SS-NMR spectra is a powerful tool to perform structural investigation on molecules of biological interest and their reciprocal interactions. One important piece of information that this technique can elucidate is the orientation of α helical peptides in a model membrane [29, 30, 31, 32].

As already seen by other authors and in the previous chapter, the powder spectra of these and analogous systems subject to uniaxial motion presents a deformation at the isotropic chemical shift, usually referred as MAH in the literature [32] . As an analytical description of the polarization behavior in proximity of this hole is still missing , its presence prevents to reach a satisfying fit quality. In the MKBE model proposed by Müller, Kumar, Baumann, and Ernst a quasi-equilibrium state must be reached to obtain undistorted CWCP powder spectra, otherwise the effects of dipolar oscillations superimpose, leading to a modulation of the line-shape [58, 59, 60]. As a consequence, one possible approach to obtain undistorted powder spectra would be to recur to long contact times, in the order of some ms for ferrocene, as demonstrated in the previous chapter. However, this approach is not feasible for samples with fast spin relaxation, such as peptides in membranes, since the CP signals decay drastically within 1 ms because of the short $T_{1\rho}$.

An additional problem is the low sensitivity, that prevents the set-up of the HH condition directly on a biological sample. The use of an external reference compound to optimize the cross-polarization may lead to severe HH condition mismatch. In these cases, is advisable to apply contact pulses with RF amplitudes varying tangentially with time, as APHH-CP, since they perform much better then traditional rectangular or ramped pulses[47].

In this chapter we are going to present a new CP scheme, called RODEO-CP, developed to obtain undistorted chemical shift powder spectra. This simple and robust sequence is efficient even at short contact times, when the (quasi)-equilibrium polarization state has not been reached yet. The method relies on slow MAS, a few tens of Hertz, to redistribute the polarization within all the frequencies. We are going to demonstrate the efficiency of the method performing the polarization exchange by mean of both CWCP and APHH-CP on a powder sample of ferrocene.

4.2 THEORY

The MBKE model

The determination of the CP dynamics from first principles is a complex problem even in the most simple static case of a single crystal of simple structure. The introduction of some approximation become unavoidable if powders of more complex structure, motions or MAS are to be included.

The classical $I-S$ model [69] describes the CP process by a thermodynamic approach that makes use of two reservoirs, the I and the S spin systems, and a large capacity bath, the lattice. The kinetics of the CP signal intensity $I(t)$ varies by double-exponential law over the contact time t: the intensity initially increase until it reaches a maximum and then it decays to zero. However, it was shown by Müller et al.[57] that ferrocene does not follow this simple law. The intensity of the $C-H$ cross polarization signal in ferrocene undergoes transient harmonic oscillations whose frequency depends on the crystal orientation with respect to the external magnetic field and as the time passes by, the oscillations are damped by the proton spin diffusion by energy exchanges (flip-flop) with homonuclear coupled bulk protons. This behavior is not compatible with the classical model assumption in which spin diffusion is fast enough to establish communications between protons and to force them to behave as a single system with a unique and uniform spin temperature, the reservoir. These considerations resulted in the MKBE model proposed by Müller, Kumar, Baumann, and Ernst.

In an ideal case of an isolated pair of spins, the magnetization would oscillate back and forward from ^1H to X nucleus at a speed proportional to their dipolar coupling constant. Instead, if the protons are coupled in a network ($I-I^*-S$ model), the proton magnetization is redistributed all over the network, "refilling" the magnetization of the proton closest to the X spin, prolonging the magnetization transfer from ^1H to X spins.

In case of strong dipolar couplings between the I and S spins, as for $^1H-^{13}C$ couples in ferrocene or $^1H-^{15}N$ in peptides, the system can be treated as a tightly coupled $I-S$ spin pair immersed in a thermal bath consisting of the remaining protons. MKBE model assumes that only one single spin I_1 interacts with the spin-bath, which is phenomenologically described. The state of the system at any time t is described by the density operator, $\sigma(t)$. If we can neglect the relaxation in the rotating frame, $T_{1\rho}$, then the evolution of σ in the double-rotating frame follows the quantum-mechanical master equation:

$$\dot{\sigma}(t) = -i\,[H, \sigma(t)] - \Gamma(\sigma(t) - \sigma(\infty)) \tag{4.1}$$

If the Hartman-Hahn conditions are satisfied, $|\omega_{1I}| = |\omega_{1S}|$, and assuming that the applied radio frequency fields are on-resonance, $\omega_{0i} \backsimeq \omega_{rf,i}$,the Hamiltonian can be expressed, in the double-rotating frame 47, 68, as:

$$H = \omega_{1I} I_z + \omega_{1S} S_z + 2bI_x S_x$$

In the static case, the dipolar constant b is given by:

$$b = -\frac{\gamma_I \gamma_S \hbar}{2r_{IS}^3}\left(3\cos^2\theta - 1\right) \tag{4.2}$$

where all the factors have the same definitions as already introduced in Chapter 2.

In presence of motions, the dipolar constant became a function of time, $b(t)$, and, in case of MAS , the time dependence is periodic [70]:

$$\begin{aligned} b(t) \quad = \quad & -\frac{\gamma_I \gamma_S \hbar}{2r_{IS}^3}\{\sqrt{2}\sin 2\beta\cos(\gamma + \omega_r t) + \\ & -\sin^2\beta\cos(2\gamma + 2\omega_r t)\} \end{aligned} \tag{4.3}$$

where β is the angle between the spinning axis and the internuclear vector $\overrightarrow{r}$, γ is an initial azimuth of $\overrightarrow{r}$ about the same axis and ω_r is the spinning speed.

The phenomenological spin diffusion super-operator Γ is introduced in the master equation (4.1) to describe the return to the thermal equilibrium of a particular I spin with the proton spins reservoir. It accounts for the dissipative interactions between the reduced spins system and the spin-bath and it imposes the relaxation of the density operator towards its equilibrium value $\sigma(\infty)$. It can be expressed as:

$$\Gamma(\sigma) = R_{df}\{[I_x,[I_x,\sigma]] + [I_y,[I_y,\sigma]]\} + R_{dp}\,[I_z,[I_z,\sigma]]$$

where the orientation dependence of the spin diffusion operator Γ is not taken in account, i.e. Γ is considered to be isotropic in the real space[1]. As R_{df} ("effective spin diffusion process" , df) is associated with the flip-flop term of the Hamiltonian (XY planar term), it describes the thermal equilibrium with the bath, i.e. the spin diffusion processes that lead to the transfer of spin order from the considered I spin to the other protons. On the other side, the parameter R_{dp} is associated with the Ising term, and it can be associated with a process where the environment *observes* the system breaking its coherences [71] driving the system to the internal quasi-equilibrium[61] ("damping" , dp, of the coherences) . A first-principle derivation of the two parameters R_{dp} and R_{df} in terms of correlation function of the system-environment random processes involved in the spin-bath interactions can be found in the PhD thesis of Alvarez [71].

In a conventional static CWCP experiment, the RF field strengths are matched to fulfill the Hartman-Hahn condition and the initial and final states are respectively I_z and $I_z + S_z$. If the additional hypothesis $|\omega_{1I}| + |\omega_{1S}| \gg |b| \gg R_{dp}, R_{df}$ is valid, the master equation (4.1) can be solved by first order perturbation theory, with the analytical solution (MBKE solution):

1 This means that the spatial directions are considered statistically independent, i.e. identical correlation times in all the spatial directions. Notably, in the *spin* space, the superoperator Γ is isotropic only if $R_{df} = R_{dp}$.

$$
\begin{aligned}
< \quad & S_z(t) >= Tr(\sigma(t)S_z) = \\
& = 1 - \frac{1}{2}\exp(-R_{df}t) - \frac{1}{2}\exp\left[-(R_{df} + \frac{R_{dp}}{2})t\right]\cos(bt)
\end{aligned}
\tag{4.4}
$$

From this equation we can deduce that, in a single crystal, the magnetization undergoes damped oscillations whose frequency, b, is directly related to the strength and orientation of the $I-S$ coupling. The decay of the oscillatory term is governed by both the R_{dp} and R_{df} constants and the final equilibrium state is approached at the speed given by R_{df}. The analytical solution (4.4) is still valid under slow MAS, i.e. when $b(t) \approx b(0)$.

It has to be noted that when the dipolar constant is zero, i.e. at the magic angle, the assumptions that lead to the equation (4.4) are not satisfied anymore. However the analytical solution can still adequately sum up the behavior of the system for a spinning sample, since the rotation consents to escape the neighborhood in which b is null and to quickly recover the validity of the assumptions previously done.

When the solution (4.4) is not applicable, a numeric integration of the master equation (4.1) becomes necessary. The recourse to numeric integration is unavoidable also for describing adiabatic passage though the Hartmann-Hahn condition.

The RODEO experiment

The RODEO-CP experiment is sketched in Figure 26. Firstly, the spin temperature of the protons is cooled down by a 90° pulse. The transfer of magnetization is realized at the Hartmann-Hahn conditions by applying two shaped pulse, (SP), on each channel. Thereafter a $\pi/2$ pulse flips the X magnetization along the z-axis. During the mixing time, t_{mix}, the system evolves under MAS, spin diffusion and molecular motion. Finally the second 90° pulse converts the X magnetization back into the plane and the FID is acquired under high power proton decoupling, such as SPINAL64 [66].

The theory applied to the RODEO experiment

If the frequency exchange during the mixing time is due solely to slow MAS and $\omega_r t_{cp} \ll 1$, the NMR signal resulting from the RODEO experiment, $G(t)$, is readily obtained by multiplying the analytical solution $< S_z(t_{CP}) >$ by the free induction decay due to the chemical shift anisotropy:

$$
\begin{aligned}
& G(t) = \\
& =< S_z(t_{CP}) > \exp\left[i\int_{\tau_m}^{\tau_m+t} \omega_{cs}(t')dt'\right] \\
& =< S_z(t_{CP}) > \exp\left(\frac{i\delta\omega_0}{2\omega_r}\left\{\frac{\sin^2\beta}{2}\left[\sin 2\Omega_{t+\tau_m} - \sin 2\Omega_{\tau_m}\right]\right.\right. \\
& \left.\left. -\sqrt{2}\sin 2\beta\left[\sin\Omega_{t+\tau_m} - \sin\Omega_{\tau_m}\right]\right\}\right)
\end{aligned}
\tag{4.5}
$$

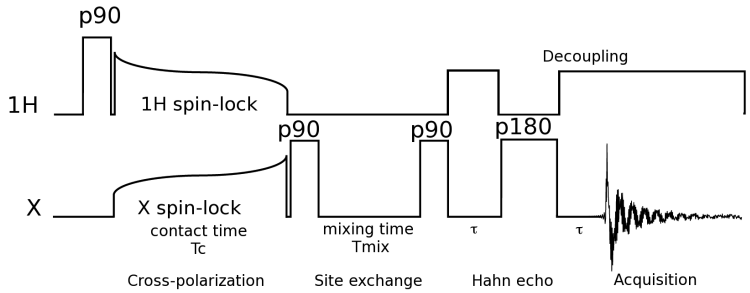

Figure 26: RODEO sequence. First a $\pi/2$ pulse is applied to cool down the ^1H spins reservoir. The CP step is realized by spin-locking the two channels during the contact time τ_c. Here the APHH-CP version is schematized with shaped pulses on both channels. The X magnetization is then flipped to the z-axis by a $\pi/2$ pulse. After the mixing time τ_m the magnetization is flipped back on the plane by another $\pi/2$ pulse. An Hahn-echo is then applied to avoid distortions. The final step is the acquisition on the X channel with a simultaneous decoupling on the proton channel.

where δ is the chemical shift anisotropy and we used the simplified notations: $\Omega_{t+\tau_m} = \gamma + \omega_r(t+\tau_m)$ and $\Omega_{\tau_m} = \gamma + \omega_r\tau_m$ where τ_m is the mixing time.

For the ferrocene rings and membrane-associated peptides undergoing fast uniaxial motion, the CSA tensor is axially symmetric (the asymmetry parameter, η, is zero) and by consequence the principal axes of the dipolar (IS) and chemical shift tensors are coincident. For the same reason (fast uniaxial motional averaging), both the CSA and the dipolar constant have to be scaled by the order parameter of the motion. For ferrocene we obtain:

$$\overline{b} = -b/2 \qquad \overline{\delta} = -\delta/2$$

From equation (4.5) it is obvious that the first factor, the evolution (CP) term, is a function of $\gamma + \omega_r t$, while the second factor, the detection (CSA) term, depends on $\gamma + \omega_r(t+\tau_m)$. The basic idea behind our method is to introduce a phase shift, $\omega_r\tau_m$, between the evolution and detection frequencies by slow MAS.

The effect of the slow MAS can be visualized in Figure 27. The magic angle hole arise from the S spins belonging to the "magic-angle cones" (the yellow cone in Figure 27a), i.e. from spins that belong to molecules whose rotational axes form an angle of $\beta^* = 54.7°$ (or close by) with the static magnetic field B_0. For these spins, equation (4.3) is constantly zero $b(\tau_{cp}) = b(0) = 0$ and, at the end of the cross-polarization step, $t = \tau_{cp}$, they are still only weakly polarized.

When τ_m is equal to zero (or an integer multiple, n, of the rotor period, T_r), there is no phase shift between evolution and detection frequencies and each orientation of the IS dipolar tensor correlates with a single (identical) orientation of the CSA tensor. In particular, the isotropic chemical shift ($\omega_{CS}(\tau_m) = 0$) is associated with $b(\tau_{cp}) = b(0) = 0$.

Instead, when the mixing time does not match the previous condition, $\tau_m \neq nT_r$, the slow MAS redistributes the magnetization thereby attenuating the line-shape distortions. This effect is maximum for $\tau_m = n\frac{T_r}{2}$.

All the vectors initially belonging to the yellow cone are characterized by the « magic-angle » evolution (CP) frequency $b(0) = 0$. After half a turn of the rotor, the frequency $b(0) = 0$ corresponds to a wide range of CSA tensor orientations (the red cone in Figure 27b) or detection frequencies characterized now by $\omega_{CS}(\tau_m) \neq 0$. We can resume the principle of RODEO-CP experiment saying that the mixing time τ_m introduce a phase shift between the evolution and detection frequencies, i.e. τ_m *decorrelates* the evolution and detection frequencies, spreading the intensity loss at the MAH over the chemical shift powder pattern.

The same effect causes also the strong reduction, or even suppression, of the line-shape distortions due to the transient dipolar oscillations. Also, as long as the $\pi/2$ pulse imperfections and T_1 relaxation can be neglected, there is no loss of signal intensity in the RODEO-CP experiment when compared to the standard CWCP pulse sequence.

In reality, the frequency decorrelation is not complete, since it is valid for all the vectors of the magic angle cone *except* those belonging to the intersection of the two cones. The intersection represents those vectors whose orientation is invariant under axial rotations around the spinner axis. The geometrically most satisfying exchange of frequencies is realized around half-turn of the spinner (Figure 27b), since the surface of intersection is made by only three lines (the rotor axis plus two other lines, see Figure 27c). [2]

4.3 MATERIALS AND EQUIPMENT

Ferrocene was purchased from Fluka Chemie and used without any further purification.

Solid-state nuclear magnetic resonance experiments were conducted on an AVANCE 500 MHz wide bore spectrometer (Bruker, Wissembourg, France) operating at a frequency of 125.7 MHz for ^{13}C. The spectrometer was equipped with a triple resonance MAS probe (operating in double mode) designed for 3.2 mm rotors.

Proton and carbon radio-frequency fields were calibrated directly on the ferrocene sample by a two-dimensional nutation experiment and adjusted to match the HH condition $\frac{\omega_{1S}}{2\pi} = \frac{\omega_{1I}}{2\pi} = 47.2$ kHz. In the APHH-CP experiments the proton field was set to 47.2 kHz while the carbon field was swept though the HH condition by the tangential time dependence give in [51] from 37.8 to 56.6 kHz.

An Hahn-echo refocusing pulse was added at the end of the RODEO experiments before the acquisition step in order to avoid the dead time problem. Proton decoupling during acquisition time was applied by SPINAL-64 scheme [66]. 192 scans were accumulated for each experiment with a recycle time of 40 s and a Lorentzian line-broadening of 100 Hz was applied prior to Fourier transform of the FID.

4.4 RESULTS

Slow MAS on CWCP experiments

We tested the effect of slow MAS during a regular CWCP experiment on a polycrystalline sample of ferrocene. The results are reported in Figure 28 for 50 µs, 150 µs, 350 µs and 1 ms of contact time performed

2 In the general case of an arbitrary rotation, the surface of intersection is made by a minimum of 2 and a maximum of 4 lines.

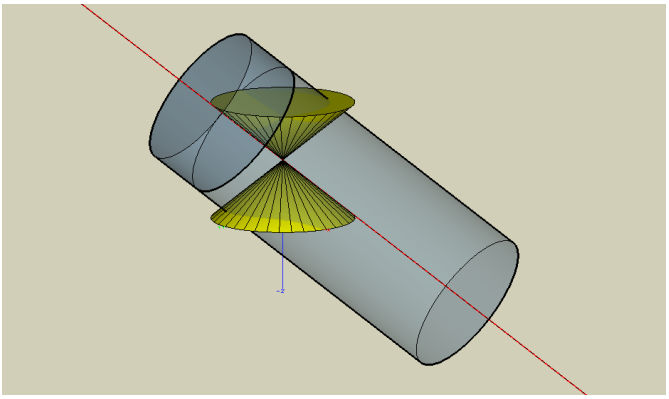

(a) The MAS spinner is oriented at the magic angle respect to the z axis. The yellow cone is the "magic-angle cone" before the mixing time, i.e. for $t = \tau_{cp}$. Every point on the surface of the cone represents spins belonging to molecules whose rotational axes form an angle of $\beta^* = 54.7°$ with the static magnetic field B_0 (in blue).

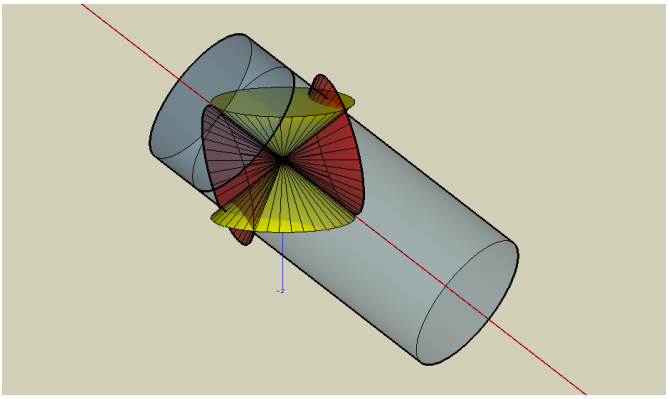

(b) Magic-angle cone after after half-turn around the rotor axis, i.e. $t = T_r/2$. The initial magic angle cone (in yellow) is transformed by the rotation in the second cone (in red).

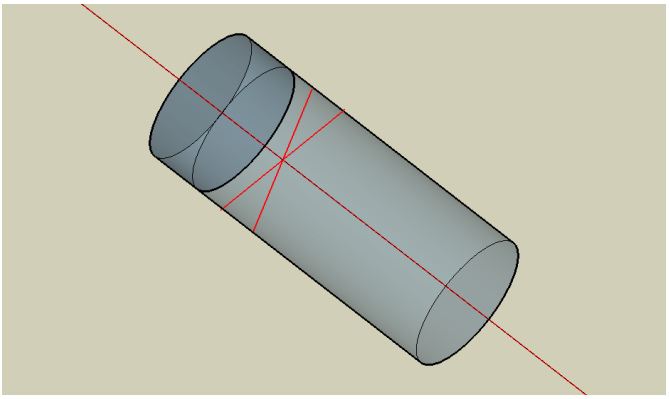

(c) Intersection between the two magic-angle cones before and after $\tau_m = T_r/2$. Only two lines (in red) plus the rotor axis conserve their orientation at the magic angle after the rotation.

Figure 27: Orientation of the « magic-angle » cones before and after the mixing time.

turning the sample at 50 Hz (in black). For comparison, we reported also the same experiment performed in static conditions with a very long contact time of 10 ms (in red), when the quasi-equilibrium state is reached.

As expected, at very short contact times the CWCP spectrum is strongly distorted because almost no signal is coming from the molecules with their rotational axes oriented at angles close to the MA. Also TOH s are not removed by the spinning. A clear improvement is visible on the line-shapes when increasing the contact time, but the recovery of the missing intensity at the isotropic CS is still not complete even for $\tau_{cp} = 1$ ms. This partial recovery of the line-shape is due to two factors, the longer CP time, that allows to approach a quasi-equilibrium state, and the slow turning, that consent to escape the neighborhood in which $b \approx 0$. Obviously, for such a slow rate, it is necessary to wait a long time before a molecule with its motional axis initially oriented at θ^* =54.7 degrees is being moved to an angle at which the dipolar coupling is effective again to drive the magnetization transfer. In particular, turning 50 µs at 50 Hz corresponds to an angle variation of less then one degree, clearly not enough to have an efficient magnetization transfer. Longer contact times of 150 µs, 350 µs or 1 ms correspond to about 3, 6 and 18 degrees respectively, so to angle variations more and more efficient. The difference between these two effect can be visualized in Figure 29: for 150 µs and 350 µs of contact time the differences between the static and the turning CWCP are barely visible, but for 1 ms there is a clear refilling due to the MAS.

Static RODEO-CP experiments

The pulse train used during RODEO-CP sequence was tested under static conditions, to check if the internal spin diffusion of ferrocene is efficient enough to refill the MAH. The spectra are reported in Figure 30 for increasing mixing times. There is only a minor refill for very long mixing times of 20 s. The total intensity of the spectra reduces of one half increasing the mixing time from 1 to 20 s: from this decrement we can estimate a T_1 of the order of 20 s. In order to recover the correct powder pattern line-shape, we should increase the mixing time to values about 3-5 times T_1, that means to dramatically prolong the acquisition time. Moreover, this kind of approach is not too general, since the efficiency is dependent from the spin dynamics of the sample.

Slow MAS RODEO-CP experiments

In Figure 31 are reported the RODEO-CP spectra on polycrystalline ferrocene under MAS recorded with different contact times for a mixing time equivalent to half-turn. When slowly turning the sample at 50 Hz, the spectral distortions are almost completely removed by RODEO-CP, even for τ_{cp} as short as 50 µs. The spectrum is close to the simulated theoretical averaged powder pattern line-shape and the unique significant discrepancy is the sightly higher intensity observed at the singularity θ=90° in the RODEO-CP spectrum. These data are in excellent agreement with calculated powder spectra using the analytical expression given by equation (4.5) as extensively shown in [72].

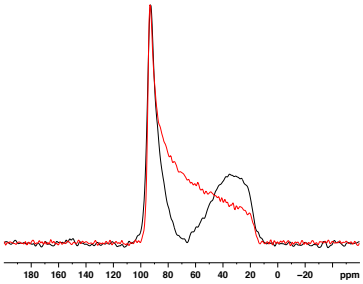

(a) CWCP performed with τ_{cp} =50 µs turning at 50 Hz (black) and the same experiment performed with τ_{cp} = 10 ms in static conditions (red).

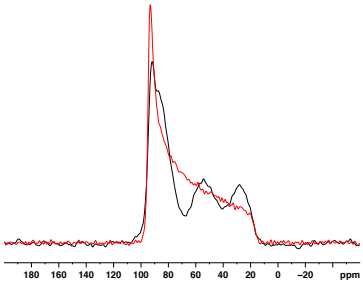

(b) CWCP performed with τ_{cp} =150 µs turning at 50 Hz (black) and the same experiment performed with τ_{cp} = 10 ms in static conditions (red).

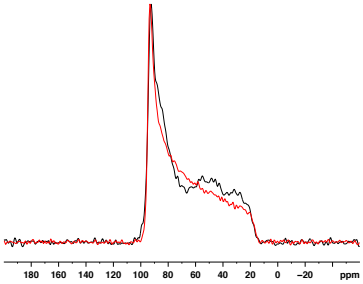

(c) CWCP performed with τ_{cp} =350 µs (black) turning at 50 Hz (black) and the same experiment performed with τ_{cp} = 10 ms in static conditions (red).

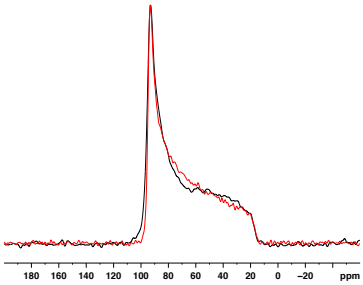

(d) CWCP performed with τ_{cp} =1 ms turning at 50 Hz (black) and the same experiment performed with τ_{cp} = 10 ms in static conditions (red).

Figure 28: Effect of slowly turning at 50 Hz on the CWCP experiment.

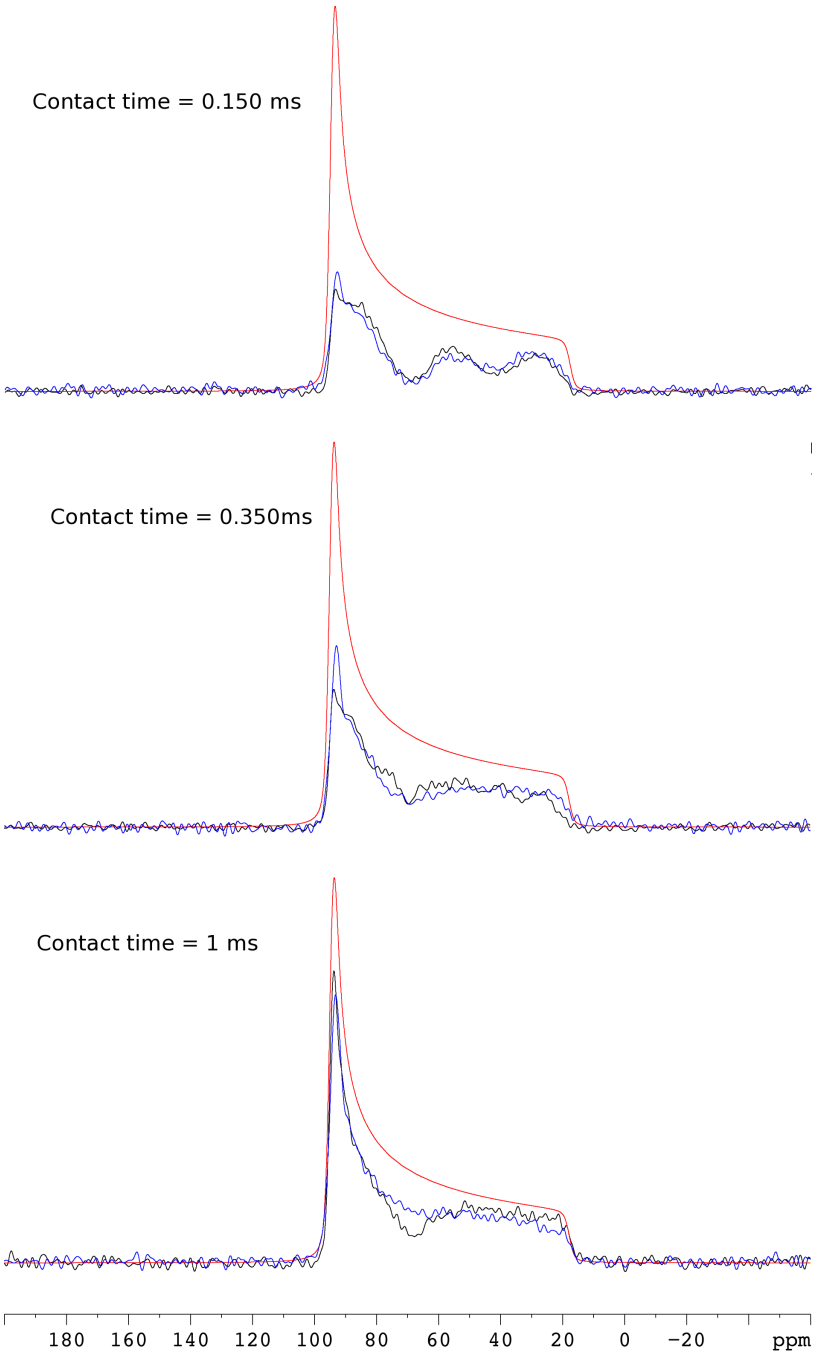

Figure 29: Static CWCP (in black) and slow MAS - CWCP (in blue) done at different contact times: 150 µs (top), 350 µs (middle) or 1 ms (bottom). In red for comparison the theoretical line shape.

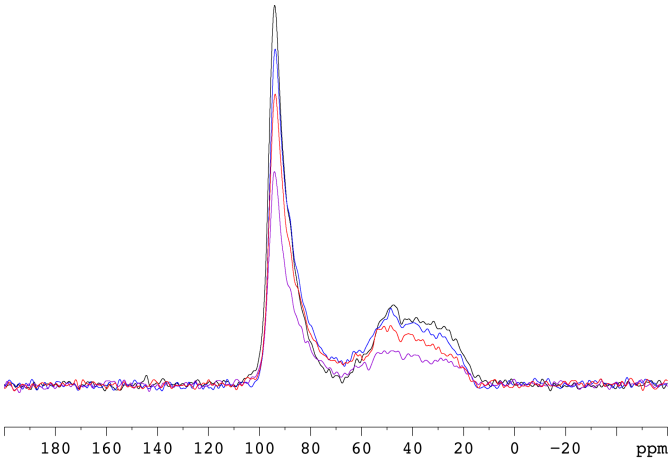

Figure 30: Static RODEO-CP various mixing times. In black τ_m=1 s, in blue τ_m=5 s, in red τ_m=10 s and in violet τ_m=20 s. All the spectra were recorded with $\tau_{cp} = 150$ µs.

RODEO-CP spectra with different mixing times are reported in Figure 32. All the experiments are accurately reproduced by calculations [72]. As expected, the optimum line-shape is recovered for $\tau_m \approxeq T_r/2$, as shown in Figure 32e, in which both the MAH and TOH are efficiently removed, even if τ_{cp} is shorter than the spin diffusion time constants $T_{df} = 1/R_{df}$, $T_{dp} = 1/R_{dp}$.

Dramatic line-shape distortions re-appear when $\tau_m = T_r$ (cf. Figure 32j) and the spectra remain significantly distorted for mixing times close to this value (cf. Figure 32a and Figure 32i).

Spectra obtained with mixing times equally distant from $\tau_m = T_r$ do not conserve this symmetry: calculations show that this phenomena is a consequence of the non-negligible effects of MAS during the detection time [72].

A perfect lock of the spinning speed may be challenging to achieve when turning just a few tens of Hertz. This is not compromising the experiment, on the contrary, a variation on the spinning speed of about 10 Hz is still acceptable and it introduces an additional degree of randomization. In fact, a random variation of the mixing time within the interval $0.5\,T_r - 0.9\,T_r$ improves the quality of the spectra, as shown in Figure 33. Although, at first sight, the small differences between the two spectra could be mistaken for experimental noise, in fact the two spectra may be distinguished on the basis of small details at the left discontinuity and at the right shoulder, as clearly reproduced by calculation in [72].

The method here presented is easily reconfigurable for other CP scheme and it is effective even when a triangular shaped-pulse (cf. Chapter 3) is used (data not shown). We implemented a pseudo-adiabatic pulse to increment the performance of the experiment and to be less sensitive to the HH condition mismatch. When APHH-CP was used as initial CP step in the RODEO sequence, undistorted line-shapes were obtained (data shown in Figure 34), with an overall intensity gain of about 1.45 respect to CWCP.

Finally, it is also possible to increase the spinning speed up to some hundreds of Hertz to avoid to deal with problems related to the stability of MAS spinning. Experiment (and simulations in [72]) demonstrated that the efficiency of our method is not altered by spinning the sample

at ca 400 Hz: as shown in Figure 35, RODEO experiment give undistorted spectra comparable with the long contact time CWCP sequence, while the MAH is clearly present in the analog experiment performed at short contact time.

4.5 CONCLUSIONS

In this chapter we present a new simple and robust method RODEO that permits to obtain undistorted chemical shift powder spectra. Our sequence takes advantage of slow MAS to redistribute the magnetization across the powder pattern and it proved to be effective not only for the recover of the MAH but even for dipolar transient holes. Also the line-shape obtained by CW-RODEO-CP for contact times as short as 150 μs was comparable with the quasi-equilibrium CWCP spectra obtained for very long contact times (10 ms).

Overall a loss of 10% in intensity was registered in CW-RODEO-CP respect to the analogue CWCP experiment, due to $\pi/2$-pulse imperfections. This minor disadvantage is abundantly compensated by the possibility to use a much shorter contact time in mobile samples with short $T_{1\rho}$, subjected to fast decay of the signal, and still obtain an undistorted powder spectra[3].

3 See Chapter A for more details.

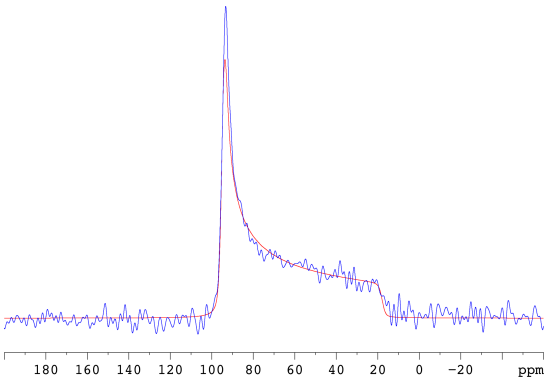

(a) Contact time $\tau_{cp} = 50\mu s$.

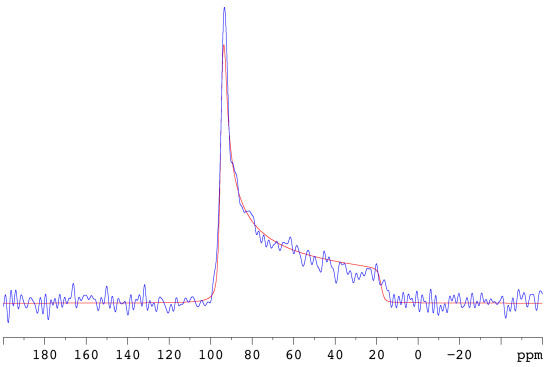

(b) Contact time $\tau_{cp} = 150\mu s$.

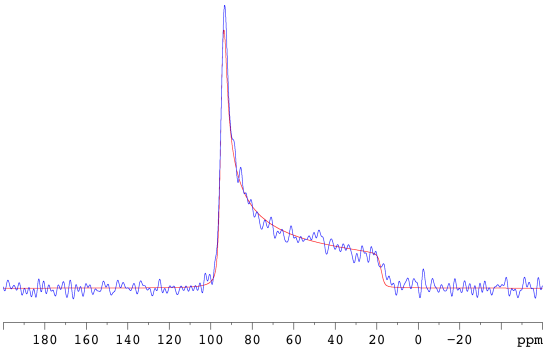

(c) Contact time $\tau_{cp} = 350\mu s$.

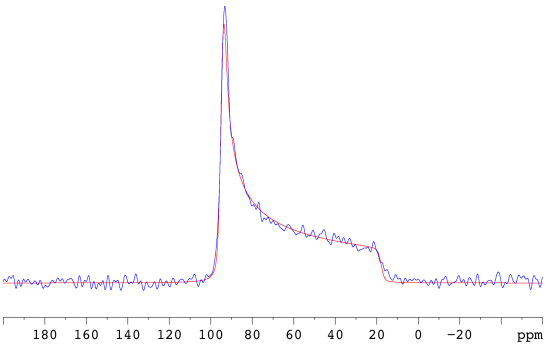

(d) Contact time τ_{cp} =1ms.

Figure 31: CW-RODEO-CP experiments performed turning the sample at 50 Hz, with τ_{mix}=10 ms (corresponding to half-turn) and at different contact times. In blue the experimental spectra, in red the theoretical fit.

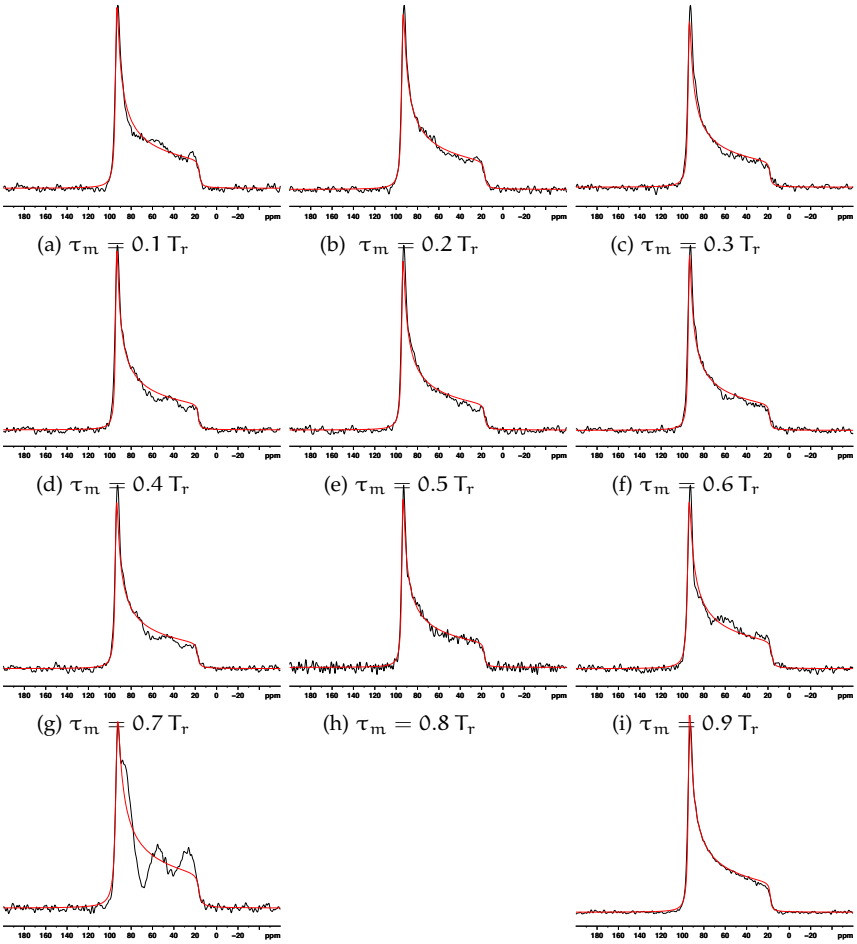

(a) $\tau_m = 0.1\ T_r$ (b) $\tau_m = 0.2\ T_r$ (c) $\tau_m = 0.3\ T_r$

(d) $\tau_m = 0.4\ T_r$ (e) $\tau_m = 0.5\ T_r$ (f) $\tau_m = 0.6\ T_r$

(g) $\tau_m = 0.7\ T_r$ (h) $\tau_m = 0.8\ T_r$ (i) $\tau_m = 0.9\ T_r$

(j) $\tau_m = T_r$ (k) CWCP with $\tau_{cp} = 10$ ms and 50 Hz MAS.

Figure 32: CW-RODEO-CP spectrum performed at various mixing times. For all the experiments a contact time of 150 µs and a spinning rate of 55 Hz were used. In black: experimental spectra. In red: theoretical averaged powder pattern fit.

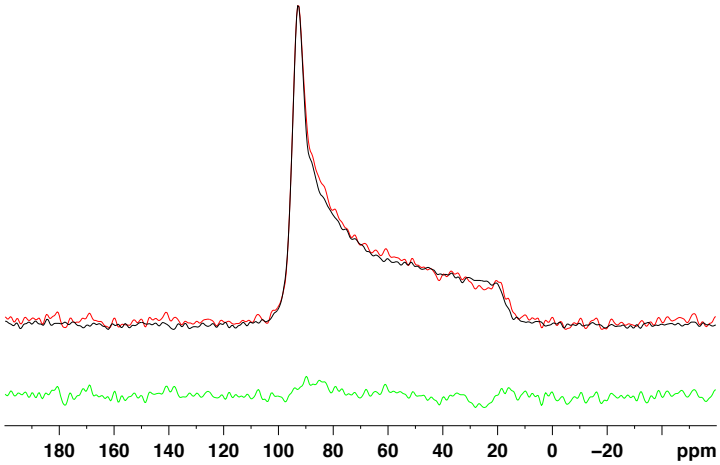

Figure 33: Confront of two spectra obtained by CW-RODEO-CP sequence using $\tau_m = 0.5\,T_r$ (in red) and averaging over several τ_m within the interval $[0.5\,T_r, 0.9\,T_r]$ (in black). In green the difference between the two spectra. Both spectra are recorded spinning the sample at the MA at 50 Hz and with a contact time of 150 µs. The use of a random variation over τ_m results in a CW-RODEO-CP spectra closest to the long contact time CWCP respect to the one obtainable applying a fixed mixing time of $\tau_m = 0.5\,T_r$.

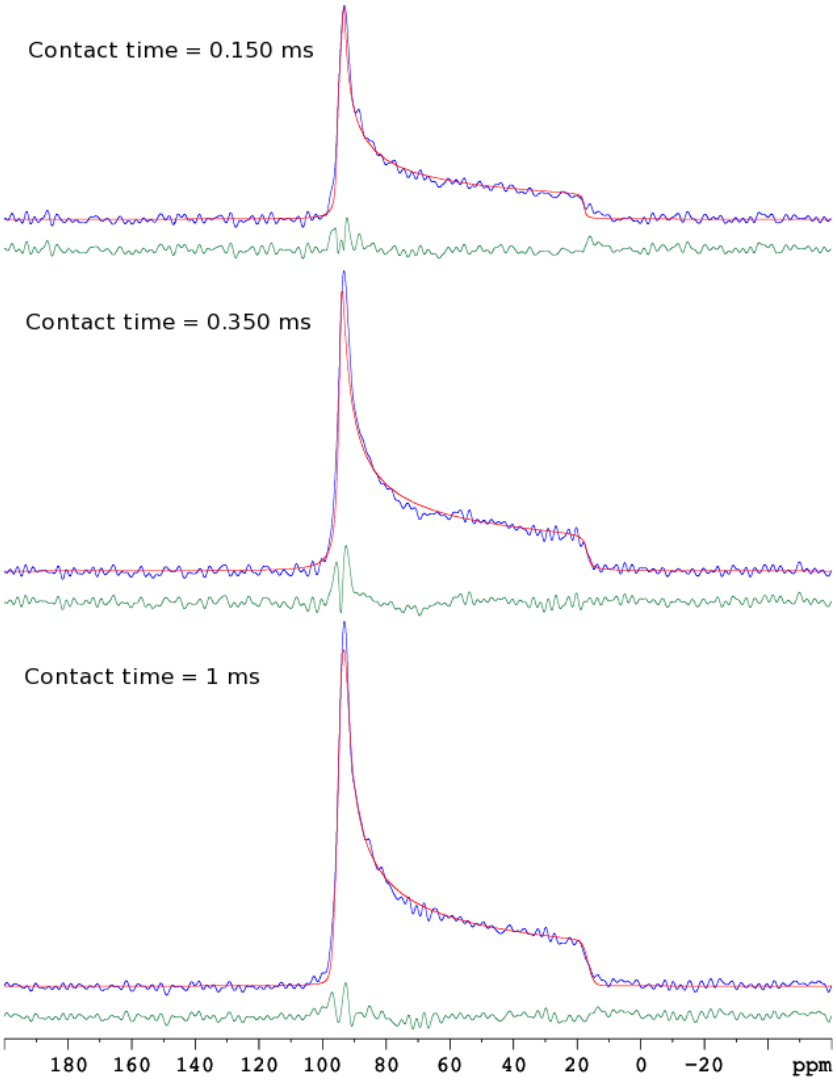

Figure 34: APHH-RODEO-CP at various contact times. Top: $t_{CP} = 150\mu s$. Middle: $t_{CP} = 350\mu s$. Bottom: $t_{CP} = 1ms$. The adiabatic passage was realized applying the *s84.3* shaped-pulse (cf. Table 4). All the experiments were recorded turning the sample at 50 Hz. A mixing time of $T_{mix} = 10$ ms was used (corresponding to half-turn exchange). In blue: experimental spectra. In red: powder pattern fit. In green: difference between experimental data and fit.

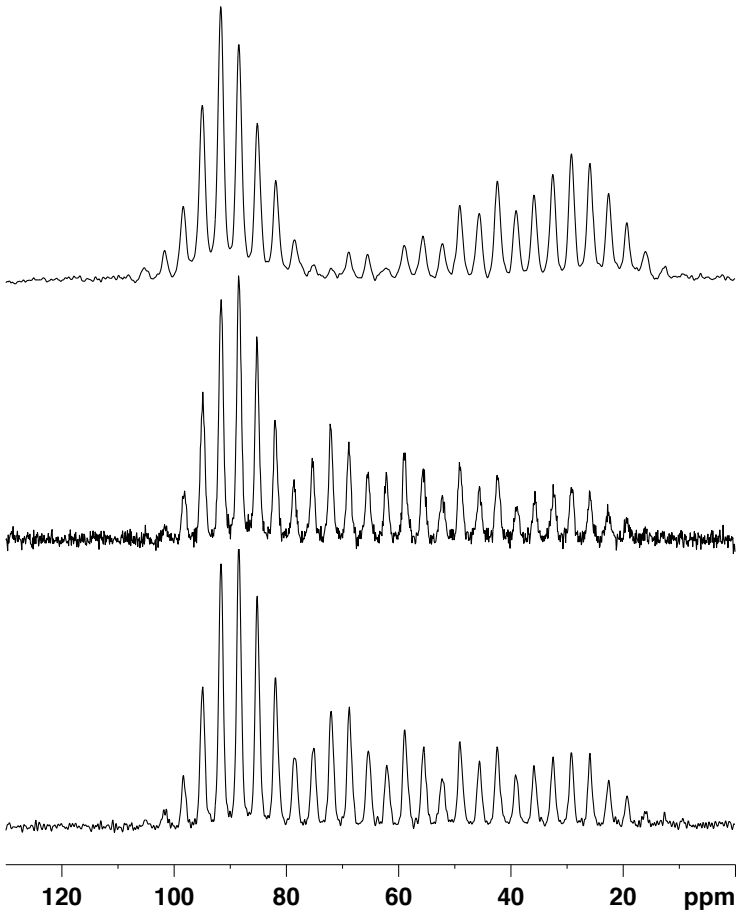

Figure 35: Experiments performed with MAS at 414 Hz. Top: CWCP with $\tau_{cp} =$ 50 µs. Middle: CW-RODEO-CP with $\tau_{cp} = 50$ µs and $\tau_m = 0.5\,T_r$. Bottom: CWCP with $\tau_{cp} = 10$ ms.

5

RODEO-CP APPLIED TO DESIGNED PEPTIDES IN UNORIENTED MODEL MEMBRANES

CONTENTS OF THE CHAPTER:

In this chapter we are going to apply the new method previously discussed to recover the powder-pattern line-shape of membrane-associated synthetic peptides that present uniaxial motion around the membrane normal. We will verify the ability of the APHH-RODEO-CP experiment to suppress the MAH. Assuming a model for the peptide dynamics, we will derive the equations expressing the tilt and pitch angles in function of the ^{15}N chemical shift tensor. Finally, fitting the unoriented SS-NMR spectra with a pure powder pattern model, we will obtain the seek values.

5.1 INTRODUCTION

Small membrane associated polypeptides or protein segment represent an important class of relevant biological structure. Antibacterial peptides, receptors and membrane penetrating anchors of viruses are examples of molecules and oligomers studied by SS-NMR that are mostly inaccessible to diffraction techniques such as X-ray crystallography. They represent also key object to develop new NMR techniques and to understand the folding of more complex membrane proteins. In this optics, KALP and KL14 are suitable candidates to test the efficiency of new NMR sequences and they reflect respectively the main characteristics of a transmembrane and an in-plane alpha helix [73]. The structural study of membrane-associated peptides by NMR techniques is complicated by their peculiar dynamics in the membrane bilayer: unlike in solution, the liquid crystal media impose an anisotropic reorientation of the solute. This unique behavior allows the persistence of orientation-dependent interactions as the chemical shift anisotropy and the dipolar coupling that usually broaden the NMR peaks. In any case, these molecules conserve a high degree of mobility with characteristic times covering several order of magnitude. Rapid internal conformational changes appear in the pico-nano seconds range, while whole-body motions, as lateral and axial diffusion, occur in the intermediate scale, from nano- to milliseconds. Finally slower off-axis re-orientations happens in the micro and milliseconds time scale due to wobble of the single molecule or to membrane undulations. All this motions are reflected, in different manners, in modifications of the orientation dependent observables, making of solid-state NMR a valuable tool to investigate structure, topology and dynamics of small objects associated to membranes. Specifically, the milliseconds range corresponds to the CSA and deuterium quadrupolar interactions, observable at frequencies of the order of 10 to 100 kHz. Proton-decoupled ^{15}N solid-state NMR spectroscopy in particular has proved to be a direct probe for the tilt angle of polypeptides in oriented samples. Only few studies so far explored theoretically [29] or experimentally [43] the possibility to obtain the membrane-relative alignment of alpha helices or beta sheets [32] from globally non-oriented samples.

In these and precedent studies [30] was already noticed the presence of a distortion and defined as the "magic angle hole"[32]. The hole appears in uni-axially mobile molecules where the chemical shift and the dipolar coupling tensor became collinear with the rotational axis, as we previously encountered with ferrocene. The analogy of ^{13}C spins in ferrocene with a system composed of single-labeled ^{15}N polypeptides in liquid crystals does not stop here. Both systems undergo transient oscillations at short contact times [74, 57] and these oscillations were even used by Tian and co-workers to selectively polarize protonated carbons versus non-protonated carbons.

The presence of deviations from the averaged powder pattern line-shape complicates dramatically the interpretation of the spectra, aggravated by the poor resolution obtained from non-oriented samples. In the presence of distorted spectra discerning populations of spins with different orientation behavior can result a difficult task. In case of multiple label present in the sample the task became even more difficult. To expand the application of this approach to the study of more complex systems and topologies, a methodology to record a undistorted spectra has to be developed. Confident with the positive results obtained with the analog spin system ferrocene, we decided to apply the RODEO-CP sequence to the study of two synthetic peptides, KALP and KL14, playing the roles of a transmembrane or surface-associated model helix. The resulting line-shape is a clean powder pattern without critical distortions.

5.2 DYNAMICS OF MEMBRANE ASSOCIATED PEPTIDES

Biological membranes are dynamic objects and can be described by the fluid mosaic model of S. J. Singer and Garth Nicolson 1972, as a two-dimensional liquid where all lipid and protein molecules diffuse more or less easily. As previously seen in Chapter 1, solid state NMR is sensitive to the orientation and dynamics assumed by peptides within the bilayers.

When the rotational diffusion is fast enough the chemical shift anisotropy is averaged to a symmetric tensor with components $\sigma_{\parallel}$ and $\sigma_{\perp}$ given by:

$$\sigma_{\parallel} = \sigma_{11}\cos^2\alpha\sin^2\beta + \sigma_{22}\sin^2\alpha\sin^2\beta + \sigma_{33}\cos^2\beta \tag{5.1}$$

$$\sigma_{\perp} = \frac{\sigma_{11}(1-\cos^2\alpha\sin^2\beta) + \sigma_{22}(1-\sin^2\alpha\sin^2\beta) + \sigma_{33}\sin^2\beta}{2} \tag{5.2}$$

where α and β are the Euler's rotation angles (cf. Figure 8). The values of the parameters $\sigma_{\parallel}$ and $\sigma_{\perp}$ are plotted in Figure 36 in function of the two angles α and β.

Unfortunately, the two parameters $\sigma_{\parallel}$ and $\sigma_{\perp}$ are not independent: they are related by the $\sigma_{iso} = \frac{\sigma_{\parallel}+2\sigma_{\perp}}{2}$. The isotropic chemical shift is, in fact, pre-determined from the principal components of the static ^{15}N amide chemical shift, so the three equations form an undetermined system in two variables. [1]

1 In other words, this indeterminacy can be seen as consequence of the assumption of the motional averaging, that imposes the additional condition $\eta \equiv 0$, and Δ becomes the only parameter free.

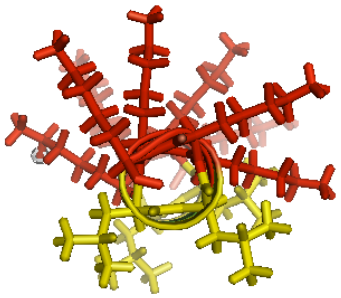

(a) KL14 peptide: helical wheel projection. The charged residues (lysines) are reproduced in red while the hydrophobic amino acids are in yellow.

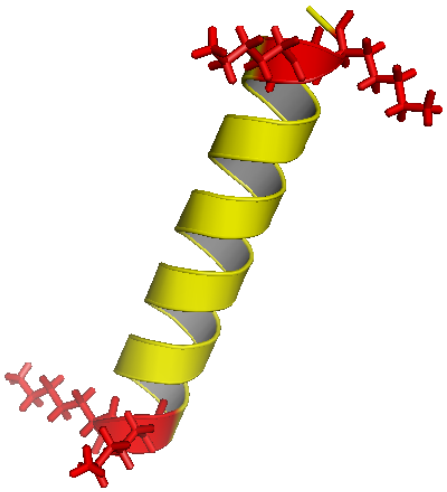

(b) KALP peptide. In red the charged anchors (lysines) and in yellow the hydrophobic core.

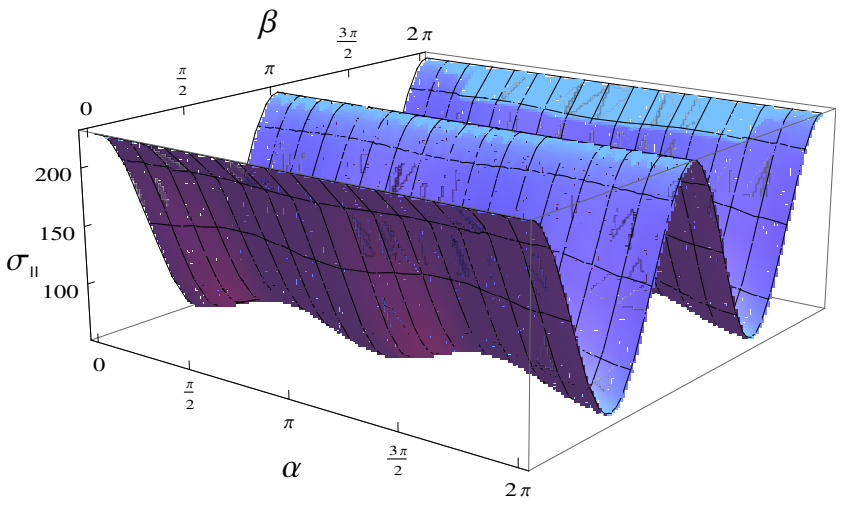

(a) Behaviour of $\sigma_{\parallel}$ with the variation of α and β angles.

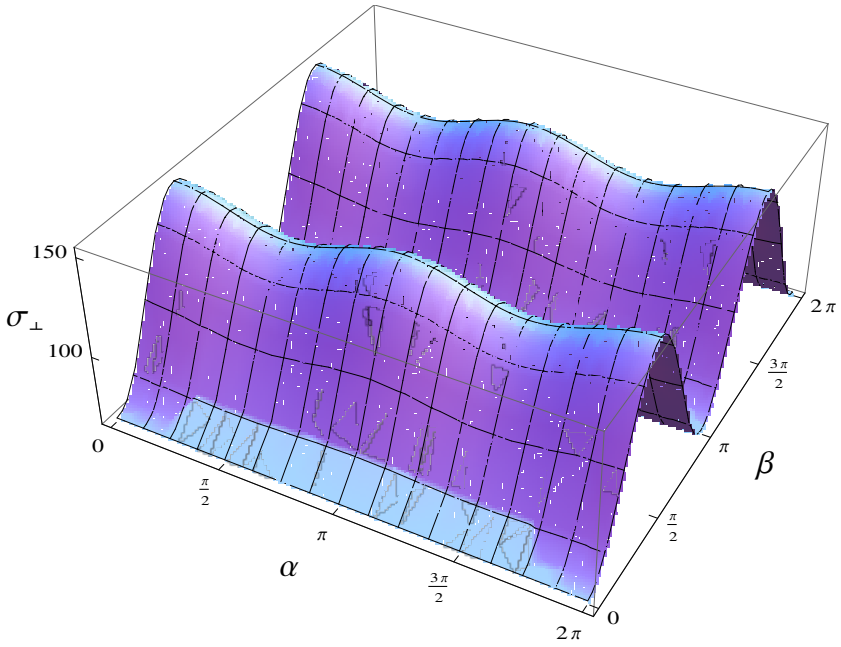

(b) Behaviour of $\sigma_{\perp}$ with the variation of α and β angles.

Figure 36: Variation of $\sigma_{\parallel}$ and $\sigma_{\perp}$ in function of the angles α and β. As principal axes values we used $\sigma_{11} = 53.84$ ppm, σ_{22} =78.06 ppm and σ_{33}=228.24 ppm.

In order to solve the system we can add an additional condition. Let first consider the two extreme case: an in-plane peptide ($\beta = \pi/2$) and a transmembrane peptide ($\beta = 0$).

For an helix inserted parallel to the membrane normal, the relations (5.1) and (5.2) become:

$$\sigma_{\parallel} = \sigma_{33} \tag{5.3}$$

$$\sigma_{\perp} = \frac{\sigma_{11} + \sigma_{22}}{2} \tag{5.4}$$

It has to be noted that, in the transmembrane case, no phase dependence persists. This is consequence of the fact that for $\beta = 0$ the normal of the membrane and the helix axis are coincident. In this configuration, only the self-rotational diffusion of the peptide around its own axis is still acting and the definition itself of the parameter α became useless, since all the angles would be physically equivalent.

This is not the case for in-plane peptides, where the phase of the helix respect to the membrane surface is indeed well defined and it corresponds to the knowledge of which residue is pointing toward the water interface and which other toward the internal hydrophobic core of the membrane.

For a perfectly surface-aligned peptide, the helix axis and the membrane normal are orthogonal and the angle β is equal to $\pi/2$. The previous relationships became then a function only of the phase α between the molecular frame xyz and the fixed frame XYZ.

$$\sigma_{\parallel} = \sigma_{11}\cos^2\alpha + \sigma_{22}\sin^2\alpha \tag{5.5}$$

$$\sigma_{\perp} = \frac{\sigma_{11}\sin^2\alpha + \sigma_{22}\cos^2\alpha + \sigma_{33}}{2} \tag{5.6}$$

The two previous equations (5.5) and (5.6) have the following extreme solutions:

$$\alpha = \tfrac{\pi}{2} \longrightarrow \begin{cases} \sigma_{\parallel} = \sigma_{22} \\ \sigma_{\perp} = \frac{\sigma_{11}+\sigma_{33}}{2} \end{cases}$$

$$\alpha = 0 \longrightarrow \begin{cases} \sigma_{\parallel} = \sigma_{11} \\ \sigma_{\perp} = \frac{\sigma_{22}+\sigma_{33}}{2} \end{cases}$$

In general, both the variables α and β are unknown. As additional conditions, we can suppose that the self-rotational diffusion of the peptide around its own axis is fast enough to allow the peptide to complete a fast rolling around the helix axis, i.e. σ_{33}. Then we can assume $< \cos^2\alpha > = < \sin^2\alpha > = 1/2$ and the equation (5.1) become:

$$\sigma_{\parallel} = \frac{\sigma_{11} + \sigma_{22}}{2}\sin^2\beta + \sigma_{33}\cos^2\beta \tag{5.7}$$

$$\sigma_{\perp} = \frac{\sigma_{11} + \sigma_{22} + (\sigma_{33} - \frac{\sigma_{11}+\sigma_{22}}{2})\sin^2\beta}{2} \tag{5.8}$$

This last assumption is a good approximation as long as we have an hydrophobic peptide inserted in the membrane with moderated tilted

angles. When the peptide present a defined hydrophilic/hydrophobic surfaces separation with an in-plane orientation, fast complete motion around the helix axis became energetically unfavorable and our approximation less realistic. However, the error introduced on the tilt angle is still limited, because the values of σ_{11} and σ_{22} are close to each other.

Since $\sin^2\alpha$ and $\cos^2\alpha$ are monotonic functions that assume values between the interval $[0, 1]$, then we can calculate the error introduced by considering $< \sin^2\alpha >=< \cos^2\alpha >= 1/2$ instead to the real unknown values of $\sin^2\alpha$ and $\cos^2\alpha$.

In the hypothesis of $\sin^2\alpha$=0, we obtain $\sigma_{\parallel} = \sigma_{11} + (\sigma_{11} - \sigma_{33})\cos^2\beta$ and if instead $\sin^2\alpha = 1$, then we would have $\sigma_{\parallel} = \sigma_{22} + (\sigma_{33} - \sigma_{22})\cos^2\beta$. The error we introduce on $\sigma_{\parallel}$ by our approximation is maximum when $\sin^2\alpha$ or $\cos^2\alpha$ are maximum, i.e. for $\alpha = k\pi$ with $k \in \mathbb{N}$, and its value is $\left|\Delta\sigma_{\parallel}\right| = \frac{\sigma_{22}-\sigma_{11}}{2}(1 - \cos^2\beta)$. The error is also a function of β: it is minimum for $\beta = 0$ and increase with β until its maximum $\frac{\sigma_{11}-\sigma_{22}}{2}$ at β=$\frac{\pi}{2}$. In the end, our approximation introduces an uncertainty on $\Delta\sigma_{\parallel} \leqslant \frac{\sigma_{22}-\sigma_{11}}{2} \simeq \pm 10\text{ppm}$.

Once recorded the motional averaged spectra, $\sigma_{\parallel}$ and $\sigma_{\perp}$ are known, and the fit of any the equations (5.7) or (5.8) with the static tensor parameters σ_{11}, σ_{22} and σ_{33} will give the seek tilt angle β:

$$(\beta)_{\alpha=\pi/4} = \arccos\sqrt{\frac{\sigma_{\parallel} - \frac{\sigma_{11}+\sigma_{22}}{2}}{\sigma_{33} - \frac{\sigma_{11}+\sigma_{22}}{2}}} \tag{5.9}$$

We can write the equation equivalent to the precedent deriving from the equation (5.8):

$$(\beta)_{\alpha=\pi/4} = \arcsin\sqrt{\frac{2\sigma_{\perp} - \sigma_{11} - \sigma_{22}}{\sigma_{33} - \frac{\sigma_{11}+\sigma_{22}}{2}}} \tag{5.10}$$

5.3 MATERIALS AND METHOD

Chemicals

KALP (GKK LALA LALA LALA LALA LKKA-CONH2) and KL14 (KKLL KKAKK LLKK -CONH2) peptides were produced by automated solid-phase synthesis using standard Fmoc chemistry on a Millipore 9050 synthesizer. At the 12^{th} position for KALP and at the 8^{th} position for KL14, Fmoc-protected ^{15}N-labeled leucine and alanine were incorporated. The purity of the products were checked by MALDI-TOF mass spectroscopy and HPLC and resulted satisfactory. The peptides were successively used without any further purification. POPC was purchased from Avanti (Avanti Polar Lipids, Inc., Alabaster, AL, USA) and used without any further purification. Chloroform and trifluoro-ethanol (Tri-fluoro ethanol (TFE)) were purchased from Sigma Aldricht.

Oriented samples preparation

The samples were prepared with about 10 mg of each peptide co-dissolved in TFE with 100 mg of POPC within a glass test-tube. Solvents were partially evaporated using a nitrogen stream and the concentrated

solutions were spread on thin glass plates. The glass plates were exposed to high vacuum over night to remove the residual solvent. After re-hydration for 2-3 days in a closed chamber in presence of a saturated solution of potassium nitrate (which gives 93% relative humidity at 25°C), the glass plates were stacked on top of each other, wrapped with Teflon® tape and sealed in plastic.

Unoriented samples preparation

Samples of freeze-dried peptide powder were prepared simply by fitting about 90mg of KALP and about 85mg of KL14 in a 7 mm rotor.

Unoriented membrane-associated peptide samples were prepared dissolving peptides (about 20 mg of KALP and about 30 mg of KL14) and lipids (ca 200 mg of POPC) with the same procedure and solvents used for the oriented sample preparation, but the mixtures were dried completely by nitrogen stream taking care to form a uniform extended film on the walls of the tubes. The tubes were successively placed in high vacuum overnight to remove all the residual traces of solvents. The dried films were re-hydrated for three days in a closed chamber in presence of a saturated solution of potassium nitrate, which gives 93% relative humidity at 25 °C. The samples were then briefly centrifuged and transferred in a 7 mm rotor.

NMR experiments

The oriented SS-NMR experiments were performed on a Bruker Avance 300 spectrometer (Larmor frequency of 30.43 and 300.33 MHz in ^{15}N and ^{1}H resonance, respectively) with a triple-resonance SS-NMR probe modified with flattened coil. Proton-decoupled ^{15}N SS-NMR spectra were acquired at room temperature using adiabatic passage though APHH-CP. Nitrogen and proton fields were swetp trough the HH conditions from 21.7 to 30.0 kHz and from 26.0 to 17.4 kHz respectively using the tangential time dependence given in [63]. Before Fourier-transformation an exponential apodization function corresponding to a line broadening of 100 Hz was applied. Recycle delay was set to 3s. 51874 and 102400 scans were recorded respectively for KL14 and KALP samples.

APHH-CP experiments

The APHH-CP experiments were carried out on a Bruker Avance 400 spectrometer (Larmor frequency of 40.54 and 400.13 MHz for ^{15}N and ^{1}H resonance, respectively) equipped with a Bruker **CPMAS!** (CPMAS!) probe for 7-mm-o.d. rotors in static conditions. The proton and nitrogen radio frequency fields were calibrated first on a reference sample ($^{15}NH_4Cl$). The experiments were performed sweeping the ^{1}H and ^{15}N RF fields through the HH condition from 24 to 36 kHz using the tangential time dependence given in [51]. Recycle time applied was 3 s and 10240 scans were recorded. An Hahn-echo refocusing pulse has been included in all the experiments before the acquisition to overcome the dead time problem. Proton decoupling during acquisition and echo times was performed by SPINAL-64 [66]. A left shift of 24 points and a Lorentzian broadening of 500 Hz were applied prior to Fourier-transform.

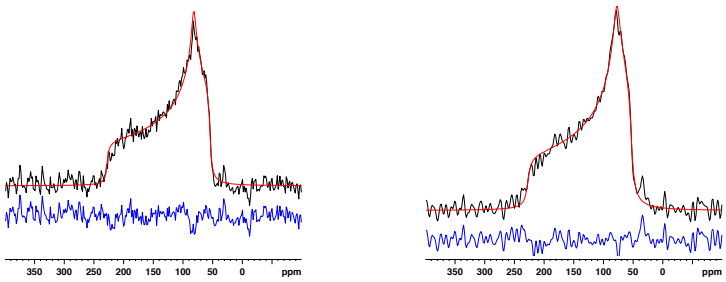

(a) freeze-dried KL14 APHH-CP powder spectra (in black) with 1ms of contact time. 2416 scans acquired and 50Hz of Lorentzian line-broadening was added prior to Fourier-transform.

(b) Freeze-dried KL14 APHH-CP powder spectra (in black) with 3ms of contact time. 1024 scans acquired and 50Hz of Lorentzian line-broadening was added prior to Fourier-transform.

Figure 37: APHH-CP spectra (in black) of freeze-dried ^{15}N-labeled KL14 recorded with different contact times. The better signal-to-noise has to be ascribed to the higher number of scans. The fit results are reported in Table 10. For comparison, the difference between experimental spectra and fit is reported below (in blue). Both experiments were conducted at room temperature.

APHH-RODEO-CP experiments

The APHH-RODEO-CP experiments were performed with the same setup and parameters of the APHH-CP experiences. The MAS frequency was fixed at 50 Hz and the applied mixing time was calibrated to randomly scan all values corresponding to the interval needed by the rotor to cover from 1/4 to 1/2 of the period.

5.4 RESULTS

In order to obtain the static chemical shift tensors for the two peptides we recorded the spectra of the KL14 Figure 37 and KALP Figure 38 freeze-dried powders. For contact times below 1ms some residual distortion of the spectra seems to flatten the spectra in the isotropic chemical shift region, while for much longer contact times as 10 ms (data not shown) the signal collapses due to T_1 relaxation. The fit of these spectra gives the parameters reported in Table 11 and Table 10.

Oriented samples

The oriented spectra of both peptides in Figure 39 show a single narrow peak, indication of a defined alignment of the peptides into the lipid bilayer. The positions of the peak for KALP and KL14 are respectively of 202.3±0.5 and 73.0±0.5 ppm. The first is indicative of a peptide oriented transmembrane while the second is characteristic of a peptide aligned on the surface of the membrane.

APHH-CP experiments

Figure 40a and Figure 40b shows the APHH-CP ^{15}N-NMR spectra of two α-helical model peptides KL14 and KALP in POPC membrane. These two peptides are known to adopt stable in-plane and transmembrane

KL14 FREEZE-DRIED PEPTIDE POWDER	$\tau_{cp} = 1ms$	$\tau_{cp} = 3ms$
fit overlap	92%	89%
σ_{33} (ppm)	228.2±0.5	228.7±0.5
σ_{22} (ppm)	78±4	82±4
σ_{11} (ppm)	54±1	55±1
σ_{iso} (ppm)	120±2	122±2
Δ_{CSA}(ppm)	108±1	107±1
η_{CSA}	0.22±0.04	0.26±0.04
Ω	174±1	173±1
K	-0.72±0.03	-0.69±0.03
line broadening (Hz)	336	209

Table 10: Chemical shift parameters obtained from the fit of (8-alanine)-^{15}N labeled KL14 as pure freeze-dried powder. The errors were estimated as the difference between the values obtained the two fits.

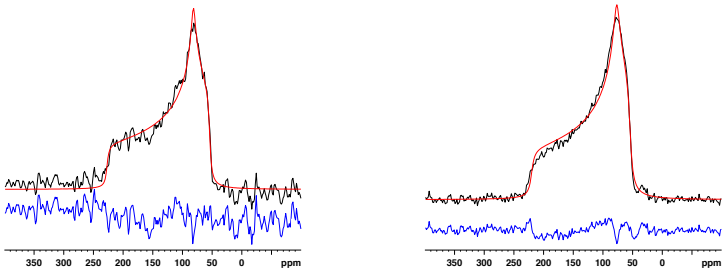

(a) Freeze-dried KALP APHH-CP powder spectra (in black) with 800µs of contact time. 2416 acquired and 50Hz of Lorentzian line-broadening was added prior to Fourier-transform.

(b) Freeze-dried KALP APHH-CP powder spectra (in black) with 3ms of contact time. 6144 scans acquired and 50Hz of Lorentzian line-broadening was added prior to Fourier transform.

Figure 38: APHH-CP spectra (in black) of freeze-dried KALP recorded with different contact times. The better signal-to-noise has to be ascribed to the higher number of scans and also the longer contact time. However at 3ms the anisotropy of the $T_{1\rho}$ seems to start acting while at 800µs the MAH is still affecting the spectra. The fitting parameters are reported in 11. For comparison, the difference between experimental spectra and fit is reported below (in blue).

KALP FREEZE-DRIED PEPTIDE POWDER	$\tau_{cp} = 800\mu s$	$\tau_{cp} = 3ms$
fit overlap	92%	93%
σ_{33} (ppm)	225±4	221±4
σ_{22} (ppm)	77.2±0.3	77.5±0.3
σ_{11} (ppm)	54.8±0.2	55.0±0.2
σ_{iso} (ppm)	119±1	118±1
Δ_{CSA}(ppm)	106±3	103±3
η_{CSA}	-0.212±0.006	-0.218±0.006
Ω	170±4	166±4
K	-0.74±0.01	-0.73±0.01
line broadening (Hz)	265	306

Table 11: Chemical shift parameters obtained from the fit of (12-leucine)-^{15}N labeled KALP as pure freeze-dried powder. The errors were estimated as the difference between the values obtained the two fits.

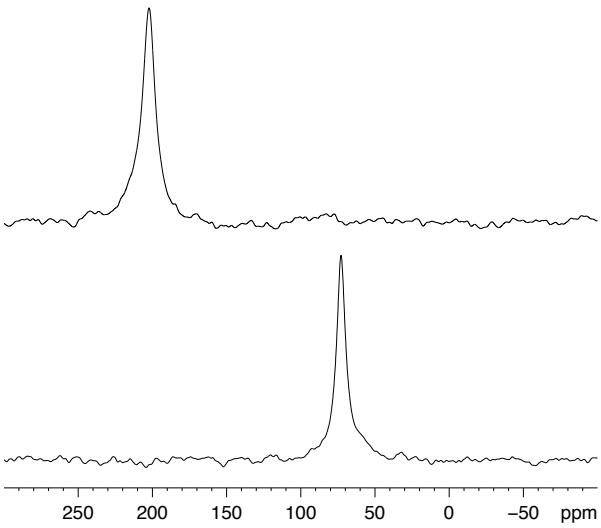

Figure 39: Spectra of peptides in oriented POPC . Top: KALP, bottom: KL14.

MEMBRANE-ASSOCIATED PEPTIDES	KL14	KALP
$\sigma_{\parallel}$ (ppm)	72±4	205±4
$\sigma_{\perp}$ (ppm)	143.5±0.5	78.7±0.3
σ_{iso} (ppm)	120±2	121±2
Δ_{CSA}(ppm)	-48±1	84±3
fit overlap	89.3%	90.7%

Table 12: Chemical shift parameters obtained from the fit of ^{15}N-single labeled KL14 and KALP in unoriented POPC. We estimate the errors on the basis of the errors obtained in the previous fits.

configuration respectively [73]. Both spectra display a magic angle hole located at the isotropic shift due to fast rotational diffusion around the bilayer normal. This MAH was previously observed with other proteins [32, 31][67, 30] and ferrocene. Both KALP and KL14 spectra present the expected line-shapes of peptides subjected to uniaxial motion around the membrane axis for a transmembrane and in-plane alignment respectively [31]. While for the transmembrane peptide a quite clear interpolation of the line-shape could still be obtained also with the MAH, for the in-plane peptide the presence of the MAH on the spectra interfere with the determination of the right shoulder. This may be due to the relatively long contact time and fast and anisotropic relaxation of KL14.

APHH-RODEO-CP experiments

As expecting from the results already seen for ferrocene, the APHH-RODEO-CP experiment efficiently suppress the MAH both for KALP and KL14 in unoriented hydrated membrane of POPC, as shown in Figure 40a and Figure 40b. The spectra follows the predicted line-shape for chemical shift powder patterns considering rotational averaging around the membrane normal [29] and were well fitted by a symmetric chemical shift tensor. The results of these fits are reported in Table 12. The σ_{iso} values of the freeze-dried peptide and membrane-associated peptide samples are only few ppm apart, indicating that there could be a slight readjustment of the screening cloud after exposure of the peptide to the hydrated membrane environment. The component of the averaged tensor parallel to the membrane normal $\sigma_{\parallel}$ of the unoriented samples is coincident within 1 ppm with abscissa of the peak originating from the oriented samples. Also, from the comparison with the APHH-CP spectra it clear that no distortion due to MAH are persisting in the APHH-RODEO-CP spectra.

5.5 DISCUSSION

From the spectra in Figure 37 of the freeze-dried peptide powder we derived the components (see Table 10) of the static tensor σ_{11}, σ_{22}, and σ_{33}, while from the fit of the APHH-RODEO-CP spectra obtained in unoriented POPC membrane in Figure 40c we got the two components of the motional- averaged tensor, $\sigma_{\parallel}$ and $\sigma_{\perp}$, for each peptide (see Table 12).

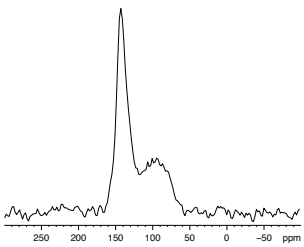

(a) Spectra of KL14 in unoriented POPC obtained by APHH-CP.

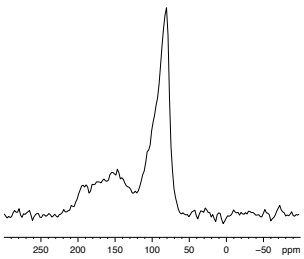

(b) Spectra of KALP in unoriented POPC obtained by APHH-CP.

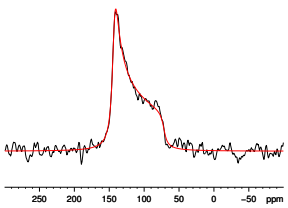

(c) Spectra (black line) and fit (red line) of KL14 in unoriented POPC obtained by APHH-RODEO-CP turning at 50Hz (MAS).

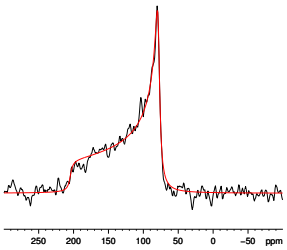

(d) Spectra of KALP in unoriented POPC obtained by APHH-RODEO-CP turning at 50Hz (MAS).

Figure 40: Static and pseudo-static spectra of peptides in unoriented POPC obtained by APHH-CP and APHH-RODEO-CP sequences.

The values that α and β can assume can be found in the intersections of the calculated geometrical surfaces $\sigma_{\parallel,\perp} = f(\alpha, \beta, \sigma_{11}, \sigma_{22}, \sigma_{33})$ given by equation (5.1) and equation (5.2) with their experimental values, i.e. the planes $\sigma_{\parallel} = \sigma_{\parallel}^{exp}$ and $\sigma_{\perp} = \sigma_{\perp}^{exp}$ (see Figure 41for KALP and Figure 42 for KL14). The intersections are two curves $\beta_{\sigma_{\parallel}} = f_{\parallel}(\alpha)$ and $\beta_{\sigma_{\perp}} = f_{\perp}(\alpha)$, that, let apart the experimental errors, should be coincident, since they are related one to the other by the implicit condition $\sigma_{\perp} = 3\sigma_{iso} - 2\sigma_{\parallel}$. Their analytical description is given by the following periodic formulas:

$$\beta_{\sigma_{\parallel}} = \pm \arccos\left(\pm\sqrt{\frac{\sigma_{\parallel} - \sigma_{11}\cos^2\alpha - \sigma_{22}\sin^2\alpha}{\sigma_{33} - \sigma_{11}\cos^2\alpha - \sigma_{22}\sin^2\alpha}}\right)$$

$$\beta_{\sigma_{\perp}} = \pm \arccos\left(\sqrt{\frac{-\sigma_{11} - \sigma_{22} + 2\sigma_{\perp}}{\sigma_{33} - \sigma_{11}\cos^2\alpha - \sigma_{22}\sin^2\alpha}}\right)$$

The curves are extensively represented in Figure 43 in the squared domain $[0, 2\pi] \times [0, 2\pi]$ for a better comprehension of their topological proprieties, even if the functions are actually periodic over a period of $\pi/2$. In particular, for the KALP peptide, the intersection of the surfaces with the experimental planes cut a topologically open curve, as shown in Figure 43a. The domain of the function $\beta = f(\alpha)$ present no restriction in α, that may assume freely all the values between 0 and 2π. Even so, the angle β is limited to values in the region 22.7°-24.5°, giving a good estimation of the tilt angle regarding the fact that no information on the helix phase α is available. We can then conclude that KALP peptide assume a transmembrane configuration in POPC bilayer and the tilt angle found by our method is in good agreement with other previously published data [75].

The topology of the curve $\beta = f(\alpha)$ change to a closed curve for the KL14 peptide, as illustrated in Figure 43b. Both α and β may assume values only in within a restricted range. As before, there are several configurations of α and β that could satisfy the experimental finding, but in this case the α and β permitted values has to stay over an elliptical curve, as a pendulum. In particular, at the minimum and maximum values permitted for α, around $\pm 63°$, the curve $\beta = f(\alpha)$ give only $\beta = 90°$ as solution, in other words the peptide is perfectly aligned with the membrane surface. If the peptide is tilted respect to the membrane ($\beta \neq 90°$), that means that the phase of the helix has to change accordingly, until the helix reach the maximum inclination: $\pm 20°$ from the membrane surface for an angle α=0°. In other words, we can conclude that the peptide assume an in-plane configuration and although our tilt angle estimation is not such as precise as for the transmembrane case, in addition we can exclude helix configurations with the σ_{11} component of the ^{15}N labeled alanine perpendicular to the membrane axis ($\alpha \backsim 90°$), since they are outside the range of values assumed by $\beta = f(\alpha)$. These findings are also in good agreement with other SS-NMR studies performed on oriented samples of KL14 [73].

5.6 CONCLUSIONS

In this chapter we demonstrated the applicability of the new method introduced in the previous chapters to recover the powder pattern line-shape of single labeled ^{15}N helical peptides subjected to uniaxial motion in model membranes. Not only the RODEO-CP sequence allows

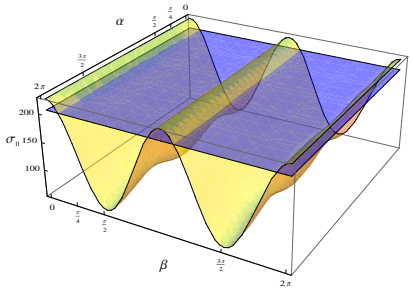

(a) Intersection of the surface given by equation (5.1) with the experimental value found for the KALP peptide, i.e. the plane $\sigma_{\parallel}$=205 ppm

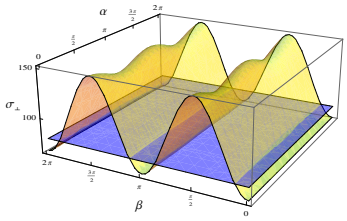

(b) Intersection of the surface given by equation (5.2) with the experimental value found for the KALP peptide, i.e. the plane $\sigma_{\perp} = 78.7$ ppm.

Figure 41: Intersections of the geometrical surfaces $\sigma_{\parallel,\perp} = f(\alpha, \beta)$ given by equation (5.1) and equation (5.2) with the experimental values found for KL14 in Table 10.

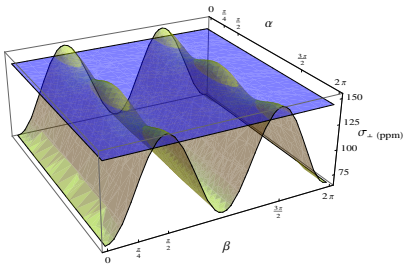

(a) Intersection of the surface given by equation (5.1) with the experimental value found for the KL14 peptide, i.e. the plane $\sigma_{\parallel} = 72.08$ ppm.

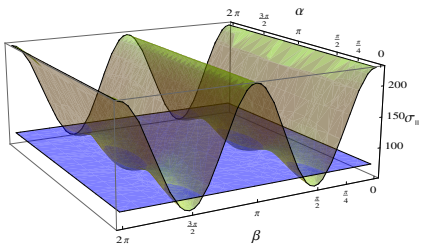

(b) Intersection of the surface given by the (5.2) with the experimental value found for the KL14 peptide, i.e. the plane $\sigma_{\perp} = 143.47$ ppm.

Figure 42: Intersections of the geometrical surfaces $\sigma_{\parallel,\perp} = f(\alpha, \beta)$ given by equation (5.1) and equation (5.2) with the experimental values found for KL14 in Table 10.

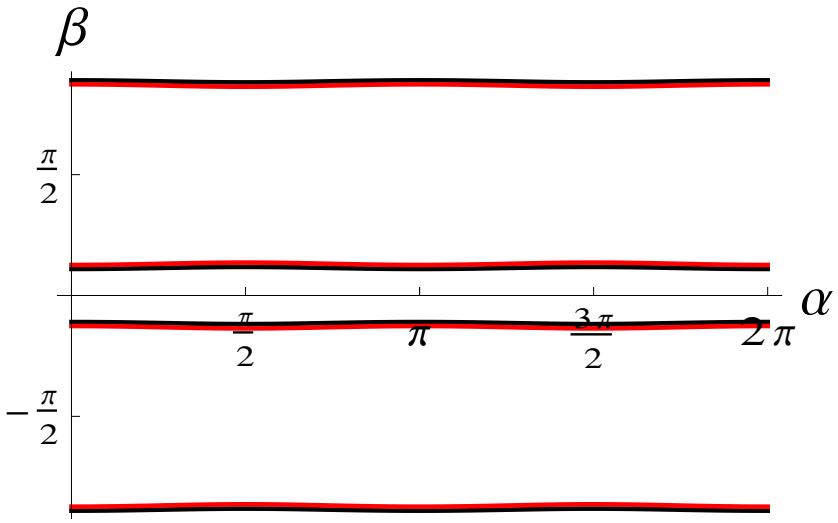

(a) The intersection of the surfaces $\sigma_\perp$ (red) and $\sigma_\parallel$ (black) with the planes representing the experimental values obtained for the transmembrane peptide KALP cut a topologically open curve $\beta = f(\alpha)$. The function present no restrictions in α, that may assume freely all the values from 0 to 2π. Even so, the angle β is limited to the region 22.7°-24.5°.

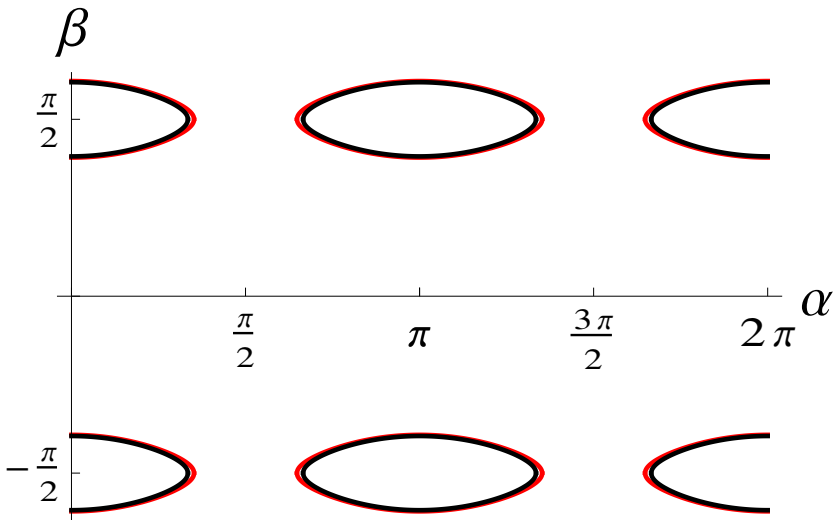

(b) The intersection of the surfaces $\sigma_\perp$(red) and $\sigma_\parallel$ (black) with the planes representing the experimental values obtained for the transmembrane peptide KL14 cut a topologically closed curve $\beta = f(\alpha)$. The function present restricted values for both α and β: the angle α is limited within $\pm 63.3°$, while the angle β is centered around $\pi/2$, within the range 70.5°-109.5°.

Figure 43: Curves $\beta = f(\alpha)$ obtained from the intersection of the surfaces $\sigma_\perp$ and $\sigma_\parallel$ with the planes representing the experimental values obtained for KALP (a) and KL14(b).

to obtain distortion-free spectra but also permits to deduce the helix orientation respect to the lipid bilayer directly from non oriented samples.

The estimation of the tilt angle is more precise for transmembrane helices, for which the uncertainty over the angle α does not affect considerably the final result. In addition, an averaging effect due to the helix self-rotational diffusion, i.e. the rotation around the helix axis, is expected to be present and to effectively average the angle α, reducing the error on β. For in-plane peptides, the calculation of helix tilt is less precise, but in exchange we obtain a rough indication on the phase of the helix.

It has to be remembered that the method is based on the approximation that the main tensor element of the ^{15}N chemical shift is parallel to the helix axis. In general, the σ_{33} and the N-H vector cover an angle comprised between 15 and 20 degrees [76]. By consequence, an additional error on the tilt angle has to be considered that depends also on the structure of the peptide. Considering an angle of 20 degrees between the main principal component of the chemical shift tensor and the actual helix axis would introduce an error of about 6% on σ_{33}. If the peptide is in a in plane configuration, this error is negligible respect to the uncertainly due to the angle α. On the contrary, it may become the main error source for transmembrane peptide, up to 8 degrees.

The advantage of this approach respect to other methods based on the use of macroscopically oriented membranes is the possibility to explore more physiological sample conditions, allowing, for example, pH and salt concentration control . It permits also a partial gain in sensitivity, due to the improved filling factor of the coil in absence of glass plates, and it eliminates systematic errors due to an imperfect or non-uniform alignment of the sample.

We have to point out that it may be not so straightforward to obtain a stable spinning speed for spinning rates as slow as 50 Hz. Sometimes spinning at few kHz is necessary to distribute the sample and equilibrating it. This process may cause dehydration of the lipids and the accumulation of the sample on the walls of the rotor living the center empty, reducing the performance of the experiment.

However it is not always necessary to spin to obtain a recovered powder patten line-shape: three-dimensional diffusion of the peptide int the lipid environment may be enough to provide the exchange of orientations needed for the MAH refilling. The application of the static version of the RODEO-CP sequence (Native Exchange of Orientations (NEO)) could open to new additional information on the reorientation correlation time of the peptide and hence the strength of the interactions of the peptide with its lipids environment.

Finally, this method is particularly useful in mobile samples such as membrane-associated peptides which have a short $T_{1\rho}$ relaxation time. For these systems the maximum magnetization transfer occur at very short contact times, of the order of hundreds of μs, where the dipolar oscillations are still strongly acting (cf. Chapter A). The use of RODEO allows to drastically shorten the contact time while still keeping undistorted line-shapes with a factor 2 in sensitivity gain (cf. Chapter A).

6

RODEO-CP APPLIED TO ANTIMICROBIAL PEPTIDES IN NATURAL MEMBRANES AND *IN VIVO*

CONTENTS OF THE CHAPTER:

In this chapter we are going to apply the APHH-RODEO-CP method to study of the interaction of the antimicrobial peptide PLAH4, analog of the LAH4 peptide, in complex systems of natural membranes such as the extract of *Escherichia coli* bacterial membrane. We will also presents the first attempt to study an antimicrobial peptide by ^{15}N-solid state NMR directly in living *Escherichia coli*.

6.1 INTRODUCTION

In-cell NMR is very enlightening since it can provide valuable structural information, elucidate interactions and investigate dynamics behavior of biomolecules in their real natural environment (for reviews, see [77, 78]). Investigations of biological macromolecules in living organisms have been developed only in the last 10 years and mainly confined to one-dimensional liquid NMR experiments [79, 80]. Only very recently multidimensional approaches have been explored after high-resolution was established in bacterial cells based on protein over-expression and sample analysis within the same cellular environment [81, 82, 83, 84].

SS-NMR methods were applied by Curtis-Fisk *et al.* [85] to elucidate the residue-specific native conformation of inclusion body proteins in whole cell, bypassing the common problem of the sequestration of the recombinant protein from the large insoluble protein aggregate.

Membrane-active peptides and proteins, so far, are studied only in model systems, as micelles or bi-layers. Rarely in lipid extracts or isolated bacterial membranes [33]. Bacteriorhodopsin in the purple membrane of *Halobacterium salinarium* is one of the few examples available [34, 35, 36]. Concerning antimicrobial peptides, PGLa and other peptides were studied in insulated native membranes [37] and in living bacteria [38] by ^{31}P. Ieronimo et *al*. also studied the orientation of PGLa by ^{19}F NMR [37] including fluoridated amino acid analogs in the peptide sequence. However, the effects of such substitution may alter the protein structure, stability or biological activity [39].

The fact that our method can be efficiently applied, as seen in Chapter 5, to obtain topological information of peptides in non-oriented samples, enable us to extend its application to more complex systems, as natural membranes. This kind of studies may open a new approach to prove the mechanism of action of antimicrobial peptides in the context of sophisticated much more complex membrane systems or *in vivo*. From these studies a more detailed description of the AMPs action may result, accounting for many additional variables that are not easily included in model membrane experiments , such as the complexity of the membrane composition or the role of the glycolipids, etc... . Additionally, the use of unoriented samples permits to obtain a good control over environmental parameters such as pH or salts concentration, that

may affect the oligomeric state of the peptide or the strength of the electrostatic interactions with the lipid surface.

6.2 MATERIAL AND METHODS

Chemicals

PLAH4 (P KKAL LALA LHHL AHLA LHLA LAL KKA-NH2) was produced by our colleague Dr. Vidovic by expression in bacteria as described in [86]. The peptide was further purified by High-Performance Liquid Chromatography (HPLC) and its molecular weight was checked by Matrix-Assisted Laser Desorption/Ionization by Time of Fly (MALDI-TOF) and corresponded with the mass of the fully ^{15}N-labeled peptide.

Escherichia Coli Total Lipid Extract, *EC*- TLE , was purchased from Avanti Polar Lipids and used without further purification.

Sample preparation

PLAH4 in Escherichia Coli *Membrane (PLAH4-TLE)*

70 mg of *EC*-TLE were dissolved in 2 ml of chloroform/methanol 1:1. The lipids were then dried under vacuum in a Rotovapor (Büchi, R200, Postfach, Switzerland) at 37°C for 10-20 minutes to form a film on the walls and successively dried overnight under vacuum to remove all the traces of solvents. 7 ml of 10 mM TRIS-base/85 mM NaCl buffer at pH 7.5 were added. Multilamellar vesicles were formed by 6 freeze/thaw cycles in liquid nitrogen/warm water bath at 38°C. The vesicles were collected after centrifuging overnight and 4.5 mg of peptide were added to reach a final peptide-to-lipid ratio about 2% molar [1]. At this stage the sample separates in a gel-like pellet and a clear solution. After checking the pH (about 5.5), the supernatant was removed by centrifuging. Finally the pellet was transferred in a 4 mm rotor and re-equilibrated in a hydration chamber for 8 hours before proceeding with the NMR experiments.

PLAH4 in In Vivo Escherichia Coli *(PLAH4-IV)*

BACTERIAL STRAINS AND GROWTH CONDITIONS The *Escherichia coli* strains used in this study were XL1-Blue purchased from Agilent Technologies (USA). The bacteria were grown in 10 ml of Lysogeny broth (LB) (20 g/l) with yeast extract (5 g/l) medium and incubated at 37 °C with shaking (200 rpm) overnight. An aliquot of 1ml was further grown in 100 ml fresh media for another 4 hours and an half.

100 ml of bacterial suspension was centrifuged for 20 minutes at room temperature . The pellet was rescued and washed 3 times with 40 ml of Tris 10 mM / NaCl 85 mM sterile buffer prepared at pH 7.5 to remove most of the nitrogen sources present in the medium. 200 µl of buffer were added to re-suspend the bacterial pellet.

SAMPLE PREPARATION FOR NMR A stock solution of 2.8 mg/ml of the peptide was prepared in 10 mM TRIS-base with 85 mM NaCl at pH=7.5. To assure an homogeneous concentration, the solution was

1 Considering an approximate composition of the *Escherichia Coli* membrane as declared from Avanti Polar Lipids: phosphatidylethanoamine 57.5%, phosphatidylglycerol 15.1% and cardiolipin 9.8%.

briefly sonicated just before to add 268 µl to the bacteria pellet re-suspended in 4.73 ml of buffer. This preparation corresponds to an approximate peptide-to-lipid molar ratio on the order of 1-2% [2] and to a final peptide concentration of about 50 µM.

To reduce the volume of the sample, the suspension was centrifuged and the pellet recovered with 300 µl of the same buffer and successively transferred into a 7 mm NMR rotor. This suspension was used also for the viability assay. The exceeding buffer was removed by centrifuging (at 10000 rpm for some minutes). The same procedure was repeated with smaller aliquots (100 µl) until the rotor was full. The total mass of bacterial pellet efficiently inserted in the rotor was about 330 mg. A control sample (232 mg of total weigh of the bacterial pellet) was prepared following the same preparation but without the peptide in order to be sure there was no ^{15}N background signal coming from the bacteria or residual medium.

NMR measurements

Cross-polarization experiments were conducted on membrane (PLAH4-TLS) and bacteria (PLAH4-IV) samples using the previously described APHH-RODEO-CP method. The CP contact time was set at 800 µs for all the experiments.

PLAH4-TLS experiments were conducted on a Bruker AVANCE 500 MHz wide bore spectrometer (Bruker, Wissembourg, France) operating at a frequencies of 500.13 MHz for ^{1}H and of 50.67 MHz for ^{15}N and equipped with a triple resonance MAS probe (operating in double resonance mode) designed for 4 mm zirconia rotors. The axis of the stator was tilted to permit the rotor to spin around 78°±1° respect to the external magnetic field[3]. HH condition and ^{15}N were determined on a reference sample of $^{15}NH_4Cl$ (spectral reference set to 41.5ppm) and successively adjusted on the sample. APHH-RODEO-CP experiment was performed sweeping the nitrogen and proton fields around the HH condition by tangential pseudo-adiabatic pulses (see Figure 44).

Three spectra were acquired at different temperatures: 298 K, 310 K and 273 K. The spinning speeds and mixing times for the three experiments were 71 Hz, 69 Hz, 72 Hz and 2.139 ms, 2.102 ms, 2.106 ms (corresponding to set the exchange angle equal to the magic angle), with a 18% random variation of the mixing time.

The PLAH4-*IV* experiments were carried out at 298K on a Bruker Avance 400 spectrometer (Larmor frequency of 40.54 MHz and 400.13 MHz in ^{15}N and ^{1}H resonance, respectively) equipped with a Bruker CPMAS probe for 7-mm-o.d. rotors in its native configuration (i.e. the rotor axis is at the magic angle). The proton and nitrogen radio frequency fields were first calibrated on a reference sample ($^{15}NH_4Cl$). The proton p_{90} field was successively determined in the sample ($B_{1p_{90}} = 40.3$ kHz) and the contact fields were adjusted accordingly, sweeping the ^{1}H and ^{15}N RF fields through the HH condition from 47.8 to 41.5 kHz and from 47.4 to 35.7 kHz using the tangential time dependencies given

2 Considering an averaged molecular weight for lipid of $811.42 g/mol$ and the fact that in *Escherichia Coli* the lipid contribute to about 2% of the total mass of the bacteria.

3 This configuration has proved to be more efficient in recovering the MAH and to allow a better geometrical coupling with the static magnetic field (data not included in the thesis work). The angle ϑ between the spinning axis and the static magnetic field B_0 was derived by the scaling of the CSA tensor with respect to the isotropic frequency by the factor of $\frac{1}{2}(3\cos^2\vartheta - 1)$[87].

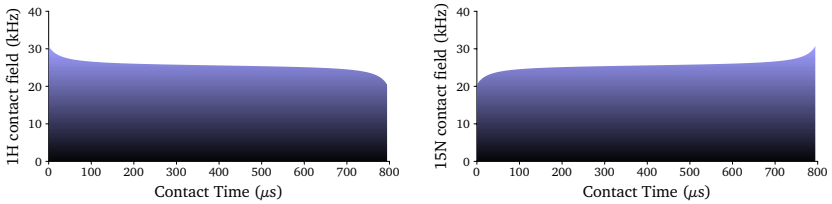

(a) Proton contact field.

(b) Nitrogen contact field.

Figure 44: Proton and nitrogen shaped-pulses used during the CP step used to record the APHH-RODEO-CP spectra on PLAH4-TLE sample.

in Figure 45. The recycle time was 4s and 75736 scans were recorded. A left shift of 2 points and a Lorentzian broadening of 300 Hz were applied prior to Fourier transform. The MAS frequency was fixed at 53 Hz and the applied mixing time (7.075 ms) was calibrated to randomly scan all values corresponding to the interval needed by the rotor to cover from 1/4 to 1/2 of the period.

The contact time of the CP step was kept constant to 800 μs and an Hahn-echo refocusing pulse has been included in all the experiments before the acquisition to overcome the dead time problem. Proton decoupling during acquisition and echo times was performed by SPINAL-64 [66].

Viability tests

To check how the bacteria were responding to the stress conditions over the time spent in the rotor (absence of oxygen and nutrients) and to the presence of the peptide, viability tests were conducted in parallel to the NMR measurements by colonies counting on LB agar gelose.

Several aliquots of bacterial pellet (20 μl) were taken at different times: t_0, coincident with the starting of the NMR experiment, t_1, t_2,t_3 corresponding to 12, 24 and 48 hours later, and t_4 after the NMR recording was finished (96 hours later).

Each aliquots was diluted in 10 ml (dilution 1: $1 \longrightarrow 500$) of buffer and used for a serial 100-fold dilutions in 5 falcon tubes (dilution 2: $1 \rightarrow 5 \cdot 10^4$, dilution 3: $1 \rightarrow 5 \cdot 10^6$, dilution 4: $1 \rightarrow 5 \cdot 10^8$, dilution 5: $1 \rightarrow 5 \cdot 10^{10}$, dilution 6: $1 \rightarrow 5 \cdot 10^{12}$).

From each dilution, 1 ml of bacterial suspension was taken and incubated in 10 ml of liquid media at 37°C with shaking. After 12 hours, the optical density of 1ml of each bacterial suspension was measured at 600 nm.

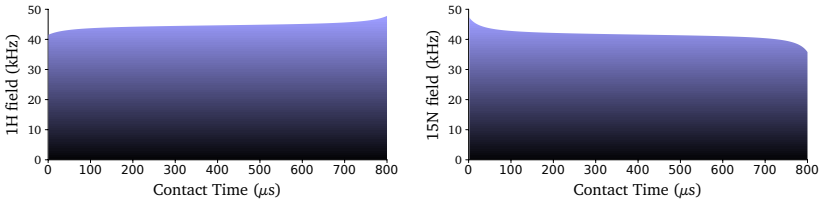

(a) Proton contact field.

(b) Nitrogen contact field.

Figure 45: Proton and nitrogen shaped-pulses used during the CP step used to record the APHH-RODEO-CP spectra on PLAH4-IV sample.

6.3 RESULTS AND DISCUSSION

6.3.1 *Solid-State NMR*

The APHH-RODEO-CP spectra of ^{15}N fully labeled PLAH4 in vesicles of *Escherichia Coli* Total Lipids Extract is reported in black in Figure 46. The spectra, recorded at 310 K, is well fitted by the sum of 6 peaks (A, B, C, D, E) as showed in red below the experimental spectra. The resulting parameters for the fit of the experimental spectrum are reported in Table 13.

The main contribution to the spectrum is coming from the central region, that can be reproduced by the superposition of an anisotropic band spanning from 142 to 78 ppm (cf. spectra A in Figure 46) and two isotropic peaks centered at 127 and 118 ppm (cf. B and F in Figure 46). The anisotropic spectra has the shape already seen in Chapter 5 for the in-plane peptide KL14 in unoriented POPC when subject to uniaxial motional averaging. It has to be noted, however, that here several amino acids contribute to the resonance band, since all nitrogens in the peptide sequence are labeled. Due to the superposition of all these contributions, we can derive only an averaged orientation of the peptide with respect to the membrane normal and not a local information on the orientation at the site of a specific residue. We can better understand this point if we have a look to the CSA tensor parameters from ^{15}N-alanine and ^{15}N-leucine labeled peptides measured from other authors and reported in Table **??**. The hypothesis of a large part of the peptide diffusing on the plane of the membrane is confirmed by the absence of signal in the $180 - 220$ ppm region, where the σ_{33} components of each ^{15}N tensor should appear. 18 amino acids over the total 27 of the peptide are leucines and alanines, so we can assume that a big part of the signal is coming from the superposition of the signals of these amino acids. Since the influence on of the structure, hydrophobicity of the environment, and of neighboring amino acids, although existing, it is only marginal

[76], we can, in first approximation, use the same average CSA tensor parameters for all the amino acids, disregarding their position in the sequence and all the other environment differences that they may be subjected to. If we assume that a large part of the peptide is subject to motional averaging on the membrane surface, then we can insert averaged values proposed in [76] in equation (5.5) and equation (5.6) to obtain an indication on the range of the $\sigma_{\parallel}$ and $\sigma_{\perp}$:

$$\begin{aligned} \overline{\sigma}_{11} &= 58\text{ppm} \\ \overline{\sigma}_{22} &= 81\text{ppm} \\ \overline{\sigma}_{33} &= 225\text{ppm} \end{aligned} \longrightarrow \begin{cases} \alpha = \frac{\pi}{2}: & \sigma_{\parallel} \approxeq 81\text{ppm}, & \sigma_{\perp} \approxeq 142\text{ppm} \\ \alpha = 0: & \sigma_{\parallel} \approxeq 58\text{ppm}, & \sigma_{\perp} \approxeq 153\text{ppm} \end{cases}$$

The estimated values of the averaged powder pattern shoulder and inflection point of an α-helical peptide of generic composition, with its axis parallel to the membrane surface, fall into the range 58-81 ppm for $\sigma_{\parallel}$ and 142-153 ppm for $\sigma_{\perp}$. In facts, the our peptide is constituted mainly of alanines and leucines, that have negligible differences in their values of chemical shift. In addition, since in our case all the amino acids are labeled, we can expect the angle α to assume all the possible values between $[0, 2\pi]$. The shoulder and discontinuity of the peak A found in Figure 46 are located respectively at 142 and 78 ppm, close to the estimated values previously discussed. Considering the low resolution of the spectra and the fact that the values of the tensor parameters we used are derived from other compounds and other experimental conditions, we can conclude that the hypothesis of a large part of the peptide undergoing to motional averaging on the surface of the membrane is reasonable.

On the top of the broad averaged in-plane resonance of the amide bonds we can see rising an isotropic peak (B), centered at 118 ppm and an additional isotropic peak could be introduced to fit the missing intensity on the $110 - 120$ ppm region (F).

The presence of isotropic peaks in the back-bone region may be explained considering a second population of the peptide not associated with lipids or associated with small vesicles, monomeric or in an aggregate form, that still can move relatively freely in the aqueous phase of the sample. Although this is a minor component of the sample, the centrifuge force to which the rotor is subject (especially in the preliminary step needed to spin-lock the spinning speed, when the sample rotates as fast as $1 - 2$ KHz) may partially extract water initially present between lipid layers and create a separated bulk-water phase on the top of the lipids.

A second reason for the presence of isotropic contribution to the spectra intensity is related to the motion of the unbounded regions of the peptide. While ^{15}N nuclei of atoms deeply involved in the lipid-peptide interactions are subject to restricted motions, labels located in less bounded zones of the peptide may undergoes to fast and more isotropic motion. This has to be be the case, for example, of proline, since it is located at the very end of the peptide sequence [4]

The other sharp peaks (C, D and E) in Figure 46 may come from isotropic motions of ^{15}N in lateral chains or lipids.

4 Unfortunately, we cannot assign its peak because no data are available in the SS-NMR literature for amine ^{15}N-labeled proline.

	A	B	C	D	E	F
σ_{iso} (ppm)	120.5±0.2	118±7	56±2	36±1	180±5	127±5
σ_{CSA} (ppm)	-42.4±0.2	0	0	0	0	0
η	0	0	0	0	0	0
Intensity (a.u.)	$100 \cdot 10^6$	$19 \cdot 10^6$	$15 \cdot 10^6$	$16 \cdot 10^6$	$13 \cdot 10^6$	$51 \cdot 10^6$
Line width (Hz)	597	683	168	136	478	526

Table 13: Parameters fitting the experimental spectra of Figure 46. The fit was performed by Top Spin software (Bruker) from 300 to -100 ppm and considering static conditions. The best overlap with the experimental spectrum after 1000 iteration cycles was of 94.74%.

The histidine lateral chain (Figure 47) may assume, under conventional conditions, three protonation states: the cationic state (imidazolium), with one positive charged shared between the two protonated ring nitrogens, and two neutral states of different tautomeric forms, with only one protonated nitrogen, either the N^{ϵ} or the N^{δ}. Wei *et al.*[5] studied the isotropic chemical shifts of the imidazole ring nitrogens for crystalline histidine-containing samples in histidines as charged and neutral species. The values, averaged over several compounds, are reported in Table 14. They could not detect any significant differences between the tensor values for the N^{δ} and the N^{ϵ} but they found much higher isotropic chemical shifts for deprotonated nitrogens then those for protonated ones. Considering the difference of referencing (we set the $^{15}NH_4Cl$ peak to 41.5 ppm) the peak E in Figure 46 is compatible with the isotropic signal coming from the protonated nitrogens in the indole group of histidines lateral chains, probably in the cationic state, as is reasonable to suppose at acidic pH.

The peak D, centered at 36 ppm, is probably coming from the ^{15}N of lysine lateral chain (see Figure 47). This sharp peak has is in good agreement with the of 34±3 ppm of the averaged isotropic chemical shift found from liquid NMR measurement (see http://www.bmrb.wisc.edu/ref_info/statsel.htm).

Gabellier *et al*. reported the signal of ^{15}N phosphocholine appearing around 43-44 ppm [88], so we can speculate that the peak located around 55 ppm belongs natural abundant ^{15}N present in the phosphocholine heads of lipids. Another possibility would be that this peak is the signal coming from the N-terminal proline. Indeed, end-term amino acids are subject to fast pseudo-isotropic motions that could explain the sharpness of the signal, but, at the best of our knowledge, no literature data are available for the isotropic chemical shift of this amino acid in the amine form.

In Figure 48 the ^{15}N cross-polarization spectra of PLAH4 in TLE at three different temperatures are shown. The dynamic of the peptide in *EC*- TLE does not change significantly decreasing the temperature from 310 to 298 K. While signals from lateral chains of lysines and ^{15}N phosphocholine heads as well as the main central band conserve their

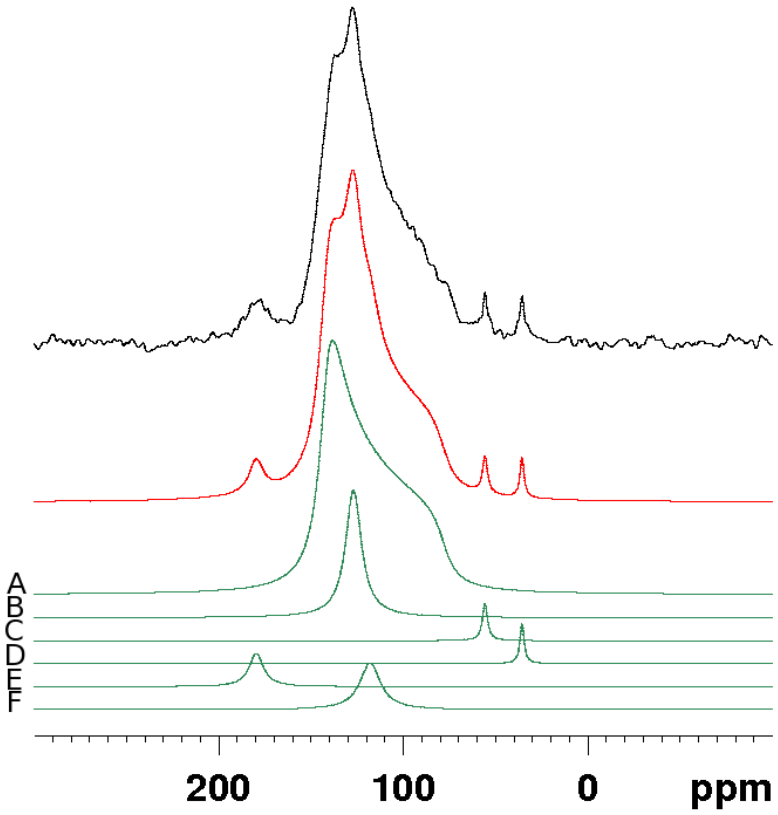

Figure 46: APHH-RODEO-CP experiment on $PLAH_4$ in unoriented *EC*- TLE performed at 310K. In black at the top: experimental spectra. In red: fit of the experimental spectra. In green: decomposition of the fitting spectra in its components: one broad peak corresponding to an axially symmetric tensor and five smaller isotropic peaks.

Histidine	atom	σ_{iso} (ppm)	N state	σ_{iso} (ppm)
neutral species	$^{15}N^{\delta 1}$	200±40	protonated	176±3
	$^{15}N^{\epsilon 2}$	182±6	deprotonated	252±2
cationic species	$^{15}N^{\delta 1}$	240±40	protonated	181±7
	$^{15}N^{\epsilon 2}$	180±9		

Table 14: Isotropic chemical shifts of the imidazole ring nitrogens for crystalline histidine-containing samples. Data averaged from [5]. Errors are calculated as the standard deviations of each data ensemble. Original data are referenced setting the peak of $^{15}NH_4Cl$ to 35.9 ppm downfield from that of liquid ammonia at -50°C, we added here 5.9 ppm in order to confront them with our reference scale ($^{15}NH_4Cl$ to 41.5 ppm).

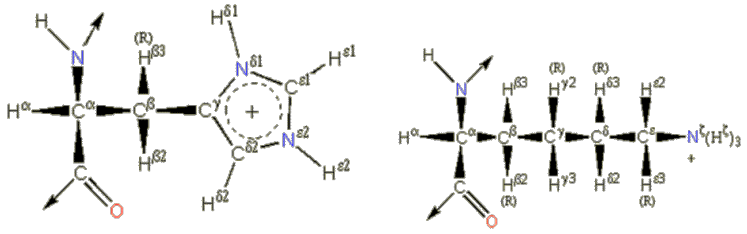

(a) Histidine residue. N is the nitrogen atom of the backbone while $N^{\delta 1}$ and $N^{\epsilon 2}$ identify the two nitrogen atoms present in the indole group of the lateral chain.

(b) Lysine residue. N is the nitrogen atom involved in the peptide bound while N^{ζ} is the lateral chain nitrogen.

Figure 47: Lateral chains of histidine and lysine. Pictures adapted from http://www.bmrb.wisc.edu/.

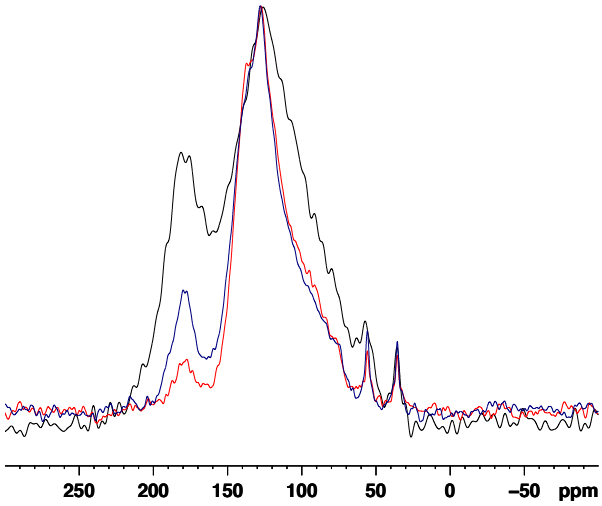

Figure 48: APHH-RODEO-CP experiment on PLAH4 in unoriented *EC*- TLE . In red: 310K. In blue: 298K. In black: 273K.

intensity and line-width, a strong intensity increase is visible from the histidines indole group region (195 − 180 ppm). The gain in intensity is related with a more efficient magnetization transfer when the lateral chain motions are slowed down.

Decreasing the temperature down to 273 K, also the line-width of all the peaks, except for lysines, is increasing. The temperature decrease may drive part of the lipids through a phase transition. In the gel phase, the lipids are more usually stiff and packed, with consequently reduced insertion and mobility of the whole peptide. Interestingly, the lateral chains of lysines are not affected by this general reduction of the dynamics, maybe because lysines are involved in specific motions related to their role as anchors [89].

In Figure 49 the ^{15}N spectra of PLAH4 in Escherichia coli obtained by the APHH-RODEO-CP sequence is shown. The total amount of time spent to record the spectra was about 4 days. The resolution is too low to proceed with an accurate analysis of the spectra. We can however distinguish a large band arising from the backbone region (70 − 200 ppm) and an additional peak centered around 40 ppm. This last peak is arising from the sum of the signals coming from the lysines lateral chains and nitrogens present in the lipids, such as the phosphocholine heads. The main signal coming from the backbone does not show clear features to drive a reasonable fitting process. The a broad peak around 120 ppm is probably due to the isotropic signals of the alanine, leucine, lysine and histidine amides. The peak appearing near 80 ppm is probably part of a powder pattern, however, due to the poor resolution, it is hard to tell if we are dealing with a static or an averaged powder pattern. The static powder pattern would be in agreement with the tendency to form aggregates of the analogous peptide LAH4 at physiological pH conditions. Their size was found to be limited to few tens of nanometers [90], suggesting a good degree of mobility, but we can not exclude the increase of their size or the reduction of their mobility

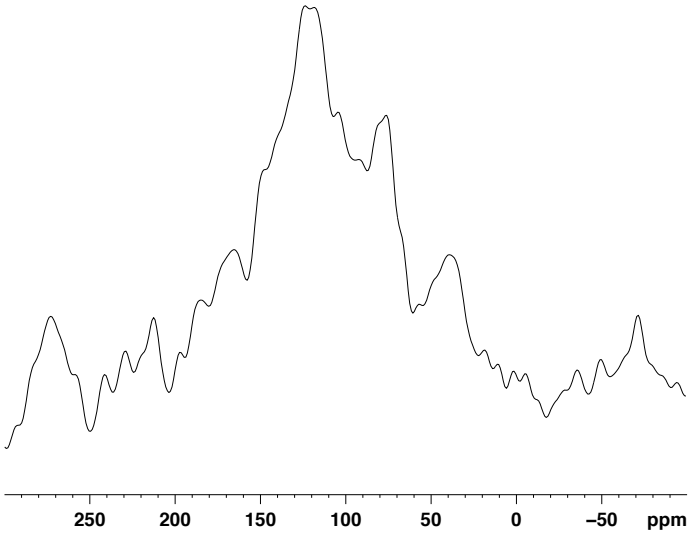

Figure 49: APHH-RODEO-CP experiment on PLAH4 in *Escherichia Coli* performed at 298K. The total amount of fully labeled peptide was less then 0.75mg.

when in presence of sterols or glycolipids. On the other hand, the idea of an averaged powder pattern line-shape as the one found for KALP in Chapter 5 would be sustained by the capability of LAH4 to assume a transmembrane orientation when the pH is increased towards neutral values [91].

It is interesting to compare the results obtained in *Escherichia coli* with the spectra acquired in the membrane. The presence of an in-plane averaged powder-pattern as in the spectra in Figure 46 is no longer evident when the same experiment is performed in *Escherichia coli* (Figure 49), suggesting that the peptide-lipid interactions are modified when we move from a model system to *in vivo*.

6.3.2 *Viability tests*

The response to the absence of oxygen and nutrients in the rotor was evaluated after several stocking times, from 0 (beginning of the NMR experiment) up to 96 hours (end of the NMR experiment) in presence and absence of PLAH4. The evaluation was performed both by optical density measurement after re-growth of bacteria in liquid media .

Viability test results measured by optical density are reported in Figure 50. There is no clear distinction in cell population grown in presence or in absence of the peptide, except for the first two dilutions. However it is hard to tell if this difference is significant, since an initial small error in the quantity of bacterial suspension inoculated in the media may cause a big gap in cell population after 12 hours of incubation.

In general, the turbidity increase with the time for all the samples until a maximum is reached, indication of proliferation of the bacteria.

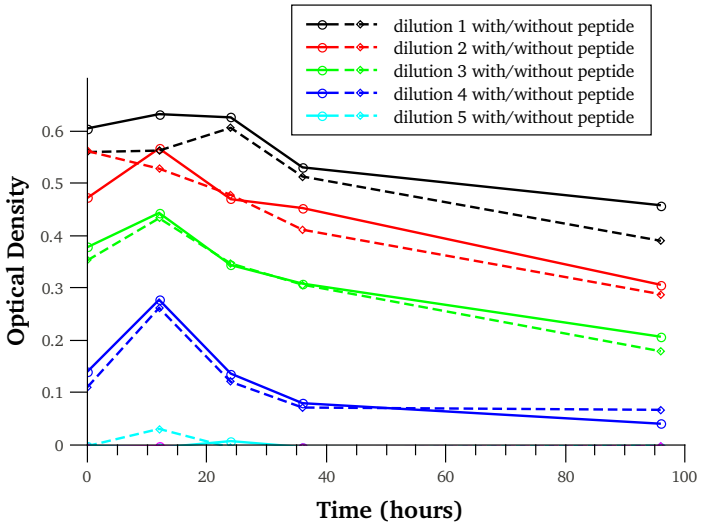

Figure 50: Optical densities in function of the stocking time of bacteria suspension in presence and absence of peptide after 12 hours of growth in liquid conditions. Dilutions 1 to 5 (see text). In the last dilution data were below the instrument accuracy.

At a certain storage time, the optical density starts to decrease and the bacteria give a reduced re-growth after the 4 days required for the NMR experiment. We can estimate a reduction of the bacteria growth of about 30% after 4 days of anaerobic conditions and in the absence of nutrients.

6.4 FUTURE DEVELOPMENTS

In this chapter we demonstrates that it is possible by our method APHH-RODEO-CP to extend the topological and dynamics study of peptides directly in membrane of very complex composition or even directly in microorganisms.

From the measurements done in *lipid extracts from Escherichia coli* we were able to assign a main component of the spectra as the signature of the in-plane configuration of the peptide. We can add to our conclusion that the peptide is still mobile enough to undergo uniaxial motional averaging both at physiological and room temperature. Part of the signal comes from the isotropic region, possibly due to a sub-population of the peptide free in solution or in small peptide or lipids-peptide aggregates.

The experiments on extracted *Escherichia coli* membrane were conducted on a fully ^{15}N-labeled PLAH4, so the results may have only a general interpretation in terms of orientation of the peptide. The use of two dimensional NMR to correlate isotropic and anisotropic chemical shifts may provide the necessary resolution to assign a specific orientation to each amino acid. This approach was already exploited *in vivo* using ultra-slow MAS for metabolic studies [82]. The extension to a 2-dimensional ^{15}N experiment is practicable for a model system

as a fully labeled peptide in a complex lipid matrix, as it gives a good signal-to-noise spectrum in a reasonable amount of time, but this is not the case for a more diluted in-cell sample.

Concerning the APHH-RODEO-CP experiment conducted in *Escherichia Coli*, viability tests showed that the bacteria ability to re-grow was partially affected after spending 4 days in the rotor. This time it is not long enough to allow the record of a 1 dimensional RODEO-CP ^{15}N spectra of satisfying quality at our peptide concentration. However, the fact that the re-grow of the bacteria has shown no major differences in the presence or in the absence of the peptide, suggests that we are still below the critical peptide-to-bacteria ratio necessary to cause a major antimicrobial effect.

To improve the quality of the spectra two strategies may be used, and eventually combined: increasing the sensitivity and/or prolonging the sample life.

Although, as demonstrated in chapter Chapter A, the use of shorter contact times could lead to a gain of a factor 2 in signal-to-noise ratio, this improvement it probably not sufficient to move forward to a 2-dimensional experience. Dynamic Nuclear Polarization (DNP) could provide the sought rise in sensitivity, as it was shown by Becerra et *al.* *[92]* that enhancements up to about 10 for ^{1}H and about 40 for ^{13}C may be reached by microwave irradiation, at room temperature, of the electron spins of doping radicals.

To achieve a prolongation of the sample life, oxygen and other nutrients necessary for the bacteria metabolism should be provided. This may be easily obtained with some modification of existing hardware, as already exist probe-heads that can handle a solution flow down to the microfluidics range for liquid NMR, as well as SS-NMR MAS -flow systems [93, 94] that allows to spin the rotor up to 3 KHz while keeping a reacting gas stream isolated from the carrier. An high MAS speed is not required for the RODEO experiment, it may actually be sufficient the chaotic motion induced by the incoming flow to provide the orientation exchange needed to obtain a powder-pattern like line-shape.

Part III

BIOPHYSICAL STUDIES ON THE ANTIMICROBIAL PEPTIDE LAH4

7

BIOPHYSICAL STUDIES OF LAH4 IN PRESENCE OF CITRATE BUFFER

CONTENTS OF THE CHAPTER:

In this chapter we are going to show that LAH4, which is commonly surface-associated to both zwitterionic and charged membranes at acidic pH, it is capable to insert into the hydrophobic core of the bilayer in presence of citrate ions. The significance of this peculiar behaviour will be discussed in the overall context of membrane-protein interaction.

7.1 INTRODUCTION

THE MEMBRANE Biological membranes are amphiphatic barriers composed of a double layer of lipids and proteins. The thickness of the biological membrane is approximately the thickness of the hydrophobic core of its lipid bilayer, while the proteins embedded inside the membrane can have very different hydrophobic length.

In order to avoid unfavourable exposure of hydrophobic surfaces to a hydrophilic environment, membranes undergo to adaptation processes in response to mismatch conditions. Since proteins are relatively rigid while lipids are more flexible, the hydrophobic match may be more easily achieved by stretching, squashing or tilting of the lipid chains. They can also assemble into another type of aggregate, leading to the disruption of the bilayer phase.

When the hydrophobic region of a protein is too extended to match the hydrophobic bilayer thickness, in order to minimize the exposed hydrophobic area, the protein may aggregate in the membrane or tilt its backbone to reduce the hydrophobic length. Furthermore, it may undergo to conformational changes to adopt a more favourable distribution of the hydrophobic and hydrophilic residues near the solvent-protein or lipid-protein interfaces.

THE PEPTIDE LAH4 is a histidine-rich peptide 26 amino acids long that has been shown to possess both antibiotic [40, 41] and DNA delivery [42, 43] capabilities. The LAH4 sequence is composed of a hydrophobic stretch of alanines and leucines interrupted by four histidines. They are clustered on one face such that an amphipathic helix is formed in the presence of membranes (see Figure 51b). Two lysines at each terminus assure the membrane anchoring and increase the peptides' solubility in polar solvents.

The imidazole side-chain of histidine has a pKa of approximately 6.0. Below a pH of 6, the imidazole ring is mostly protonated and the positive charge is equally distributed between both nitrogens and stabilized by two resonance structures. The pK values of these residues where precisely determined by Bechinger [91] using solution NMR spectroscopy in the presence of dodecylphosphocholine micelles by following the ^{1}H chemical shift of the imidazole protons (pK values found are 5.4, 5.8, 5.9, and 6.0). Because of the protonation of the imidazole rings, LAH4 increases its overall net charge from +5 to +9

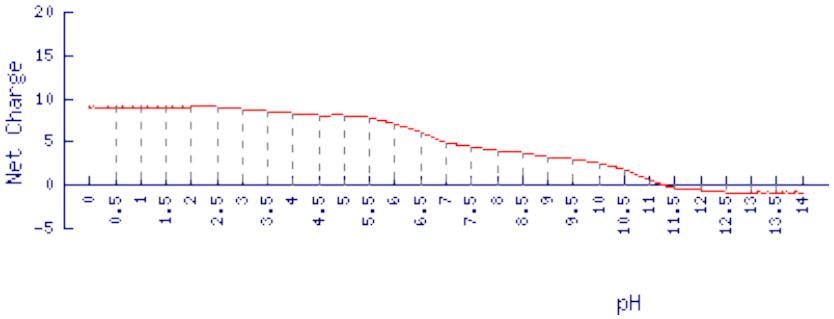

(a) Nominal charge of the peptide at different pHs.

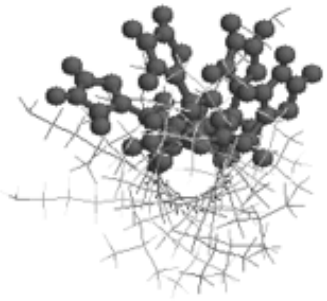

(b) Helical wheel diagram for LAH4 (reprinted from [41]).

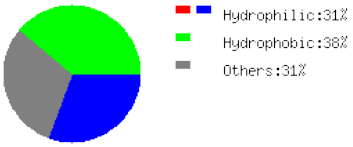

(c) Percentage of hydrophilic and hydrophobic residues in LAH4.

Figure 51: LAH4 properties. Nominal charge and hydrophobicity residue distribution calculated by the on-line tool developed by GenScript USA Inc. (USA) available at https://www.genscript.com/ssl-bin/site2/peptide_calculation.cgi.

in response to the acidification of the environment from the neutral condition to pH ca. 5, as illustrated in Figure 51a.

This property of histidines have been used previously to control the membrane interactions of model peptides, since their orientation in the target membrane depends on the total charge and charge distribution of the peptide. It was shown [40, 44] that at acidic pH, when the histidines are protonated, the LAH4-helix adopts an in-plane orientation at the membrane surface, however, at neutral pH, the uncharged histidine residues can be accommodated in the hydrophobic core of the membrane and the peptide adopts a trans-membrane orientation with the lysine residues acting as anchors at the membrane surfaces.

An overview on published strucural and activity data is reported in Table 15.

THE BUFFER Mixture of sodium citrate and citric acid solutions are commonly used to buffer pHs between 3.0 and 6.2. Citric acid is a polyprotic acid with three dissociation constants: $pK_{a1} = 3.13$, $pK_{a2} = 4.76$, $pK_{a3} = 6.40$. The dissociation process in aqueous solution is described by the three equilibria:

$$\begin{aligned} H_3Cit &\rightleftarrows H^+ + H_2Cit^- & K_{a1} &= \frac{[H_2Cit^-][H^+]}{[H_3Cit]} \\ H_2Cit^- &\rightleftarrows H^+ + HCit^{2-} & K_{a2} &= \frac{[HCit^{2-}][H^+]}{[H_2Cit^-]} \\ HCit^{2-} &\rightleftarrows H^+ + Cit^{3-} & K_{a3} &= \frac{[Cit^{3-}][H^+]}{[HCit^{2-}]} \end{aligned}$$

pH controlled by	orientation	ref.	lipids	technique
+NaOH	depending on pH	[44]	POPC	OSS-NMR*
phosphate	depending on pH	[95]	POPC	ARFTIR
+NaOH	depending on pH	[91]	POPC	OSS-NMR
acetate (?)	50%, pH6	[96]	POPC	OSS-NMR

(a) Topological studies of LAH4 peptide by direct alignment measurements.

pH controlled by	structural information	ref.	lipids	technique
citrate	helix	[44]	SDS	liquid NMR*
acetate	random (13 -26% helical content at pH4.5 and 5.5)	[40]	-	CD
Tris-HCl (pH7.5)	weakly helix (39% helical content)	[40]	-	CD
ethanolammina (pH8.5)	weakly helix (43% helical content)	[40]	-	CD
acetate	weakly helix (55% helical content)	[40]	POPC	CD
acetate	helix (70%helical content)	[40]	POPG	CD
acetate/Tris-HCl	Triptophane emission red shifted at pH5 (acetate) respect to pH7 (Tris-HCl)	[40]	-	fluorescence*
acetate/Tris-HCl	Triptophane emission blue shifted in presence of liposomes	[40]	POPC	fluorescence*

(b) Structural information of LAH4 peptide by in solution or in presence of membrane mimicking systems.

pH controlled by	membrane disruption activity	ref.	lipids	technique
acetate	same as pH7	[40]	POPC /POPG	calceine release
acetate (?)	bigger and faster at pH7	[46]	POPC /POPS	calceine release
citrate	AM activity>>pH7	[45]	Ecoli	OD_{600}

(c) Membrane perturbation efficiency of LAH4 measured as calceine release from liposomes or as antimicrobial activity on Escherichia Coli.

Table 15: Overview of structural and activity data of LAH4 from the literature. *An LAH4-analogue was used. (?) unclear from the text.

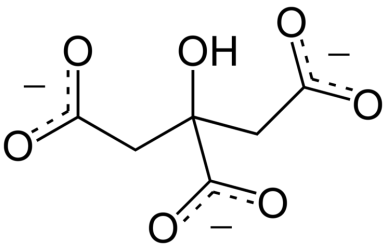

(a) Citrate anion ($C_3H_5O(COO)_3^{3-}$).

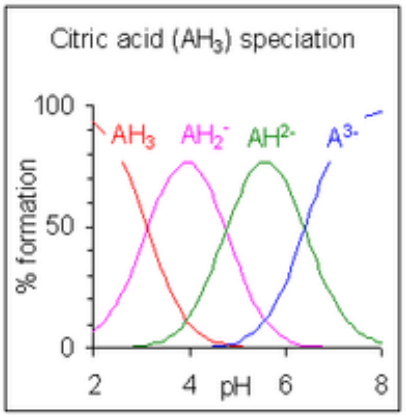

(b) % species formation for a 10 millimolar solution of citric acid at various pH.

Figure 52: Citric acid and chemical speciation in function of the pH of the solution.

Citric acid is a slightly stronger acid than typical carboxylic acids because the anion (see Figure 52a) can be stabilized by intramolecular hydrogen-bonding from other protic groups on citric acid. At pH=5, in solution are present most exclusively citric acid mono- and bi-hydrate ions, with almost identical concentration (cf. Figure 52b).

In this chapter we are going to show that LAH4, which is usually surface-associated to both zwitterionic and charged membranes at acidic pH, it is capable to insert into the hydrophobic core of the bilayer in the presence of citrate ions.

7.2 MATERIAL AND METHODS

7.2.1 *Chemicals*

LAH4 (KKAL LALA LHHL AHLA LHLA LAL KKA-NH2) and LAH4-$^{15}N_3$ peptides were produced by automated solid-phase synthesis using standard Fmoc chemistry on a Millipore 9050 synthesizer. At the 16^{th} position for LAH4 and at the 6^{th}, 16^{th} and 22^{nd} positions for LAH4-$^{15}N_3$, Fmoc-protected ^{15}N-labeled alanines were incorporated. The purity of the products were checked by MALDI-TOF mass spectroscopy and HPLC and resulted satisfactory. The peptides were successively used without any further purification. All the lipids were purchased from Avanti Polar Lipids Inc. (Alabaster, AL, USA) and used without any further purification. Chloroform and trifluoro-ethanol (TFE) were purchased from Sigma Aldrich.

A concentrated citrate buffer solution was prepared by mixing the appropriate amounts of 0.1 M citric acid and 0.1 sodium citrate solutions. The working buffer was prepared by dilution 1:10 of the stock solution. The final pH was adjusted after dilution by adding few µl of concentrated HCl 1M or NaOH 1M.

7.2.2 *Small angle x-ray scattering*

Sample preparation

Respective quantities of lipids (to give 0%, 1%, 2% and 4% peptide-to-lipids molar ratio) were co-dissolved with 1 mg of peptide in TFE (for POPC) or chlorophorm/methanol 7:3 (for POPG and POPC/ POPG 3:1). Solvents were evaporated under a nitrogen stream to form lipid films and stored under vacuum overnight to remove all traces of solvents. Dried films were re-hydrated by adding the corresponding amount of citrate buffer (10 mM, pH=5.07) to reach a final lipid concentration of about 50 mg/ml. The liposomal preparations were successively subjected to 4 cycles of 1 min of vigorous vortex following by 10 min resting well above the main phase transition of the lipids. 60 µl of each lipid dispersion were filled into 1mm thick quartz capillaries, sealed, and equilibrated for 10 minutes at each temperature before the experiments.

SAXS experiments

SAXS diffraction experiments were performed on a modified Kratky compact camera (HECUS X-ray System 3, Graz, Austria). Ni-filtered CuK_α radiation ($\lambda = 1.54$ Å) was generated from a x-ray tube generator (Seifert, Ahrensburg, Germany) operating at 2 kW. The x-ray beam size was 0.5 mm $\times$ 3.5mm and the camera was equipped with linear, one-dimensional, position sensitive detectors (PSD 50-M, HECUS, Graz, Austria). Calibration of the small-angle region was performed with silver stearate. 1800 s of exposure time was used .

SAXS data were back-ground corrected and analyzed using the program GAP (global analysis program) described in [4, 97, 98]. From the full q-range analysis we were able to deduce the membrane thickness as:

$d_B = 2(z_H + 2\sigma_H)$

where the parameters z_H and σ_H are respectively the position and width of the Gaussian used to describe the electron-density of the head group. The membrane *hydrophobic* thickness, d_{CC}, was derived as: $d_{CC} = d_B - 10$Å [4, 99].

7.2.3 *Oriented Circular Dichroism*

Sample preparation

To investigate if the citrate is affecting the peptide alone or if it requires the presence of the lipids to pre-form some sort of supra-molecular assemblies, we measured the Oriented Cicular Dichroism (OCD) of LAH4 in DMPC prepared by two different methods. One sample was made by co-dissolving lipids and peptide together before adding the buffer, and the second was obtained by dissolving first the peptide in the buffer and adding this solution to the pre-formed lipid film.

For the first sample, 1.9 mg of $LAH4_{3\times^{15}N}$, dissolved in TFE, were dispersed, by vigorous vortex mixing, in 25 mg of DMPC dissolved in few hundreds of microliters of a chloroform/methanol (1:1) solution. The solvents were evaporated by a nitrogen stream and all residual traces were eliminated by vacuum for at least 2 hours. The dried film was re-hydrated with 500 µl of 10 mM citrate buffer prepared at pH

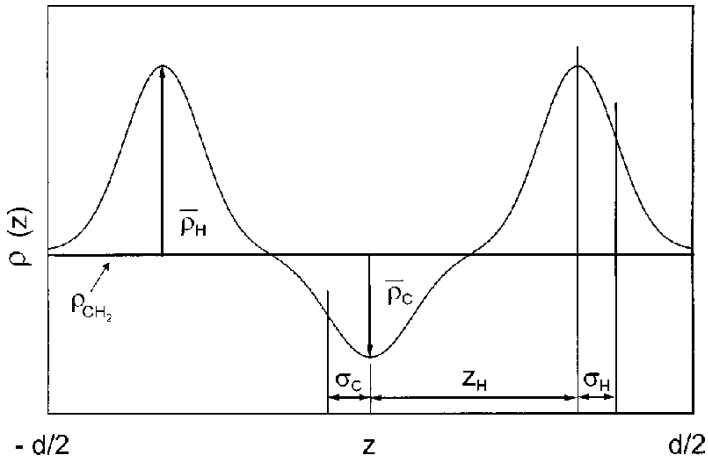

Figure 53: Definitions used for the calculation of the membrane thickness. d = lamellar repeat distance. z_H =position of the headgroup Gaussian of the electron density profile. σ_H =standard variation (width) of the headgroup Gaussian.σ_C = standard variation (width) of the Gaussian describing the hydrocarbon tails. ρ_C = amplitude of the tail Gaussian relative to that of the headgroup Gaussian. Adopted from 4.

4.8. An aliquots of 30 µl was spread on the top of a quartz window. Once dried, the window was placed in a closed chamber in contact with a saturated solution of potassium nitrate. After one night, the hydrated lipid film was squeezed with the help of a second quartz window, avoiding to exert any kind of torsions or shear forces. The two windows were then placed in a cell-holder and stored in the hydration chamber before to proceed with the CD measurements. The surface covered by the film was a circular spot of about 17 mm in diameter. A baseline sample was prepared, by the same procedure, with 25.5 mg of DMPC in the absence of peptide.

For the second sample, 25 mg of DMPC were dissolved in a few hundreds of microliters of a chloroform/methanol (1:1) solution. The solvents were evaporated by nitrogen stream and all residual traces were eliminated under vacuum for at least 2 hours. 1.8 mg of $LAH4_{3\times^{15}N}$ were dissolved in 500 µl of citrate buffer 10 mM prepared at pH 4.8 and added to the lipid film by steps of 100 µl followed by vigorous vortex mixing. After incubation for two hours at 310 K, the sample was mixed by vortexing again. After one hour 30 µl of solution was deposited on a clean quartz window, dried, re-hydrated and sealed as the previous sample. The surface covered by the film was a circular spot of about 15 mm of diameter. A new baseline sample was prepared with 25.1 mg of DMPC by the same procedure but in the absence of peptide.

Oriented CD experiments

Spectra were recorded on an Aviv 62DS spectropolarimeter, scanning the wavelength in the range 178-280 nm by 1 nm steps with 1 nm of bandwidth and an averaging time of 2 s. Three scans were averaged for each spectrum. In order to minimize linear dichroism artefacts arising from inhomogeneities of the sample or the quartz plates, the cell was positioned in a special holder that could be rotated in the plane

perpendicular to the incident light beam, as already proposed by Vogel *et al.*[100]. CD spectra were recorded every 45 degrees of rotation of the cell and the 8 spectra were subsequently averaged. Spectra were baseline corrected and scaled to zero based on the intensity measured between 255-265 nm.

7.2.4 *Solid-state NMR*

Sample preparation

LAH4 IN PRESENCE OF CITRATE BUFFER 23.4 mg of DMPC were dissolved in chloroform/methanol (1:1) within a glass test-tube. Solvents were evaporated using a nitrogen stream and the film was exposed to high vacuum over night to remove the residual traces of solvents. Successively, lipids were re-suspended with 500 µl of $LAH4_{3\times^{15}N}$ solution (8 mg/ml) in 10 mM citrate buffer pH=4.8 and the suspension was spread over 25 thin glass plates (9×22mm). About 10 µl of solution was deposited on each plate. After gently drying under a stream of nitrogen and re-hydration overnight at 313 K in a closed chamber in presence of a saturated solution of potassium nitrate, the glass plates were stacked on top of each other, wrapped with Teflon® tape and sealed in plastic wrapping.

LAH4 IN THE ABSENCE OF BUFFER To verify that the insertion of LAH4 is due to an interaction of the peptide with the citrate buffer and not a direct effect of the peptide with the lipids, we tested another sample prepared in absence of buffer. About 2 mg of $LAH4_{3\times^{15}N}$ were co-dissolved with 20 mg DMPC in chloroform/methanol (1:1) within a glass test-tube. Solvents were partially evaporated using a nitrogen stream and the concentrated solutions were spread on 15 thin glass plates. The glass plates were exposed to high vacuum over night to remove the residual solvent. For the re-hydration and sealing, we proceeded as done for the previous sample.

Samples of LAH4 in POPC, POPG and mixed POPC/POPG 3:1 were prepared in absence of buffer following the same procedure.

Solid-state NMR experiments

The oriented SS-NMR experiments were performed on a Bruker Avance 300 spectrometer (Larmor frequency of 30.43 and 300.33 MHz in ^{15}N and ^{1}H resonance, respectively) with a triple-resonance SS-NMR probe modified with flattened coil. Proton-decoupled ^{15}N SS-NMR spectra were acquired using adiabatic passage though Hartmann-Hahn condition cross polarization (APHH-CP) with a contact time of 800 µs. Nitrogen and proton fields were swept trough the HH conditions using the tangential time dependence give in [63]. Before Fourier-transformation an exponential apodization function corresponding to a line broadening of 200 Hz was applied. The recycle delay was set to 3 s.

7.3 RESULTS

Small Angle X-ray Scattering

SAXS experiments were performed to address the effect of LAH4 on the membrane thickness of the lipids.

In Figure 54 are reported the SAXSs, on a logarithmic scale, for POPC (Figure 54a), POPG (Figure 54b) and POPC/POPG 3:1 (Figure 54c) in absence and in the presence of 1%, 2% and 4% LAH4 (peptide-to-lipid molar ratio). All the data from our lipid dispersions exhibit diffuse scattering, which become dominant, in the presence of the peptide, at higher scattering angles. The presence of diffuse scattering is the signature of positionally uncorrelated bilayers [98], e.g., layers that do not "see" each other because of defects, undulations, or other reasons, such as the presence of **LUV!** (LUV!)s. The absence of Bragg peaks of higher order then two or three is characteristic for fully hydrated samples in the fluid L_α phase and we found two *quasi*-Bragg peaks in the SAXS profile of POPC in absence of peptide (cf.Figure 54a). All the other samples do not present Bragg peaks except for the mixed membrane at the highest peptide concentration studied (cf. Figure 54c). The pure diffuse modulations originating from positionally uncorrelated bilayers are the result of electrostatic repulsion of the anionic lipids. In the zwitterionic liposomes, it may be due to the electrostatic interactions caused by the presence of the peptide.

From the scattering vector profiles, we derived the electron density profiles, that are reported in Figure 55, and from them, we estimated the membrane thickness (Figure 56).

All the samples present the same pattern of membrane response in presence of the peptide: a first increase of the membrane thickness is registered for low concentrations (1-2 % molar peptide-to-lipids) followed by a second phase in which the membrane thickness decreases, at higher peptide-to-lipid ratios. The variations of the hydrophobic membrane thickness after addition of at various concentration of LAH4 are reported in Table 16.

The maximum increase in membrane thickness occurs in bilayers constituted of pure POPC (about 2.3 Å) while it is much milder in negatively charged lipids (<0.6Å) and it has an intermediate character in the mixed membrane ($\lesssim$1 Å).

For the zwitterionic membrane, after a first increase in membrane thickness, adding more peptide tends to bring back the system to the initial membrane thickness of pure POPC, indicating a different interaction mode with less effect on the lipid packing.

For negatively charged membranes, the modifications of the membrane thickness are less pronounced, with only a slight increase at low concentrations. Interestingly, when the peptide/lipid ratio reaches 4%, the hydrophobic core of the bilayer appears thinner respect to the pure POPG, indicating that a different mechanism is acting on the membrane.

Concerning the mixed membrane, we can see that its hydrophobic thickness matches the hydrocarbon chains length of the negatively charged membrane, suggesting that a partial stretch of the POPC tails is already occurring in absence of the peptide. Exposing the lipids to small concentrations of LAH4 ($\lesssim$ 2% molar), the membrane responds

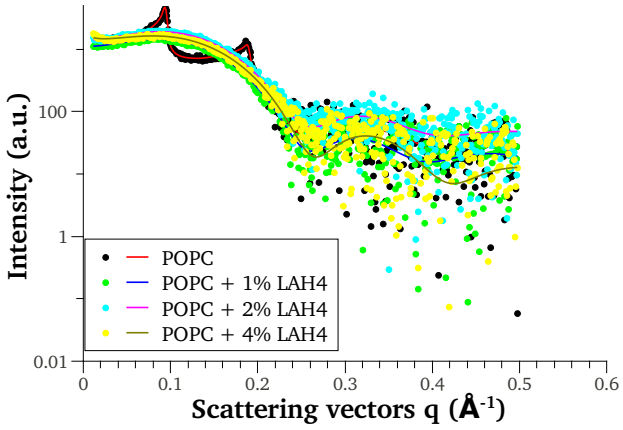

(a) Small angle scattering of POPC in the absence of LAH4 and in the presence of 1%, 2% and 4% peptide-to-lipid molar ratio.

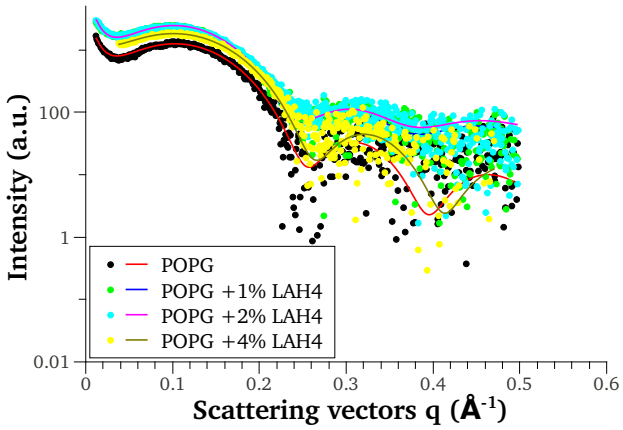

(b) Small angle scattering of POPG in the absence of LAH4 and in the presence of 1%, 2% and 4% peptide-to-lipid molar ratio.

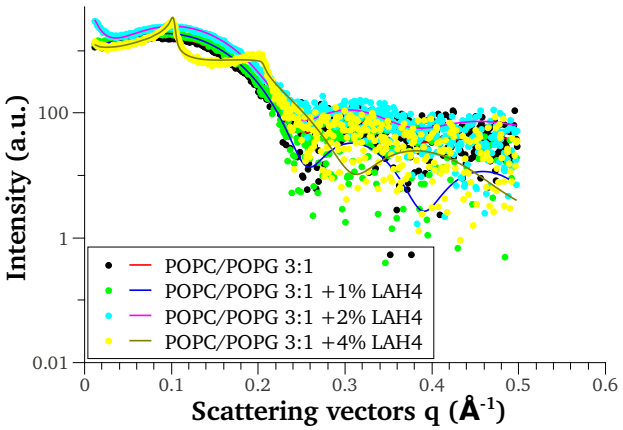

(c) Small angle scattering of POPC / POPG 3:1 in the absence of LAH4 and in the presence of 1%, 2% and 4% peptide-to-lipid molar ratio.

Figure 54: Small angle scattering of POPC, POPG and POPC/POPG 3:1 in the absence and in the presence of 1%, 2% and 4% LAH4 (peptide-to-lipid molar ratio). Full circles represent the observed intensity, lines show model fits to the data.

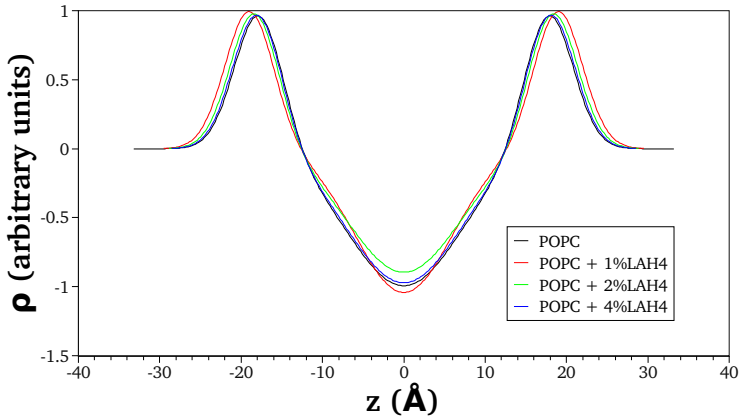

(a) POPC density profiles with increasing amount of LAH4.

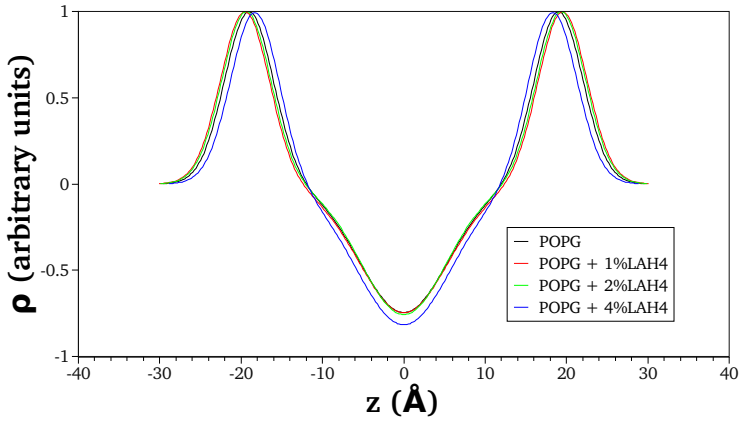

(b) POPG density profiles with increasing amount of LAH4.

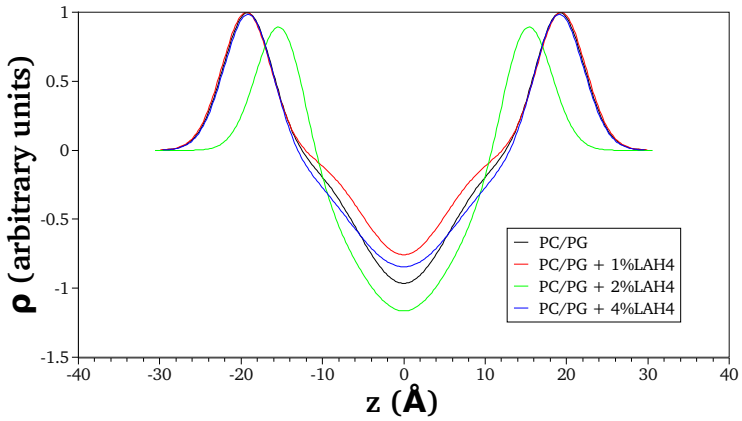

(c) POPC /POPG 3:1 density profiles with increasing amount of LAH4.

Figure 55: Electron density profiles for POPC, POPG and mixed POPC /POPG 3:1 vesicles at 298 K in 10 mM citrate buffer at pH~ 5.

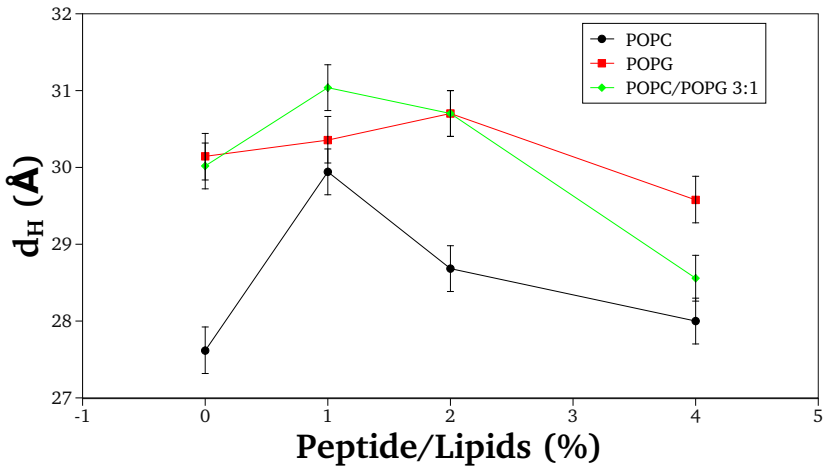

Figure 56: Hydrophobic thickness of the membrane obtained from SAXS data (see 7.2.2) for increasing LAH4 peptide-to-lipids ratios in POPC, POPG and POPC/POPG 3:1 in 10 mM citrate buffer pH 5.

% LAH4	Δd_H (Å)
POPC + 1% LAH4	2.3±0.3
POPC + 2%LAH4	1.1±0.3
POPC + 4%LAH4	0.4±0.3
POPG + 1% LAH4	0.2±0.3
POPG + 2%LAH4	0.6±0.3
POPG + 4%LAH4	-0.6±0.3
PC/PG + 1% LAH4	1.0±0.3
PC/PG + 2%LAH4	0.7±0.3
PC/PG + 4%LAH4	-1.5±0.3

Table 16: Increase of the hydrophobic membrane thickness after addition of LAH4.

with a small but significant stretch of the fatty acyl chains. Higher concentrations of the peptide decrease the hydrophobic thickness of the bilayer, until at 4% peptide-to-lipid ratio. At this concentration there is not only a drastic decrease of the hydrophobic thickness to values close to the pure POPC, but also the Bragg peak reappears. These two fact suggests that the peptide induces a phase segregation leading to pure POPC and POPG domains enriched in peptide.

Oriented Circular Dichroism

To support our interpretation of the SAXS measurements, we investigated the orientation of the peptide in POPC membranes by a more direct approach, as OCD.

The use of circular dichroism to investigate the orientation of polypeptides in membranes is still a technique used only by few despite its

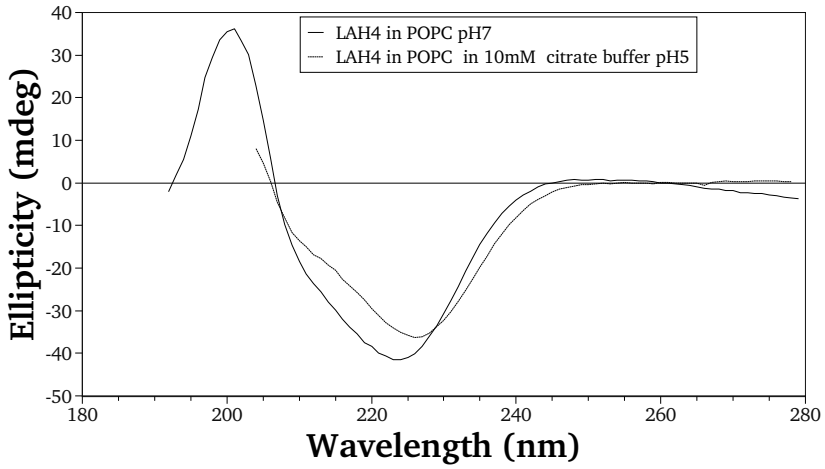

Figure 57: Oriented CD spectra of LAH4 in POPC hydrated films at 30°C. Samples prepared co-dissolving lipids and peptide in organic solvent before to add the buffer. The buffer used were 10 mM sodium citrate/citric acid solution at pH=5 and sodium phosphate monoacid/citric acid solution at pH=7 (final pH in the sample estimated between 6.2 and 6.5). Only the region of the spectra which gave a HT signal below 500 V are considered in the figure. The higher absorption of the sample at pH~7, that prevent us to record an reliable spectrum below 202 nm, is due to the higher amount of sample deposited on the quartz plate (30 µl respect to 10 µl for the sample at pH=5).

low material requirement and relatively cheap set-up. The principle of the method is based on the Moffit's theory [101, 102, 103]. The electronic transitions $n\pi^*$ and $\pi\pi^*$ are the key transitions for proteins in the far ultraviolet region (from ~ 290 to ~ 190 nm). They characterized by transition moments that posses a defined direction with respect to the molecular axis system, so the resulting spectra are sensible to the alignment of the carbonyl bond with respect to the incident light. Specifically, the intensity at 208 nm of an oriented helical polypeptide may be used as a fingerprint of the helix alignment [104].

As we can see in Figure 57, the OCD spectrum of LAH4 at pH~5 resembles closely to the spectrum obtained at neutral pH. The absence of the negative band around 208 nm is the indication that the peptide is aligned parallel to the incident light, meaning inserted in a transmembrane manner.

To better understand the mechanism of insertion of the peptide, we compared the oriented CD spectra of LAH4 in DMPC prepared by two different protocols. In the first case, we co-dissolved in organic solvent the peptide with the lipids to form a homogeneous film and later the film was re-hydrated with citrate buffer. In the second case, the administration of the peptide was done only after lipid film formation, by adding an appropriate amount of peptide dissolved in citrate buffer. The first procedure forces the peptide in an α-helix conformation and favours the peptide-lipid binding, while the second favour the citrate-peptide electrostatic interactions and screen the phospholipid charges. The spectra of these two samples are reported in Figure 58. Both curves

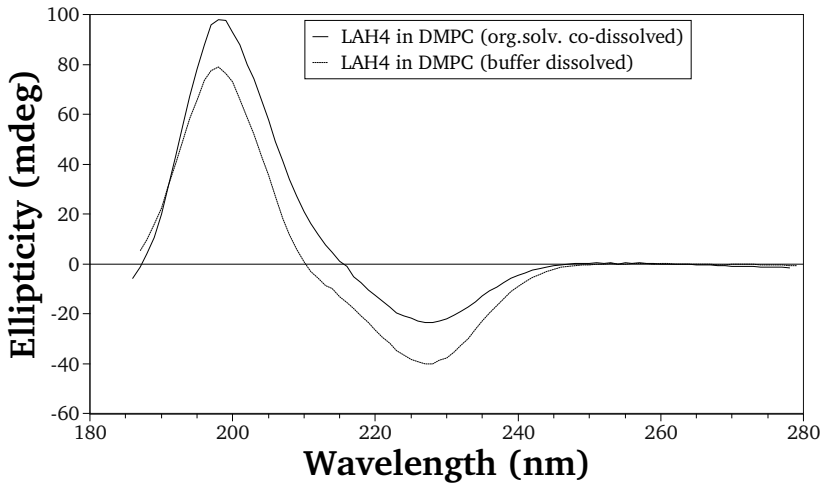

Figure 58: Oriented CD spectra of LAH4 in DMPC hydrated films at 40°C. Samples prepared co-dissolving lipids and peptide in organic solvent before to add the buffer (continuous line) or by adding the peptide dissolved in buffer to the pre-formed lipid film (dashed line). The buffer used was a 10 mM sodium citrate/citric acid solution at pH=5. Spectra recorded at 40 °C. Only the regions of the spectra with below 500 mV are considered in the figure.

present only two peaks, one positive centred around 298 nm, and another negative around 227 nm. In particular, no band around 208 nm is detectable in both spectra, which is characteristic an helical peptide with its axis oriented parallel to the incident beam. The differences in intensity ratio are most probably due to a non-perfect baseline subtraction, due to the high absorption of the lipids and buffer around 180 nm, linear dichroism and inhomogeneities of the film.

To investigate the insertion of the peptide in function of the membrane properties, we recorded the oriented CD spectra of LAH4 in different states of the DMPC membrane. When the lipids are in the gel state or in a low hydration state, the spectra show two negative bands centred around 208 and 227 nm respectively, plus a third positive band appearing at the lower wavelength limit of the spectra. This pattern indicates that part of the peptide is aligned perpendicular to the beam (i.e. parallel to the membrane surface). Softening the membrane by increasing the temperature above the main phase transition or by increasing the hydration state of the mutilayers modifies the oriented CD spectra. The negative band centered around 208 nm progressively disappears, highlighting a transition towards a transmembrane state.

Solid-state NMR

Previously it has been shown[105], that oriented SS-NMR spectroscopy can be used to follow the alignment of helical peptides in membranes. The ^{15}N chemical shift is a sensitive indicator of helical tilt angles when α-helices are incorporated in oriented phospholipid bilayers oriented with the normal parallel to the magnetic field direction. The measurement of chemical shifts < 100 ppm is indicative of helix orientations

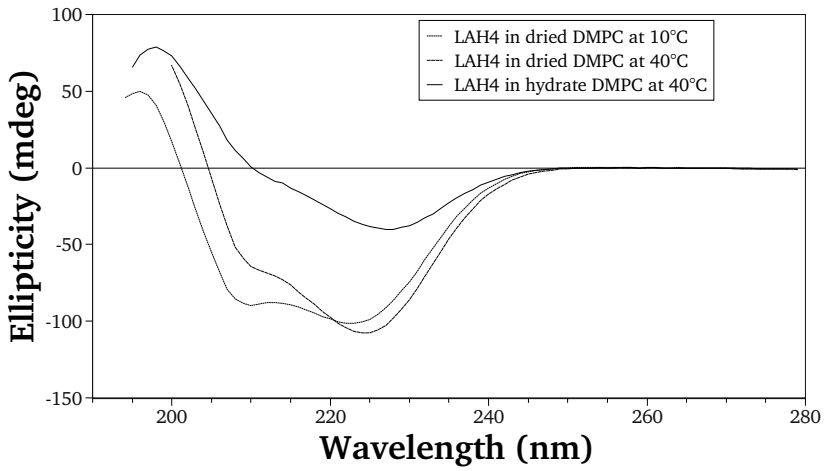

Figure 59: Oriented CD spectra of LAH4 in dried and hydrated films of DMPC. The peptide was dissolved in buffer prior to add it to the pre-formed lipid film. The sample was measured before re-hydration at 10 °C (short dashed line) and 40 °C (long dashed line), and again at 40°C after being exposed at high humidity for one night (continuous line). Only the regions of the spectra with HT signal below 500 V are considered in the figure.

parallel to the membrane surface, whereas resonances > 180 ppm agree with transmembrane helix alignments. We applied oriented SS-NMR spectroscopy to have an additional measure complementing the OCD and x-ray scattering data on LAH4 samples reconstituted in zwitterionic, charged and mixed lipids in absence of buffer. Due to the acidity of the peptide, the environment of the hydrated membrane is at pH around 5, so the differences in alignment has to be addressed to the citrate-peptide or citrate-membrane interactions.

In Figure 60 are reported the spectra proton-decoupled spectra of ^{15}N single labelled peptide reconstituted in hydrated POPC and POPG unoriented membranes. Since all the orientations of the local phospholipid bilayer are present, the resulting spectra is an averaged powder pattern, as described in Chapter 5, provided that the peptide motion around the bilayer normal is fast compared to the time scale of the ^{15}N CS anisotropy. The spectrum obtained in both cases is close to the calculated spectra of an in-plane peptide subject to uniaxial motional averaging around the membrane normal, with a symmetric tensor of components $\sigma_{\parallel} \approxeq 140$ and $\sigma_{\perp} \approxeq 80$ ppm.

We additionally tested if the peptide-concentration dependence of the peptide alignment found by x-ray diffraction persists also in the absence of buffer. When oriented sample of mixed POPC and POPG are loaded with increasing concentration of peptide, the spectra show no significant modifications (spectra are shown in Figure 61).

In Figure 62 are reported two ^{15}N SS-NMR spectra obtained in the presence (bottom) and in the absence (top) of citrate buffer at 318 K. When LAH4 is reconstituted in hydrated DMPC well above the main lipids phase transition, a sharp peak appears around 80 ppm, indication of a well oriented sample with the peptide oriented parallel to the

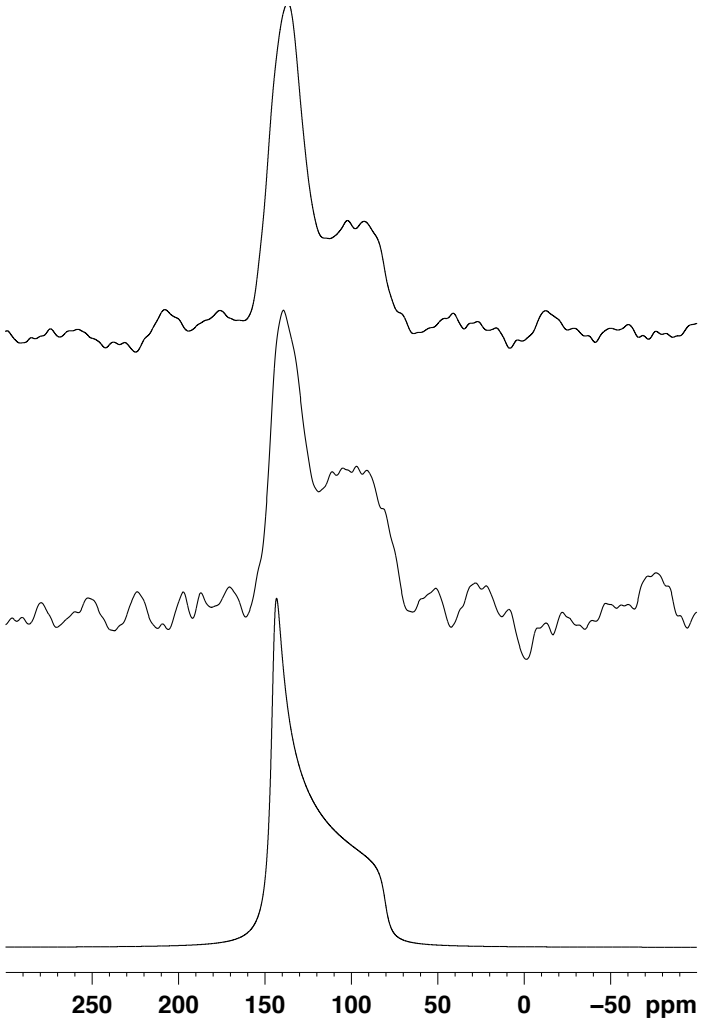

Figure 60: SS-NMR APHH-CP spectra of LAH4 in unoriented POPC (Top) and POPG (Middle). Both spectra were recorded at 37 °C. At the bottom the theoretical spectrum of a an in-plane peptide subject to uniaxial rotational motion around the membrane normal. Note the presence of the MAH at the isotropic CS frequency (for details, cf. Chapter 4).

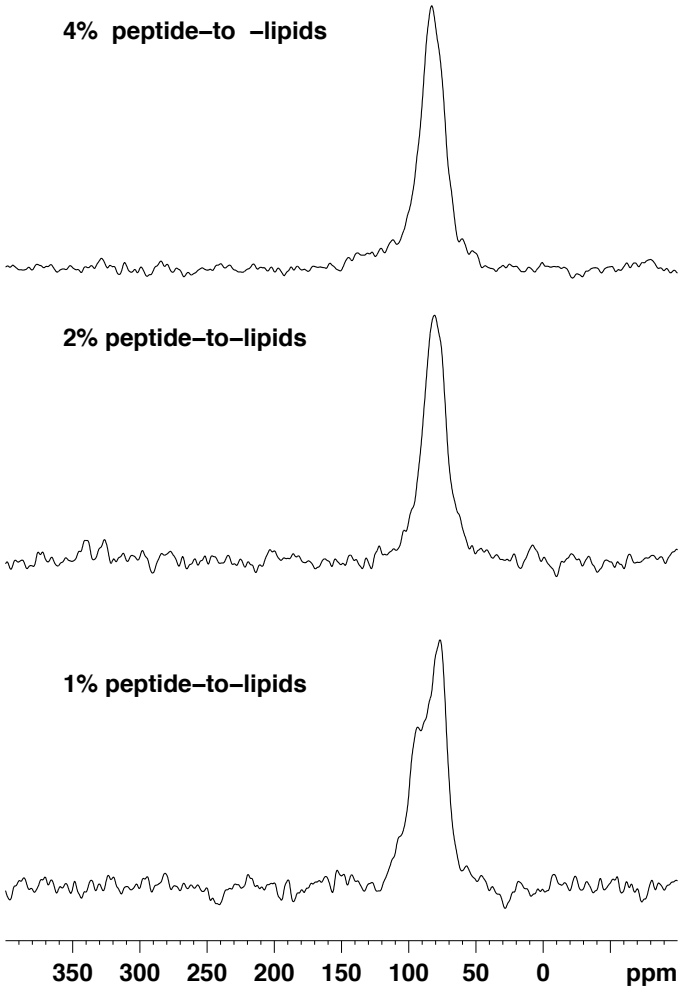

Figure 61: Oriented SS-NMR of LAH4 in mixed membranes of POPC/ POPG 3:1 at different peptide-to-lipid molar ratios. All the spectra were recorded at 313 K.

freeze-dried powder	LAH4(^{15}N-ala$_{16}$)
σ_{11}	(219±3) ppm
σ_{22}	(86±3) ppm
σ_{33}	(66±3) ppm

(a) Tensor parameters obtained from the static powder pattern spectra of freeze-dried LAH4(^{15}N-ala$_{16}$).

Averaged powder pattern	$\sigma_{\parallel}$	$\sigma_{\perp}$
POPC	(80±5) ppm	(145±5) ppm
POPG	(74±5) ppm	(144±5) ppm
in plane alignment*	(76±6) ppm	(147±6) ppm

(b) Tensor parameters obtained from the averaged powder pattern spectra of LAH4 in unoriented POPC and POPG. The last line of the table reports the calculated parameters in case of uniaxial rotational motion around the membrane axis and in-plane alignment, using the values of σ_{ii} found above. *Values calculated as described in Chapter 5.

Table 17: The tensor parameters values obtained with LAH4 reconstituted in unoriented POPC and unoriented POPG are compatible within the errors, with the corresponding calculated parameters for an in-plane peptide subject to uniaxial rotational motion around the membrane axis.

membrane surface. On the other side, when lipids and peptide are in the presence of citrate buffer, the main contribution to the spectrum comes from the region of chemical shifts higher then 200 ppm, that is a clear indication of transmembrane orientation of the peptide.

7.4 DISCUSSION

In this chapter we demonstrated that the presence of citrate buffer modify the peptide-lipids interactions of LAH4 in zwitterionic membranes. When the acidity of the sample is not controlled by the use of citrate buffer, the peptide is surface-bounded, as shown in Figure 62, Figure 61, and Figure 60, and as confirmed in several previous publications for LAH4 [91] and LAH4 analogues [44] in which the pH control was achieved by adding NaOH or by the use of phosphate [95]. This behaviour is independent from the membrane chosen, as showed by SS-NMR in DMPC, POPC and POPG (cf. Figure 60 and Figure 62) and from the peptide concentration (cf. Figure 61).

Instead, when the peptide is in contact with citrate buffer, it penetrates in the membrane core and inserts in a transmembrane manner, as showed by our oriented CD and NMR spectra in DMPC and POPC (Figure 58, Figure 57).

These findings support the interpretation of the enhanced hydrophobic thickness, shown by the x-ray results, as a consequence of LAH4 transmembrane insertion. Indeed, the peptide sequence is constituted of an hydrophobic core region of 21 amino acids. Calculating 1.5 Å per residue, we obtain an estimated hydrophobic length of 31.5 Å, very close to the maximum values found in Figure 56. The extensive stretch

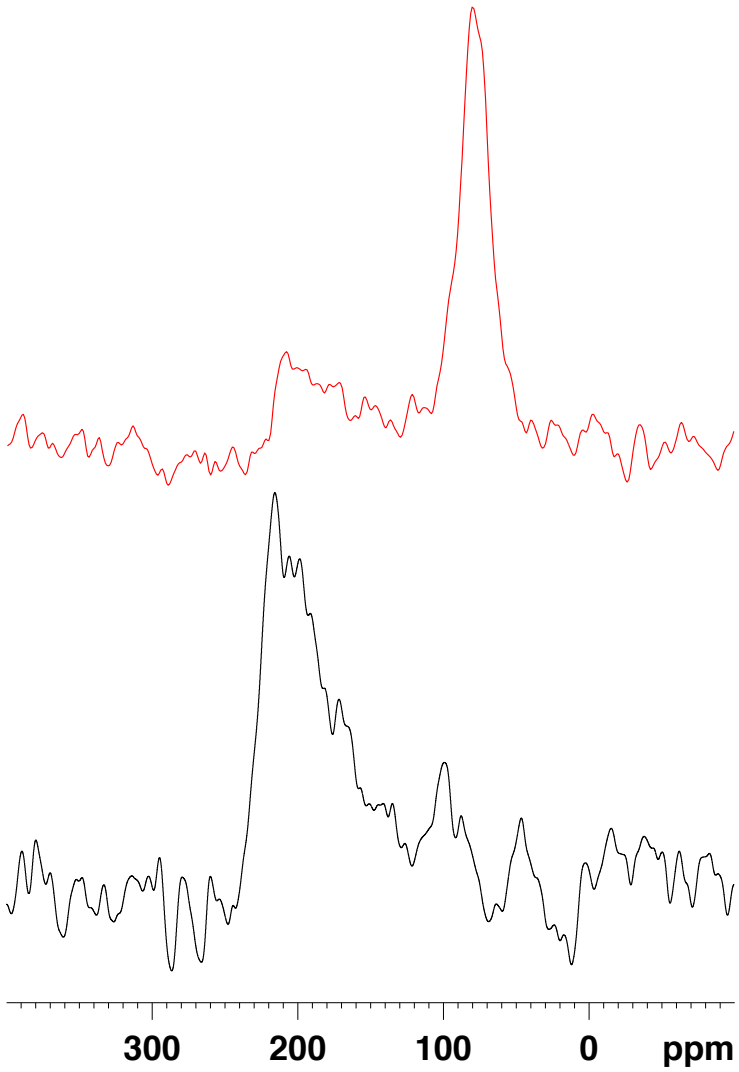

Figure 62: Oriented SS-NMR of LAH4 in DMPC. Top: LAH4, 2%mol peptide-to-lipids, without buffer (pH≈5). Bottom: LAH4, 4%mol peptide-to-lipids, in presence of citrate buffer pH≈5. Both spectra were recorded at 318 K.

of the zwitterionic membrane observed at low concentrations may then be explained as the response of the bilayer to the peptide insertion in order to minimize the exposure of hydrophobic residues to the charged phospholipid head region and to the aqueous environment. Rising the peptide concentration may lead to aggregation and a re-arrangement of the helices tilt, with a consequent minor stretch for the membrane.

The negatively charged membrane is subject to only a very mild increase of the membrane thickness followed by a drastic decrease at 4 % P/L, at which the length of the hydrophobic layer decrease below the value for pure POPG. The hydrophobic thickness of the charged bilayer is very close to the hydrophobic peptide length, so the moderate lengthening can be due both to a transmembrane insertion mechanism or to a membrane-curvature effect due to the association of the peptide with the charged surface of the lipids. The membrane-thinning effect observed at higher concentrations may be due to the installation of a detergent mechanism upon the achievement of a threshold concentration.

What is the role of citrate in the insertion mechanism of the peptide? A reduced peptide aggregation of β-amyloid was observed previously by other authors [106] in presence of citrate. They speculated that the anionic carboxylic groups of citrate ion-pair with cationic residues of Aβ. Although this may happens also in our case, the binding in solution of the citrate anionic species to LAH4 would lead to a neutralization of the peptide, and a consequent increase in hydrophobicity that should be reflected in a major propensity to form large aggregates. This proposed mechanism is not supported by the experimental findings by Marquette *et al.*[46]. They measured the hydrodynamic diameter of LAH4 in citrate buffer at pH=5 by Dynamic Light Scattering (DLS), and concluded that the peptide is present in small oligomers or, more likely, in an extended monomeric form. Also, OCD measurements demonstrate that the insertion of LAH4 occurs if the sample is prepared by initially co-dissolving peptide and lipids in organic solvent but also if the peptide is added in citrate solution to the pre-formed lipid film. These two facts suggest that the insertion of peptide into the membrane is not due to macroscopic structures pre-existing in aqueous solution but it is indeed a process driven by the presence of the membrane-peptide interactions.

Studies to verify eventual structural modifications happening in solution are still missing. However, if the action of citrate is related to its amphiphatic nature, with a negatively charged carboxylic groups at one end and an apolar group at the other end, acetic acid and other organic acids currently used as buffers may have the same behaviour. Solution CD data in acetate buffer at pH 4.5 and 5.5 show that LAH4 does not fold in an helix, as it does in neutral conditions, but it stays in a random coil conformation. Moreover, LAH4 does fold in an amphiphatic helix when POPC or POPG vesicles are added to the solution, independently from the solution pH [40]. The folding of the peptide in an amphiphatic helix was shown also for LAH4 analogues in citrate buffer in presence of Sodium dodecyl sulfate (SDS) micelles [44].

Once the peptide is folded, the histidine charges of the peptide can be neutralized by the citrate anions. As mentioned before, at pH~5, in the citrate buffer solution, citric acid mono- and bi-hydrate anions are present with roughly the same concentration. Electrostatic interactions may drive the negatively charged citrate anions to bind the charged histidines of LAH4, neutralizing the core of the peptide and favour-

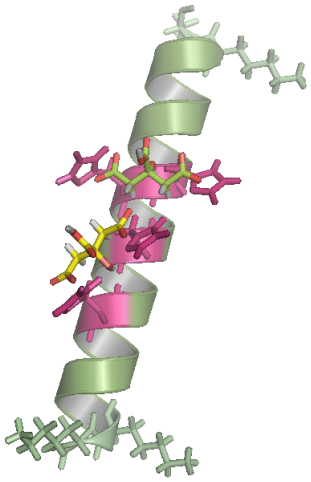

Figure 63: Neutralization of charged histidines may occur by binding of two $HCit^{2-}$. In our figure, the binding is between His_{10}-His_{11} and His_{14}-His_{18}. Of course, many other permutations could be explored, especially if the binding of single-charged $H_2Cit^-$are introduced. Finally, the flexibility of the histidines' lateral chains may easily overcome the eventual distance or orientational mismatch of the carboxylic group of the citrate and the positive charged imidazole ring of the histidines.

ing its insertion in the membrane due to hydrophobic effect. In two studies [91, 44] on the energetics of the membrane-peptide topological equilibrium of LAH4 and LAH4-analogues, the authors assume that the spontaneous insertion of the peptide may occur only under neutralization of the four histidines. The four positive charges may be neutralized by the direct interaction with two citric acid mono-hydrate anions, $HCit^{2-}$, or four H_2Cit^- bi-hydrate anions or a combination of citric acid mono- and H_2Cit^- bi-hydrate anions. In the first hypothesis, the double charged $HCit^{2-}$ are lodged between consecutive histidines of the same helix (see a representation in Figure 63), but, a priori, other stoichiometries of the citrate-LAH4 complex are possible. Another hypothesis would be that the citrate anion act as a bridge between two LAH4 molecules and lead to dimerization (cf. Figure 64a). The hydroxyl group of the citrate is also available to form H-bonds that may stabilize the supramolecular structure (Figure 64b).

Some modifications of the membrane properties can be expected in response to the ionic strength of the buffer or to the sequestration of calcium ions by the mild chelating activity of citrate. Recent investigations (unpublished results) showed a different antibiotic activity of LAH4 in the presence of EDTA. However, the effects of citrate on the lipids alone can hardly be responsible for the insertion of a peptide carrying 4 positive charges. Anyhow the process of peptide insertion seems to require a high fluidity of the membrane, as illustrated by the decrease of the transmembrane component on the OCD spectra in dried DMPC at 10°C (cf. Figure 59).

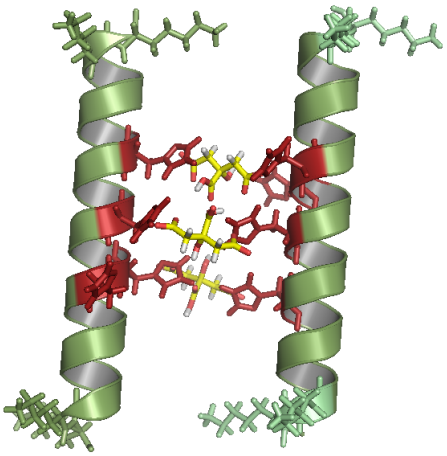

(a) Citrate may induces dimerization by forming a bridge between two or more LAH4 molecule. Here it is represented an hypothetical dimer built by two helices and three $HCit^{2-}$ ions bounding three couples of histidines. The two other histidine may be neutralized by a mono-charged H_2Cit^- ion or promote the aggregation with other helices.

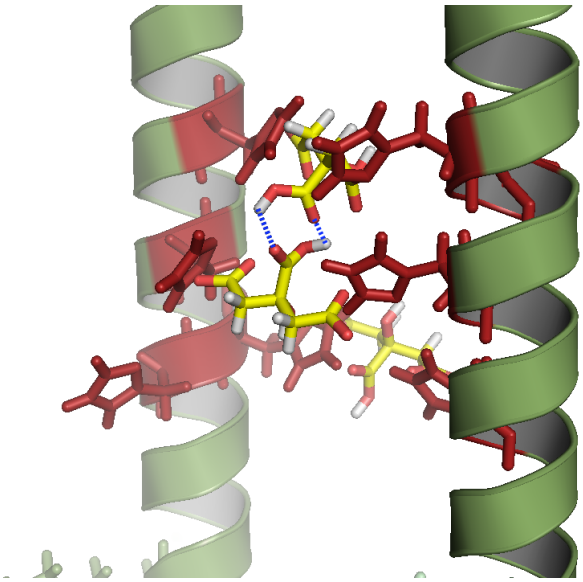

(b) The protonated carboxylic group of citrate may promote the formation of H-bounds (in blue) that could concur to stabilize the structure.

Figure 64: Hypothetical LAH4-citrate complexes. Figures are reported only for visualization purposes, they are not real models.

7.5 CONCLUSIONS

Our NMR and OCD data demonstrate that LAH4, at acid pH and in presence of citrate buffer, inserts in a transmembrane fashion into zwitterionic membranes. Interestingly, the x-ray lamellar diffraction experiments suggest that the insertion may occur also when negatively charged and mixed membranes are used, at least below a certain threshold concentration.

The process of insertion seems to be independent from the preformation of aggregates in solution, favouring a mechanism in which the fold of the peptide happens with the contact of the membrane, leaving the charged histidines in contact with the buffer solution. The citrate anions may then associate with the cationic residues, neutralizing the peptide. The insertion of the peptide is then favoured by hydrophobic effects.

Once inserted, the peptide may be subject to conformational changes, tilt or aggregation to minimize the contact of the hydrophilic core with the water phase.

More investigations are needed to understand if this phenomenon is a peculiar behaviour related to LAH4-citrate binding or if it is indeed a general property of the buffer that may be extended to other organic acid-based buffers. In any case, this study highlight the fact that the complexity of the membrane-peptide behaviours cannot be understood without taking in account also external factors, such as the specific ionic environment.

Part IV

APPENDIX

A

CONTACT TIME OPTIMIZATION FOR APHH-RODEO-CP EXPERIMENTS

CONTENTS OF THE CHAPTER:

As demonstrated in the first chapters of this thesis, the RODEO method redistributes the magnetization and recovers the line-shape for very short contact times. The efficiency of the CP experiments on peptides in unoriented model membranes may be greatly increased by choosing shorter contact times over the otherwise much longer intervals needed to reach a quasi-equilibrium state in a classical APHH-CP sequence.

INTRODUCTION

As reported by Tian and Cross [74], nitrogen CWCP spectra of single labeled peptides in oriented model membrane are subject to dipolar transient oscillations. In particular, in their study, the intensity of the signal do not follow a monotone increment with contact time until the relaxation starts to act, as commonly happens to many other solids, but positive and negative variations are superimposing to the magnetization build-up curve. The oscillations are visible until ca 1 ms, region where the $T_{1\rho}$ begins to act and the signal start to decrease.

It was found by Müller [57] that single crystals of ferrocene oscillate to different frequencies depending on the orientation of the crystal with respect to the external magnetic field. Samples containing a homogeneous distribution of all the possible spin orientations will then present a distribution of frequencies of dipolar oscillations, one for each spin orientation. These frequencies may interact destructively and, through relaxation processes, drive the system to behave like a classical *I-S* model with a unique spin temperature.

Also the use of adiabatic schemes such as APHH-CP or variable-amplitude CP are known to smooth out the dipolar oscillations.

Despite all these factors that diminish the impact of the dipolar oscillations, in this study we are going show that they still persist in a sample where a peptide has been reconstituted in an unoriented membrane even if the spectrum is recorded using an APHH-CP sequence.

As demonstrated in Chapter 4 of this thesis, the RODEO method is able to re-distribute the magnetization and to recover the line-shape even for contact times as short as 150 µs. The efficiency of the CP experiments on peptides in unoriented model membranes may be greatly increased by choosing shorter contact times over the otherwise much longer intervals needed to reach a quasi-equilibrium state in a traditional CP sequence. This is an especially critical parameter for biological samples, in which the numerous sources of mobile protons causes a fast decay of the magnetization in the plane.

MATERIAL AND METHODS

Chemicals

KALP (GKK LALA LALA LALA LALA LKKA-CONH2) and KL14 (KKLL KKAKK LLKK -CONH2) peptides were produced by automated solid-phase synthesis using standard Fmoc chemistry on a Millipore 9050 synthesizer. At the 12^{th} position for KALP and at the 8^{th} position for KL14, Fmoc-protected ^{15}N-labeled leucine and alanine were incorporated. The purity of the products were checked by MALDI-TOF mass spectroscopy and HPLC and resulted satisfactory. The peptides were successively used without any further purification. POPC was purchased from Avanti Polar Lipids, Inc. (Alabaster, AL, USA) and used without any further purification. Chloroform and trifluoro-ethanol were purchased from Sigma Aldrich (Sigma-Aldrich Chimie S.a.r.l. Lyon, France).

Samples preparation

Unoriented membrane-associated peptide samples were prepared by dissolving peptides and lipids with the same procedure and solvents used for the oriented sample preparation, but the mixtures were dried completely by nitrogen stream taking care to form a uniform extended film on the walls of the tube. The tubes were successively placed in high vacuum overnight to remove all the residual traces of solvents. The dried films were re-hydrated in a closed chamber in presence of salt at 93% relative humidity for three days. The samples were then transferred in a 7 mm MAS rotor by mild centrifuging.

APHH-CP experiments

The APHH-CP experiments were carried out on a Bruker Avance 400 spectrometer (Larmor frequency of 40.54 and 400.13 MHz in ^{15}N and ^{1}H resonance, respectively) equipped with a Bruker **CPMAS!** probe for 7 mm-o.d. rotors under static conditions.

The proton and nitrogen radio-frequency fields were calibrated first on a reference sample ($^{15}NH_4Cl$) and carefully adjusted on freeze-dried KALP trough a two-dimensional nutation experiment. The experiments were performed sweeping the ^{1}H and ^{15}N RF fields through the HH condition $\omega_{1I}/2\pi = \omega_{1S}/2\pi = 43.4$ kHz using the tangential time dependencies of Figure 65c and Figure 65d. Proton pulses were readjusted on the membrane sample.

Cross-polarization dynamics were evaluated on a set of 13 experiments increasing the contact time from 50 µs to 2 ms. Recycle time applied was 4 s and 10240 scans were recorded. An Hahn-echo refocusing pulse has been included in all the experiments before the acquisition to overcome the dead time problem. Proton decoupling during acquisition and echo times was performed by SPINAL-64. A left shift of 24 points and a Lorentzian broadening of 500 Hz were applied prior to Fourier transformation.

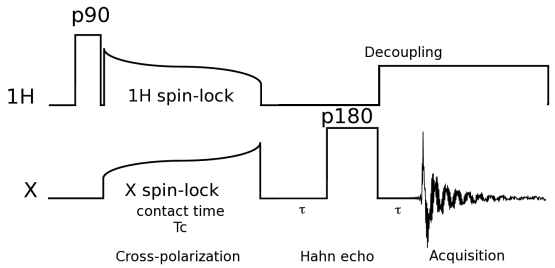

(a) APHH-CP sequence.

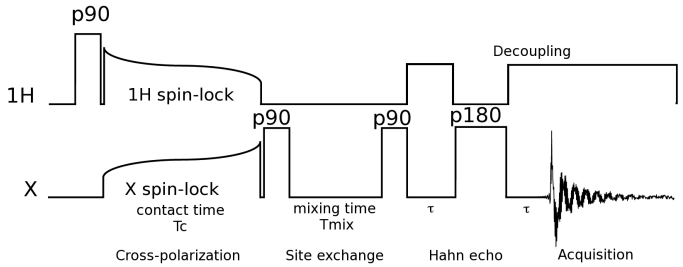

(b) APHH-RODEO-CP sequence.

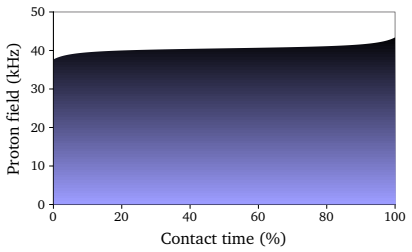

(c) Tangential time dependency of proton field during cross-polarization step.

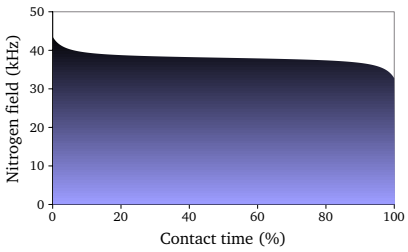

(d) Tangential time dependency of nitrogen field during cross-polarization step.

Figure 65: Example of possible configurations for membrane-associated peptides.

RESULTS AND CONCLUSIONS

We investigated the dynamics of the adiabatic CP process for of a peptide in hydrated non oriented lipids by performing APHH-CP experiments at various contact times. The results are reported in Figure 66. The integrals of each spectrum are reported in Figure 67.

Figure 66 shows that the intensities of the discontinuities are subject to oscillations: this effect is due to the dipolar oscillations, as already described in ferrocene in the previous chapters and as already found in analogues samples of peptides in oriented lipid bilayers by Tian and Cross [74]. Therefore, the adiabatic passage though the Hartmann-Hahn condition is not sufficient to completely remove dipolar oscillations in membrane samples for short contact times and the oscillations disappear only when the interval approaches 1 ms. Waiting a contact time of about 1ms is advisable in order to exit the transient regime and to

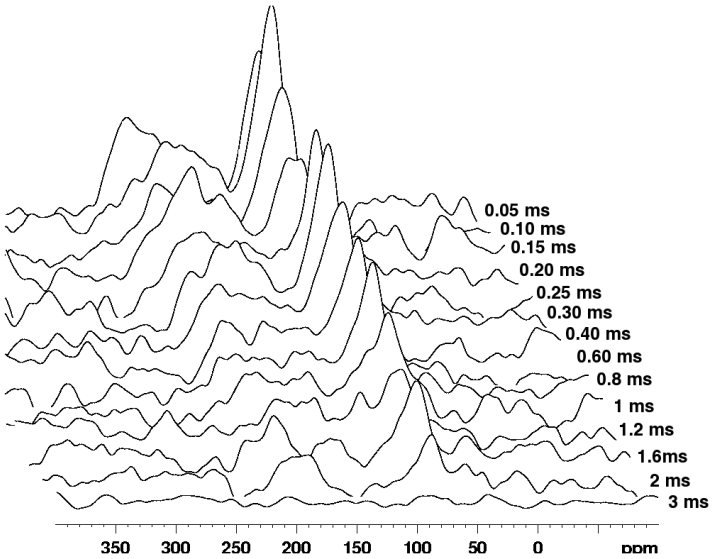

Figure 66: APHH-CP dynamics of single site ^{15}N-labelled KALP in POPC . On the right scale, increasing contact times of each recorded spectra.

avoid distortions, however using a shorter contact time of 100µs would give twice more signal. This last strategy is indeed possible thanks to the capability of the RODEO method to recover undistorted powder pattern line-shapes even at contact times as short as 150 µs.

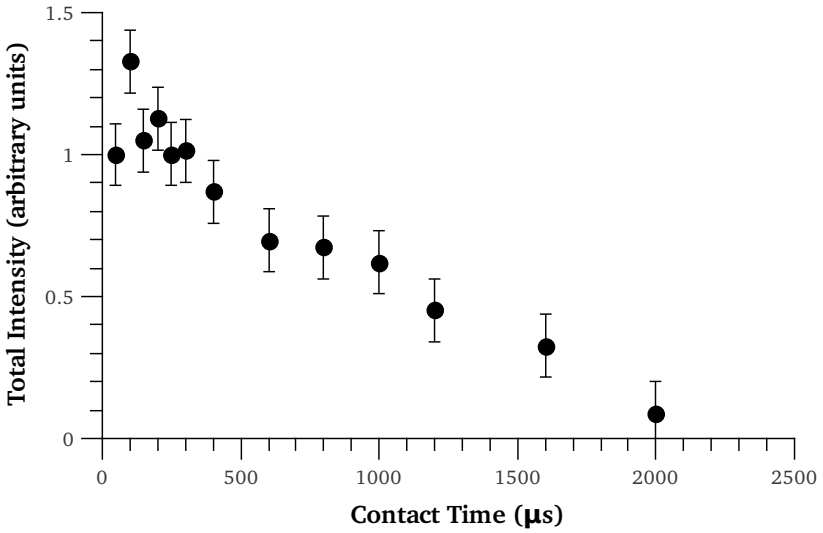

Figure 67: APHH-CP dynamics of KALP in POPC . All peaks were integrated from 227 to 59 ppm. Absolute error was assigned from the noise level of the spectra.

BIBLIOGRAPHY

[1] Orsolya Toke, Lynette Cegelski, and Jacob Schaefer. Peptide antibiotics in action: Investigation of polypeptide chains in insoluble environments by rotational-echo double resonance. *Biochimica et Biophysica Acta (BBA) - Biomembranes*, 1758(9):1314 – 1329, 2006. Membrane Biophysics of Antimicrobial Peptides. (Cited on pages xv and 5.)

[2] Burkhard Bechinger and Karl Lohner. Detergent-like actions of linear amphipathic cationic antimicrobial peptides. *Biochim Biophys Acta*, 1758(9):1529–1539, Sep 2006. (Cited on pages xv, 6, 7, 8, and 17.)

[3] Burkhard Bechinger. Rationalizing the membrane interactions of cationic amphipathic antimicrobial peptides by their molecular shape. *Current Opinion in Colloid & Interface Science*, 14(5):349 – 355, 2009. (Cited on pages xvi, 6, and 9.)

[4] G. Pabst, M. Rappolt, H. Amenitsch, and P. Laggner. Structural information from multilamellar liposomes at full hydration: Full q-range fitting with high quality x-ray data. *Physical Review E*, 62:4000–4009, September 2000. (Cited on pages xxi, 109, and 110.)

[5] Yufeng Wei, Angel C. de Dios, and Ann E. McDermott. Solid-state 15n nmr chemical shift anisotropy of histidines: Experimental and theoretical studies of hydrogen bonding. *Journal of the American Chemical Society*, 121(44):10389–10394, 1999. (Cited on pages xxvi, 95, and 97.)

[6] Huey W Huang. Molecular mechanism of antimicrobial peptides: the origin of cooperativity. *Biochim Biophys Acta*, 1758(9):1292–1302, Sep 2006. (Cited on pages 4 and 16.)

[7] M. S. Sansom. Alamethicin and related peptaibols–model ion channels. *Eur Biophys J*, 22(2):105–124, 1993. (Cited on pages 4 and 16.)

[8] K. Matsuzaki, O. Murase, N. Fujii, and K. Miyajima. An antimicrobial peptide, magainin 2, induced rapid flip-flop of phospholipids coupled with pore formation and peptide translocation. *Biochemistry*, 35(35):11361–11368, Sep 1996. (Cited on pages 4 and 16.)

[9] H. W. Huang. Action of antimicrobial peptides: two-state model. *Biochemistry*, 39(29):8347–8352, Jul 2000. (Cited on page 4.)

[10] H. Steiner, D. Andreu, and R. B. Merrifield. Binding and action of cecropin and cecropin analogues: antibacterial peptides from insects. *Biochim Biophys Acta*, 939(2):260–266, Apr 1988. (Cited on pages 6 and 17.)

[11] D. Juretic, R. W. Hendler, F. Kamp, W. S. Caughey, M. Zasloff, and H. V. Westerhoff. Magainin oligomers reversibly dissipate delta microh+ in cytochrome oxidase liposomes. *Biochemistry*, 33(15):4562–4570, Apr 1994. (Cited on pages 6 and 17.)

[12] L. Silvestro, K. Gupta, J. N. Weiser, and P. H. Axelsen. The concentration-dependent membrane activity of cecropin a. *Biochemistry*, 36(38):11452–11460, Sep 1997. (Cited on pages 6 and 17.)

[13] T. Wieprecht, M. Dathe, M. Beyermann, E. Krause, W. L. Maloy, D. L. MacDonald, and M. Bienert. Peptide hydrophobicity controls the activity and selectivity of magainin 2 amide in interaction with membranes. *Biochemistry*, 36(20):6124–6132, May 1997. (Cited on pages 6 and 17.)

[14] H. Duclohier, G. Molle, and G. Spach. Antimicrobial peptide magainin i from xenopus skin forms anion-permeable channels in planar lipid bilayers. *Biophys J*, 56(5):1017–1021, Nov 1989. (Cited on pages 6 and 17.)

[15] R. A. Cruciani, J. L. Barker, S. R. Durell, G. Raghunathan, H. R. Guy, M. Zasloff, and E. F. Stanley. Magainin 2, a natural antibiotic from frog skin, forms ion channels in lipid bilayer membranes. *Eur J Pharmacol*, 226(4):287–296, Aug 1992. (Cited on pages 6 and 17.)

[16] B. Christensen, J. Fink, R. B. Merrifield, and D. Mauzerall. Channel-forming properties of cecropins and related model compounds incorporated into planar lipid membranes. *Proc Natl Acad Sci U S A*, 85(14):5072–5076, Jul 1988. (Cited on pages 6 and 17.)

[17] P. Schlieper and E. De Robertis. Triton x-100 as a channel-forming substance in artificial lipid bilayer membranes. *Arch Biochem Biophys*, 184(1):204–208, Nov 1977. (Cited on pages 6 and 17.)

[18] E. Grant, T. J. Beeler, K. M. Taylor, K. Gable, and M. A. Roseman. Mechanism of magainin 2a induced permeabilization of phospholipid vesicles. *Biochemistry*, 31(41):9912–9918, Oct 1992. (Cited on pages 6 and 17.)

[19] T. D. Madden and P. R. Cullis. Stabilization of bilayer structure for unsaturated phosphatidylethanolamines by detergents. *Biochim Biophys Acta*, 684(1):149–153, Jan 1982. (Cited on pages 6 and 17.)

[20] M. Wu, E. Maier, R. Benz, and R. E. Hancock. Mechanism of interaction of different classes of cationic antimicrobial peptides with planar bilayers and with the cytoplasmic membrane of escherichia coli. *Biochemistry*, 38(22):7235–7242, Jun 1999. (Cited on pages 6 and 18.)

[21] Kim A Brogden. Antimicrobial peptides: pore formers or metabolic inhibitors in bacteria? *Nat Rev Microbiol*, 3(3):238–250, Mar 2005. (Cited on pages 6, 9, and 18.)

[22] Christian Ostermeier and Hartmut Michel. Crystallization of membrane proteins. *Current Opinion in Structural Biology*, 7(5):697 – 701, 1997. (Cited on pages 10 and 19.)

[23] Raymond C Stevens. High-throughput protein crystallization. *Current Opinion in Structural Biology*, 10(5):558 – 563, 2000. (Cited on pages 10 and 19.)

[24] S. J. Opella. Nmr and membrane proteins. *Nat Struct Biol*, 4 Suppl:845–848, Oct 1997. (Cited on pages 10 and 19.)

[25] Lydia Prongidi-Fix, Philippe Bertani, and Burkhard Bechinger. The membrane alignment of helical peptides from non-oriented 15n chemical shift solid-state nmr spectroscopy. *J Am Chem Soc*, 129(27):8430–8431, Jul 2007. (Cited on pages 11, 20, and 37.)

[26] M. Hong, K. Schmidt-Rohr, and D. Nanz. Study of phospholipid structure by 1h, 13c, and 31p dipolar couplings from two-dimensional nmr. *Biophysical Journal*, 69(5):1939 – 1950, 1995. (Cited on pages 11 and 20.)

[27] Mei Hong and Tim Doherty. Orientation determination of membrane-disruptive proteins using powder samples and rotational diffusion: A simple solid-state nmr approach. *Chemical Physics Letters*, 432(1-3):296 – 300, 2006. (Cited on pages 11, 20, and 51.)

[28] Edward W. Abel, Nicholas J. Long, Keith G. Orrell, Anthony G. Osborne, and Vladimir Sik. Dynamic nmr studies of ring rotation in substituted ferrocenes and ruthenocenes. *Journal of Organometallic Chemistry*, 403(1-2):195 – 208, 1991. (Cited on page 11.)

[29] Burkhard Bechinger and Christina Sizun. Alignment and structural analysis of membrane polypeptides by 15n and 31p solid-state nmr spectroscopy. *Concepts in Magnetic Resonance Part A*, 18A(2):130–145, 2003. (Cited on pages 12, 30, 31, 37, 55, 73, and 83.)

[30] U. S. Sudheendra and Burkhard Bechinger. Topological equilibria of ion channel peptides in oriented lipid bilayers revealed by 15n solid-state nmr spectroscopy. *Biochemistry*, 44(36):12120–12127, 2005. PMID: 16142910. (Cited on pages 12, 37, 55, 74, and 83.)

[31] Lydia Prongidi-Fix, Philippe Bertani, and Burkhard Bechinger. The membrane alignment of helical peptides from non-oriented 15n chemical shift solid-state nmr spectroscopy. *J Am Chem Soc*, 129(27):8430–8431, Jul 2007. (Cited on pages 12, 33, 51, 55, and 83.)

[32] Mei Hong and Tim Doherty. Orientation determination of membrane-disruptive proteins using powder samples and rotational diffusion: A simple solid-state nmr approach. *Chem Phys Lett*, 432(1-3):296–300, Dec 2006. (Cited on pages 12, 37, 55, 73, 74, and 83.)

[33] Daniel J. Fowler, Robert M. Weis, and Lynmarie K. Thompson. Kinase-active signaling complexes of bacterial chemoreceptors do not contain proposed receptor-receptor contacts observed in crystal structures. *Biochemistry*, 49(7):1425–1434, 2010. PMID: 20088541. (Cited on pages 12, 21, and 89.)

[34] Ingrid Wallat Maarten P. Heyn & Anthony Watts Anne S. Ulrich. Re-orientation of retinal in the m-photointermediate of bacteriorhodopsin. *Nature Structural Biology*, 2:190–192, 1995. (Cited on pages 12, 21, and 89.)

[35] Miya Kamihira, Thomas Vosegaard, A. James Mason, Suzana K. Straus, Niels Chr. Nielsen, and Anthony Watts. Structural and orientational constraints of bacteriorhodopsin in purple membranes determined by oriented-sample solid-state nmr spectroscopy. *Journal of Structural Biology*, 149(1):7 – 16, 2005. (Cited on pages 12, 21, and 89.)

[36] Michael F. Brown, Maarten P. Heyn, Constantin Job, Suhkmann Kim, Stephan Moltke, Koji Nakanishi, Alexander A. Nevzorov, Andrey V. Struts, Gilmar F.J. Salgado, and Ingrid Wallat. Solid-state 2h nmr spectroscopy of retinal proteins in aligned membranes. *Biochimica et Biophysica Acta (BBA) - Biomembranes*, 1768(12):2979 – 3000, 2007. NMR Structural Studies on Membrane Proteins. (Cited on pages 12, 21, and 89.)

[37] Marco Ieronimo, Sergii Afonin, Katja Koch, Marina Berditsch, Parvesh Wadhwani, and Anne S. Ulrich. 19f nmr analysis of the antimicrobial peptide pgla bound to native cell membranes from bacterial protoplasts and human erythrocytes. *Journal of the American Chemical Society*, 132(26):8822–8824, 2010. (Cited on pages 12, 21, and 89.)

[38] Chia B.C.S., Lam Y.-H., Dyall-Smith M., Separovic F., and Bowie J.H. A 31p nmr study of the interaction of amphibian antimicrobial peptides with the membranes of live bacteria. *Letters in Peptide Science*, 7:151–156(6), May 2000. (Cited on pages 12 and 89.)

[39] J.T. Gerig. Fluorine nmr of proteins. *Progress in Nuclear Magnetic Resonance Spectroscopy*, 26(Part 4):293 – 370, 1994. (Cited on pages 12, 21, and 89.)

[40] Titus C. B. Vogt and Burkhard Bechinger. The interactions of histidine-containing amphipathic helical peptide antibiotics with lipid bilayers. *Journal of Biological Chemistry*, 274(41):29115–29121, 1999. (Cited on pages 13, 22, 105, 106, 107, and 123.)

[41] A. James Mason, Amélie Martinez, Clemens Glaubitz, Olivier Danos, Antoine Kichler, and Burkhard Bechinger. The antibiotic and dna-transfecting peptide lah4 selectively associates with, and disorders, anionic lipids in mixed membranes. *The FASEB Journal*, 20(2):320–322, 2006. (Cited on pages 13, 22, 105, and 106.)

[42] Antoine Kichler, Christian Leborgne, Olivier Danos, and Burkhard Bechinger. Characterization of the gene transfer process mediated by histidine-rich peptides. *Journal of Molecular Medicine*, 85:191–201, 2007. 10.1007/s00109-006-0119-4. (Cited on pages 13, 22, and 105.)

[43] Lydia Prongidi-Fix, Masae Sugawara, Philippe Bertani, Jesus Raya, Christian Leborgne, Antoine Kichler, and Burkhard Bechinger. Self-promoted cellular uptake of peptide/dna transfection complexes. *Biochemistry*, 46(40):11253–11262, Oct 2007. (Cited on pages 13, 22, 73, and 105.)

[44] Christopher Aisenbrey, Christina Sizun, Joachim Koch, Meike Herget, Rupert Abele, Burkhard Bechinger, and Robert TampÃ©. Structure and dynamics of membrane-associated icp47, a viral inhibitor of the mhc i antigen-processing machinery. *J Biol Chem*, 281(41):30365–30372, Oct 2006. (Cited on pages 13, 22, 106, 107, 121, 123, and 124.)

[45] Antoine Kichler, Christian Leborgne, Josefine März, Olivier Danos, and Burkhard Bechinger. Histidine-rich amphipathic

peptide antibiotics promote efficient delivery of dna into mammalian cells. *Proc Natl Acad Sci U S A*, 100(4):1564–1568, Feb 2003. (Cited on pages 13, 22, and 107.)

[46] Arnaud Marquette, A. James Mason, and Burkhard Bechinger. Aggregation and membrane permeabilizing properties of designed histidine-containing cationic linear peptide antibiotics. *Journal of Peptide Science*, 14(4):488–495, 2008. (Cited on pages 13, 22, 107, and 123.)

[47] M.J. Duer. *An Introduction to Solid-State NMR*. Blackwell Science Ltd, 2004. (Cited on pages 25, 38, 55, and 56.)

[48] S. R. Hartmann and E. L. Hahn. Nuclear double resonance in the rotating frame. *Phys. Rev.*, 128(5):2042–2053, Dec 1962. (Cited on page 29.)

[49] O. B. Peersen, X. L. Wu, I. Kustanovich, and S. O. Smith. Variable-amplitude cross-polarization mas nmr. *Journal of Magnetic Resonance, Series A*, 104(3):334 – 339, 1993. (Cited on pages 30 and 37.)

[50] S. Hediger, B.H. Meier, and R.R. Ernst. Cross polarization under fast magic angle sample spinning using amplitude-modulated spin-lock sequences. *Chemical Physics Letters*, 213(5-6):627 – 635, 1993. (Cited on page 30.)

[51] S. Hediger, B. H. Meier, and R. R. Ernst. Adiabatic passage hartmann-hahn cross polarization in nmr under magic angle sample spinning. *Chemical Physics Letters*, 240(5-6):449 – 456, 1995. (Cited on pages 30, 51, 60, and 79.)

[52] A. C. Kolbert and A. Bielecki. Broadband hartmann-hahn matching in magic-angle spinning nmr via an adiabatic frequency sweep. *Journal of Magnetic Resonance, Series A*, 116(1):29 – 35, 1995. (Cited on page 30.)

[53] Riqiang Fu, Philippe Pelupessy, and Geoffrey Bodenhausen. Frequency-modulated cross-polarization for fast magic angle spinning nmr at high fields: relaxing the hartmann-hahn condition. *Chemical Physics Letters*, 264(1-2):63 – 69, 1997. (Cited on page 30.)

[54] John Glushka, Maria Lee, Scott Coffin, and David Cowburn. Nitrogen-15 chemical shifts of backbone amides in bovine pancreatic trypsin inhibitor and apamin. *Journal of the American Chemical Society*, 111(20):7716–7722, 1989. (Cited on page 30.)

[55] Eric Oldfield. Chemical shifts and three-dimensional protein structures. *Journal of Biomolecular NMR*, 5:217–225, 1995. 10.1007/BF00211749. (Cited on page 30.)

[56] Doree Sitkoff and David A. Case. Theories of chemical shift anisotropies in proteins and nucleic acids. *Progress in Nuclear Magnetic Resonance Spectroscopy*, 32(2):165 – 190, 1998. (Cited on page 30.)

[57] Luciano Müller, Anil Kumar, Thomas Baumann, and Richard R. Ernst. Transient oscillations in nmr cross-polarization experiments in solids. *Phys. Rev. Lett.*, 32(25):1402–1406, Jun 1974. (Cited on pages 37, 51, 56, 74, and 129.)

[58] P. Palmas, P. Tekely, and D. Canet. Local-field measurements on powder samples from polarization inversion of the rare-spin magnetization. *Journal of Magnetic Resonance, Series A*, 104(1):26 – 36, 1993. (Cited on pages 37 and 55.)

[59] A. Naito and C.A. McDowell. Anisotropic behavior of the 13c nuclear spin dynamics in a single crystal of l-alanine. *J. Chem. Phys.*, 84:4181–4186, April 1986. (Cited on pages 37 and 55.)

[60] Xiaoling Wu and Shanmin Zhang. Selective polarization inversion and depolarization of 13c in cross relaxation in nmr. *Chemical Physics Letters*, 156(1):79 – 81, 1989. (Cited on pages 37 and 55.)

[61] M. H. Levitt, D. Suter, and R. R. Ernst. Spin dynamics and thermodynamics in solid-state nmr cross polarization. *The Journal of Chemical Physics*, 84(8):4243–4255, 1986. (Cited on pages 37 and 57.)

[62] G. Metz, X. L. Wu, and S. O. Smith. Ramped-amplitude cross polarization in magic-angle-spinning nmr. *Journal of Magnetic Resonance, Series A*, 110(2):219 – 227, 1994. (Cited on page 37.)

[63] S. Hediger, B.H. Meier, Narayanan D. Kurur, Geoffrey Bodenhausen, and R.R. Ernst. Nmr cross polarization by adiabatic passage through the hartmann–hahn condition (aphh). *Chemical Physics Letters*, 223(4):283 – 288, 1994. (Cited on pages 37, 79, and 111.)

[64] A. Bax. *Two-dimensional NMR in Liquids*. Delft University Press, Delft, 1984. (Cited on page 38.)

[65] M. Baldus, D. G. Geurts, S. Hediger, and B. H. Meier. Efficient 15n-13c polarization transfer by adiabatic-passage hartmann-hahn cross polarization. *Journal of Magnetic Resonance, Series A*, 118(1):140 – 144, 1996. (Cited on page 38.)

[66] B. M. Fung, A. K. Khitrin, and K. Ermolaev. An improved broadband decoupling sequence for liquid crystals and solids. *J Magn Reson*, 142(1):97–101, Jan 2000. (Cited on pages 38, 58, 60, 79, and 92.)

[67] Sarah D Cady, Catherine Goodman, Chad D Tatko, William F DeGrado, and Mei Hong. Determining the orientation of uniaxially rotating membrane proteins using unoriented samples: a 2h, 13c, and 15n solid-state nmr investigation of the dynamics and orientation of a transmembrane helical bundle. *J Am Chem Soc*, 129(17):5719–5729, May 2007. (Cited on pages 51 and 83.)

[68] M. H. Levitt, D. Suter, and R. R. Ernst. Spin dynamics and thermodynamics in solid-state nmr cross polarization. *The Journal of Chemical Physics*, 84(8):4243–4255, 1986. (Cited on pages 51 and 56.)

[69] Waclaw Kolodziejski and Jacek Klinowski. Kinetics of cross-polarization in solid-state nmr: A guide for chemists. *Chemical Reviews*, 102(3):613–628, 2002. PMID: 11890752. (Cited on page 56.)

[70] M.Matti Maricq and J. S. Waugh. Nmr in rotating solids. *The Journal of Chemical Physics*, 70(7):3300–3316, 1979. (Cited on page 57.)

[71] Gonzalo Augustin Alvarez. *Decoherence of many-spin systems in NMR: From molecular characterization to an environmentally induced quantum dynamics phase transition*. PhD thesis, Universidad National de Cordoba, 2007. (Cited on page 57.)

[72] J. Raya, B. Perrone, B. Bechinger, and J. Hirschinger. Chemical shift powder spectra obtained by using rotor-directed exchange of orientations cross-polarization (rodeo-cp). *Chemical Physics Letters*, 508:155–164, 2011. (Cited on pages 62 and 65.)

[73] Christopher Aisenbrey and Burkhard Bechinger. Tilt and rotational pitch angle of membrane-inserted polypeptides from combined 15n and 2h solid-state nmr spectroscopy. *Biochemistry*, 43(32):10502–10512, 2004. PMID: 15301548. (Cited on pages 73, 83, and 85.)

[74] Tian and Cross. Dipolar oscillations in cross-polarized peptide samples in oriented lipid bilayers. *J Magn Reson*, 125(1):220–223, Mar 1997. (Cited on pages 74, 129, and 131.)

[75] Ulrike Harzer and Burkhard Bechinger. Alignment of lysine-anchored membrane peptides under conditions of hydrophobic mismatch: A cd, 15n and 31p solid-state nmr spectroscopy investigation. *Biochemistry*, 39(43):13106–13114, 2000. (Cited on page 85.)

[76] Evgeniy Salnikov, Philippe Bertani, Jan Raap, and Burkhard Bechinger. Analysis of the amide 15n chemical shift tensor of the c-alpha tetrasubstituted constituent of membrane-active peptaibols, the alpha-aminoisobutyric acid residue, compared to those of di- and tri-substituted proteinogenic amino acid residues. *Journal of Biomolecular NMR*, 45:373–387, 2009. 10.1007/s10858-009-9380-5. (Cited on pages 88 and 94.)

[77] Zach Serber and Volker Dötsch. In-cell nmr spectroscopy. *Biochemistry*, 40(48):14317–14323, 2001. PMID: 11724542. (Cited on page 89.)

[78] Zach Serber, Lorenzo Corsini, Florian Durst, and Volker Dötsch. In-cell nmr spectroscopy. In Thomas L. James, editor, *Nuclear Magnetic Resonance of Biological Macromolecules*, volume 394 of *Methods in Enzymology*, pages 17 – 41. Academic Press, 2005. (Cited on page 89.)

[79] Zach Serber, Adrian T. Keatinge-Clay, Richard Ledwidge, Alexander E. Kelly, Susan M. Miller, and Volker Dötsch. High-resolution macromolecular nmr spectroscopy inside living cells. *Journal of the American Chemical Society*, 123(10):2446–2447, 2001. (Cited on page 89.)

[80] Zach Serber, Richard Ledwidge, Susan M. Miller, and Volker Dötsch. Evaluation of parameters critical to observing proteins inside living escherichia coli by in-cell nmr spectroscopy. *Journal of the American Chemical Society*, 123(37):8895–8901, 2001. (Cited on page 89.)

[81] Daisuke Sakakibara, Atsuko Sasaki, Teppei Ikeya, Junpei Hamatsu, Tomomi Hanashima, Masaki Mishima, Masatoshi

Yoshimasu, Nobuhiro Hayashi, Tsutomu Mikawa, Markus Walchli, Brian O. Smith, Masahiro Shirakawa, Peter Guntert, and Yutaka Ito. Protein structure determination in living cells by in-cell nmr spectroscopy. *Nature*, 458(7234):102–105, 03 2009. (Cited on page 89.)

[82] Robert A. Wind, Jian Z. Hu, and Paul D. Majors. Localized in vivo isotropic-anisotropic correlation 1h nmr spectroscopy using ultraslow magic angle spinning. *Magnetic Resonance in Medicine*, 55(1):41–49, 2006. (Cited on pages 89 and 100.)

[83] J. M. Wieruszeski, A. Bohin, J. P. Bohin, and G. Lippens. In vivo detection of the cyclic osmoregulated periplasmic glucan of ralstonia solanacearum by high-resolution magic angle spinning nmr. *Journal of Magnetic Resonance*, 151(1):118 – 123, 2001. (Cited on page 89.)

[84] Kohsuke Inomata, Ayako Ohno, Hidehito Tochio, Shin Isogai, Takeshi Tenno, Ikuhiko Nakase, Toshihide Takeuchi, Shiroh Futaki, Yutaka Ito, Hidekazu Hiroaki, and Masahiro Shirakawa. High-resolution multi-dimensional nmr spectroscopy of proteins in human cells. *Nature*, 458(7234):106–109, 03 2009. (Cited on page 89.)

[85] Jaime Curtis-Fisk, Ryan M. Spencer, and David P. Weliky. Native conformation at specific residues in recombinant inclusion body protein in whole cells determined with solid-state nmr spectroscopy. *Journal of the American Chemical Society*, 130(38):12568–12569, 2008. (Cited on page 89.)

[86] Verica Vidovic, Lydia Prongidi-Fix, Burkhard Bechinger, and Sebastiaan Werten. Production and isotope labeling of antimicrobial peptides in escherichia coli by means of a novel fusion partner that enables high-yield insoluble expression and fast purification. *J Pept Sci*, 15(4):278–284, Apr 2009. (Cited on page 90.)

[87] Naresh K. Sethi, David M. Grant, and Ronald J. Pugmire. 13c chemical shielding anisotropy studied by variable-angle sample spinning. *Journal of Magnetic Resonance (1969)*, 71(3):476 – 479, 1987. (Cited on page 91.)

[88] Cristina Gabellieri, Steven Reynolds, Arnon Lavie, Geoffrey S. Payne, Martin O. Leach, and Thomas R. Eykyn. Therapeutic target metabolism observed using hyperpolarized 15n choline. *Journal of the American Chemical Society*, 130(14):4598–4599, 2008. (Cited on page 95.)

[89] J Antoinette Killian and Thomas KM Nyholm. Peptides in lipid bilayers: the power of simple models. *Current Opinion in Structural Biology*, 16(4):473 – 479, 2006. Membranes / Engineering and design. (Cited on page 98.)

[90] Arnaud Marquette, Bernard Lorber, and Burkhard Bechinger. Reversible liposome association induced by lah4: A peptide with potent antimicrobial and nucleic acid transfection activities. *Biophysical Journal*, 98(11):2544 – 2553, 2010. (Cited on page 98.)

[91] Burkhard Bechinger. Towards membrane protein design: ph-sensitive topology of histidine-containing polypeptides. *Journal of Molecular Biology*, 263(5):768 – 775, 1996. (Cited on pages 99, 105, 107, 121, and 124.)

[92] Lino R. Becerra, Gary J. Gerfen, Richard J. Temkin, David J. Singel, and Robert G. Griffin. Dynamic nuclear polarization with a cyclotron resonance maser at 5 t. *Phys. Rev. Lett.*, 71(21):3561–3564, Nov 1993. (Cited on page 101.)

[93] M. Hunger, T. Horvath, and J. Weitkamp. Conversion of propan-2-ol on zeolite lanay investigated by in situ mas nmr spectroscopy under continuous-flow conditions. In Son-Ki Ihm Hakze Chon and Young Sun Uh, editors, *Progress in Zeolite and Microporous Materials, Preceedings of the 11th International Zeolite Conference*, volume 105 of *Studies in Surface Science and Catalysis*, pages 853 – 860. Elsevier, 1997. (Cited on page 101.)

[94] Zalusky-A. Lewis D.H. Douskey M.C. Pomije M.J. Mann K.R. Munson E.J. Isbester, P.K. Nmr probe for heterogeneous catalysis with isolated reagent flow and magic-angle spinning. *Catalysis Today*, 49(4):363–375, 1999. cited By (since 1996) 24. (Cited on page 101.)

[95] Burkhard Bechinger, Jean-Marie Ruysschaert, and Erik Goormaghtigh. Membrane helix orientation from linear dichroism of infrared attenuated total reflection spectra. *Biophysical Journal*, 76(1):552 – 563, 1999. (Cited on pages 107 and 121.)

[96] Evgeniy Salnikov, Christopher Aisenbrey, Verica Vidovic, and Burkhard Bechinger. Solid-state nmr approaches to measure topological equilibria and dynamics of membrane polypeptides. *Biochimica et Biophysica Acta (BBA) - Biomembranes*, 1798(2):258 – 265, 2010. Membrane Protein Dynamics by NMR: Correlation of Structure and Function. (Cited on page 107.)

[97] Georg Pabst, Richard Koschuch, Beatriz Pozo-Navas, Michael Rappolt, Karl Lohner, and Peter Laggner. Structural analysis of weakly ordered membrane stacks. *Journal of Applied Crystallography*, 36(6):1378–1388, Dec 2003. (Cited on page 109.)

[98] Georg Pabst. Global proprieties of biomimetic membranes: perspectives on molecular features. *Biophysical Reviews and Letters (BRL)*, 1:57–84, 2006. (Cited on pages 109 and 112.)

[99] Georg Pabst, Stephan L Grage, Sabine Danner-Pongratz, Weiguo Jing, Anne S Ulrich, Anthony Watts, Karl Lohner, and Andrea Hickel. Membrane thickening by the antimicrobial peptide pgla. *Biophys J*, 95(12):5779–5788, Dec 2008. (Cited on page 109.)

[100] H. Vogel. Comparison of the conformation and orientation of alamethicin and melittin in lipid membranes. *Biochemistry*, 26(14):4562–4572, Jul 1987. (Cited on page 111.)

[101] W. Moffitt. The optical rotatory dispersion of simple polypeptides. ii. *Proc Natl Acad Sci U S A*, 42(10):736–746, Oct 1956. (Cited on page 116.)

[102] W. Moffitt and J. T. Yang. The optical rotatory dispersion of simple polypeptides. i. *Proc Natl Acad Sci U S A*, 42(9):596–603, Sep 1956. (Cited on page 116.)

[103] W. Moffitt, D. D. Fitts, and J. G. Kirkwood. Critique of the theory of optical activity of helical polymers. *Proc Natl Acad Sci U S A*, 43(8):723–730, Aug 1957. (Cited on page 116.)

[104] H. H. de Jongh, E. Goormaghtigh, and J. A. Killian. Analysis of circular dichroism spectra of oriented protein-lipid complexes: toward a general application. *Biochemistry*, 33(48):14521–14528, Dec 1994. (Cited on page 116.)

[105] Christina Sizun and Burkhard Bechinger. Bilayer sample for fast or slow magic angle oriented sample spinning solid-state nmr spectroscopy. *J Am Chem Soc*, 124(7):1146–1147, Feb 2002. (Cited on page 117.)

[106] Yong Hoon Park, Young-Jin Kim, Il Hong Son, and Hyun Duk Yang. Inhibition of beta-amyloid(1-40) peptide aggregation and neurotoxicity by citrate. *Korean J Physiol Pharmacol*, 13(4):273–279, Aug 2009. (Cited on page 123.)

ACKNOWLEDGMENTS

First and foremost it is my very pleasant duty to thank Prof. B.Bechinger for accepting me as his student, directing and supporting me during - as it turned out - many years. He always seemed to believe in my abilities (even when I had serious doubts) and was thus vital in motivating me to finish the work I had started.

I am equally grateful to Prof. B.Wallace for her support and encouragement. I want to especially acknowledge her to especially reschedule her plans for my thesis defense. Thanks a lot!

Many collaborators contributed to the acquisition and the discussion of the data reported in this work. I thank Dr. Andrew Miles for helping me countless number of times with the CD experiments and for the warnings about radioactive spiders' hallucinations at the synchrotron at the break of the day. I would also like to thank Dr. Georg Pabst and prof. Karl Lohner for allowing me to use their experimental facilities and for helping with SAXS experiments and discussions of the results.

At last, but not the least, I want to thank my colleagues - Dr. Jésus Raya and Dr. Jérôme Hirshinger - what I may say I know about SS-NMR, I own this knowledge to them. Special thanks to Jésus for all the occasions in which he helped me when I could not launch my experiment because of a hidden parameter or a missing insert or a broken pre-amplifier or God (Jésus) knew why. Dr. Elise Glattard - there are too many reasons to thank for and I don't know where to begin. Thanks for the help with the experiments, including the sleepless nights counting bacteria; for all the work done in the lab (even if it is not her duty); for always participating in the social activities I proposed; for all the discussion about the future and the time when we will get old (i.e. from this year...). Many thanks to all of the above for their priceless comments on this manuscript. Also, thanks to Dr. Verica Vidovic for providing me the PLAH4 peptide and Delphine Hatey for synthesizing and purifying some of the peptides I used for this work.

Among the other colleagues, I want to explicitly thank Anna, comrade-in-arms in the never ending war against "The Bureaucracy", for her "never give up" attitude. I am often jealous of her energy and organization skills. Christopher deserves all the gratitude for his efforts to fix anything broken in the lab (or, at least, to disassemble it) and for his masterpiece - the rhubarb cake. I want to thank Arnaud and Philippe for their helpful suggestions about DLS and NMR and for the serious conversations on mountaineering and food. I thank Evgueniy for his fairness both in science and volleyball. I don't want to forget all the other present and past lab-mates Marie-Catherine, James, Svetlana, Sebaastian, Victor, Fatou, Omar, Mathias, Patricia, Marc, Caroline, François-Marie, Malika, Hiba and Karim, who contribute to the lively atmosphere of the lab.

Many other people that lessened my loneliness in Strasbourg deserve my honest gratitude, most of whom are "colleagues next door" or "next floor": Lucas, Linas, Adi, Corinna, Giangi, Andrea, Maria, Chiara,

Silvia, Emanuele, Pierre, Gael, Ilaria, Garreth and all the other hard-core people of the "Monday Climbing + Beer", later shrank into "Monday Beer". With them I was always able to release the stress of a long weekend of failed experiments with conceited verbal exchanges about science, religion, alcoholic adventures... and topics that should not be mentioned in a thesis.

A special thanks to my last flatmate, Cristina, as we tried to keep ourselves together in the difficult times when we were both inexperienced-over-specialized job seekers. I would like to offer in advance my sincere apologies to my current flatmate and colleague, Nataliia, because she is going to see the worst of me some days before (and probably after) my thesis defence.

No Italian can end a PhD thesis without a word for his/her mother - so many thanks mum - if I made it, it is also because of you. An additional hug to my two restless nephews for their very special contributions to this dissertation while my computer was unattended...

Many, many, many thanks to Denis to keep up with me after all these years and all these kilometers.

Finally, I would like to express my gratitude to the European Union 6^{th} Framework Marie Curie Actions for financial support and all the people of the Biocontrol Network to build such an lively group.

DECLARATION

I hereby declare that this thesis is my own work and effort and that it has not been submitted anywhere for any award. Where other sources of information have been used, they have been acknowledged.

Strasbourg, France, September 2011

Barbara Perrone

COLOPHON

This thesis was typeset with LyX, a document processor released under a Free Software/Open Source license and available in several languages http://www.lyx.org/.

The typographic style was written for LaTeX by André Miede in homage to Bringhurst's "The Elements of Typographic Style". The LyX port of the original package, "classicthesis", was written by Nick Mariette and it is available at http://soundsorange.net/resources/classic-thesis-for-lyx/.

Final Version as of October 25, 2011 at 17:40.